STUDY OF SERINE PALMITOYLTRANSFERASE AND DE NOVO SYNTHESIS OF SPHINGOLIPIDS

A Dissertation
Presented to
The Academic Faculty

by

Jia Wei

In Partial Fulfillment
of the Requirements for the Degree
Doctor of Philosophy in the
School of Biology

Georgia Institute of Technology
May, 2009

STUDY OF SERINE PALMETOYLTRANSFERASE AND DE NOVO SYNTHESIS OF SPHINGOLIPIDS

Approved by:

Dr. Alfred Merrill, Advisor
School of Biology
Georgia Institute of Technology

Dr. Kirill Lobachev
School of Biology
Georgia Institute of Technology

Dr. Gang Bao
Biomedical Engineering
Georgia Institute of Technology

Dr. Marion Sewer
School of Biology
Georgia Institute of Technology

Dr. Yury Chernoff
School of Biology
Georgia Institute of Technology

Date Approved: March 23rd, 2009

To my wonderful husband

ACKNOWLEDGEMENTS

I would like to thank my advisor Dr. Alfred Merrill for his invaluable instruction and guidance. With his enthusiasm, his inspiration, and his great efforts to explain things clearly and simply, he helped to make biology research fun for me.

I would like to thank my thesis committee members, Dr. Yury Chernoff, Dr. Marion Sewer, Dr. Kirill Lobachev, Dr. Gang Bao and previous member Dr. Harish Radhakrishna for support, encouragement, feedback and suggestions.

I thank Elaine Wang, Samuel Kelly, Jeremy Allegood, Hyejung Park, Amin Momin, Chris Haynes, Ying Liu and other Merrill lab members for help and suggestions.

I wish to thank my parents. I am indebted to my father for his care and love. Although he is no longer with us I am sure he shares our joy and happiness in the heaven. I cannot ask for more from my mother. She gave me constant support and love throughout my whole life.

I would like to thank my son, my lovely sunshine, who brought me happiness and energy when I felt sad and tired.

My deepest gratitude goes to my wonderful husband, Qiang Fu. Without his love and support, this dissertation is impossible. To him I dedicate this thesis.

TABLE OF CONTENTS

LIST OF TABLES

LIST OF FIGURES

CHAPTER 1

CHAPTER 2

CHAPTER 3

LIST OF SYMBOLS OR ABBREVIATIONS

1-deoxySa 1-deoxy sphinganine
1-desoxMe-Sa 1-desoxy-methyl sphinganine
1-deoxy-DHCer 1-deoxy-dihydroceramide
1-desoxMe-DHCer 1-desoxy-methyl dihydroceramide
4HPR 4 hydroxyphenylretinamide
aa amino acid
AMP adenosine monophosphate
aSMase acid sphingomyelinase
BSA bovine serum albumin
C6-NBD Sphingomyelin N-[6-[(7-nitro-2-1,3-benzoxadiazol-4-yl)amino]hexanoyl]-sphingomyelin
Cer ceramide
Cer-1-P ceramide-1-phosphate
CHO Chinese hamster ovary cells
CMH ceramide monohexoside (monohexosylceramide)
DEAE diethylaminoethyl
DES1 dihydroceramide desaturase 1
DES2 dihydroceramide desaturase2
DHCer dihydroceramide
DHCMH dihydroceramide monohexoside
DHSM dihydrosphingomyelin
DTT dithiotreitol
ER endoplasmic reticulum
ESI LC-MS/MS liquid chromatography electrospray tandem mass spectrometry
FB1 fumonisin B1
Gal galactose
GalCer galactosylceramide
GFP green fluorescent protein
Glu glucose
GluCer glucosylceramide
HEK293 human embryonic kidney cells
HeLa human cervical cancer cells
HPLC high performance liquid chromatography
HSN1 hereditary sensory neuropathy type I
K_2HPO_4 dipotassium phosphate
KCl potassium chloride
KOH potassium hydroxide
kDa kilo Dalton
LYB Chinese hamster ovary cells with SPT1 deficiency
$MgCl_2$ magnesium chloride
NaCl sodium chloride
NADPH Nicotinamide adenine dinucleotide phosphate
nSMase, neutral sphingomyelinase
PBS phosphate buffered saline

QRT-PCR, quantitative real-time PCR
Sa sphinganine
So sphingosine
SDS sodium dodecyl sulfate
SDS-PAGE sodium dodecyl sulfate polyacrylamide gel electrophoresis
SM sphingomyelin
SMase sphingomyelinase
SPT serine palmitoyltransferase
SPT1/2 HEK293 cells stably overexpressing SPT1 and SPT2
TBS tris buffered saline

SUMMARY

Sphingolipids are membrane components in eukaryotes, some prokaryotes and viruses. They play important roles in membrane structure, biological recognition and signal transduction (3-5). Serine palmitoyltransferase (SPT) catalyzes the first unique step of *de novo* sphingolipid biosynthesis, the condensation of serine and palmitoyl-CoA to form the sphingoid base backbone (6). We have studied the molecular and biological consequences of overexpression of SPT using HEK293 cells stably transfected with plasmids containing the cDNA for *SPTLC1* and *SPTLC2* (termed "SPT1/2 cells"). The effects of the elevated SPT activity were analyzed by measuring the sphingolipid amounts and types in these cells as well as by following the incorporation of [^{13}C] palmitate into the sphingoid base (and/or fatty acid) backbones, which were analyzed by liquid chromatography, electrospray ionization-tandem mass spectrometry (LC-ESI-MS/MS). These studies revealed that most sphingolipid subspecies were elevated in SPT1/2 cells (with disproportionate increases in dihydrosphingolipids and subspecies with stearic acid in the ceramide backbone); however, sphingomyelins were lower. The lower sphingomyelin does not appear to be caused by faster degradation, but possibly by substitution by dihydrosphingomyelins. Despite large increases in ceramide, a growth inhibitory and pro-apoptotic mediator in many cell types, the SPT1/2 cells did not display higher numbers of dead cells but, instead, grew faster than HEK293 cells. Thus, increased de novo sphingolipid biosynthesis via this manipulation has uncovered several new features of this pathway that warrant further investigation.

In the course of these studies, we noted by confocal microscopy that SPT1 is not only found in the endoplasmic reticulum, but also in the nucleus and focal adhesions. This unexpected localization was confirmed in several cell lines, and by finding that SPT1 is co-immunoprecipitated with vinculin using an anti-vinculin antibody. The association of SPT1 with focal adhesions may indicate that it plays a role in cell morphology and migration, and consistent with this hypothesis, focal adhesion staining of SPT1 is seen mainly before cells in culture reach confluence, and reappears when proliferation and migration is reinitiated by a standard scratch-wound healing assay. Furthermore, elimination of SPT1 using *SPTLC1* siRNA causes cell rounding that does not appear to be due to interference with *de novo* sphingolipid biosynthesis. Thus, in addition to its "traditional" role in de novo sphingolipid biosynthesis in the ER, SPT1 is present in other cellular compartments and is required for normal cell morphology and migration.

SPT1 was hypothesized to be present in cells in more than one isoform because GenBank has at least three putative SPT1 transcipts that can be rationalized to be produced by alternative splicing. The predicted amino acid sequence of one isoform (which we term *SPTLC1L*) is longer than the SPT1 that has heretofore been associated with SPT activity, and this isoform appears to be expressed in Hek cells because a polypeptide of the predicted size was found by antibodies against its unique amino acid sequence. The functions of the alternative isoforms are not yet clear; however, their existence futher underscores how much remains to be learned about the biochemistry and regulation this pathway and its components.

CHAPTER 1

Review of Serine Palmitoyltransferase

1.1 Sphingolipid

1.1.1 Structure and *de novo* synthesis of sphingolipid molecules

Sphingolipids are a family of phospholipids and glycolipids built upon sphingoid base backbones. There are three major types of sphingoid bases, sphingosine (So), sphinganine (Sa, dihydrosphingosine) and phytosphingosine (4-hydroxydihydrosphingosine). The majority of the sphingoid bases in cells are N-acylated with long-chain fatty acids to produce ceramides (Cer) (Fig. 1.1). By adding a head group at 1-hydroxy position ceramide can be converted to sphingomyelin (SM) or ceramide monohexoside (CMH) including glucosylceramide (GluCer) and galactosylceramide (GalCer). CMH would be converted to various glycosphingolipids (GSL) by adding more carbohydrate groups.

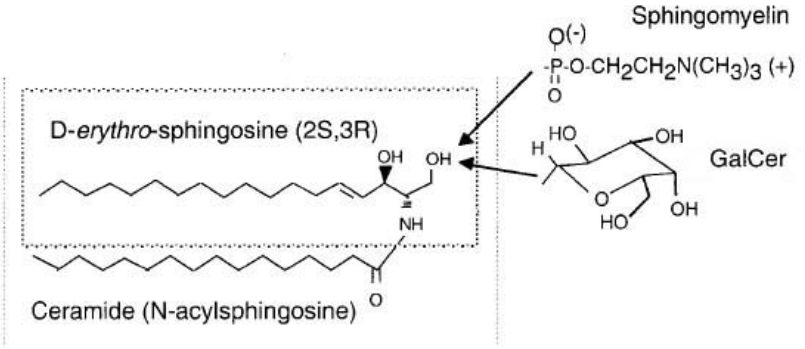

Figure 1.1 Structure of sphingolipid molecules (1)

Intracellular sphingolipids are from extracellular uptake, *de novo* synthesis and turnover from complex sphingolipids. The capacity for *de novo* sphingolipid biosynthesis (Fig. 1.2) is widespread among cell types and tissues (2). The pathway starts from condensation of serine and palmitoyl-CoA by SPT to form 3-keto-sphinganine (3-keto-Sa) which is quickly converted to Sa by 3-keto-sphinganine reductase. The desaturated form of Sa is So and both of them can be phosphorylated to form sphinganine-1-phosphate (Sa1P) and sphingosine (S1P) which are bioactive signaling molecules. Unlike Sa, So is only derived from turnover of ceramide. Both Sa and So can be N-acylated by (dihydro)ceramide synthase (CerS) to form dihydro-ceramide (DHCer) and Cer sequentially. Then DHCer and Cer are further converted to more complex Sphingolipids (DHSM, DHCMH, SM, CMH etc.) by adding different head groups.

In the absence of an exogenous sphingoid base source, loss of this pathway by mutation of SPT or its inhibition by ISP1/myriocin or sphingofungin B affects growth and viability. It is intriguing that this pathway contains so many compounds, which affect cell behavior when added exogenously or formed via sphingolipid turnover, that the consequences can be growth arrest and cytotoxicity or growth stimulation or inhibition of apoptosis.

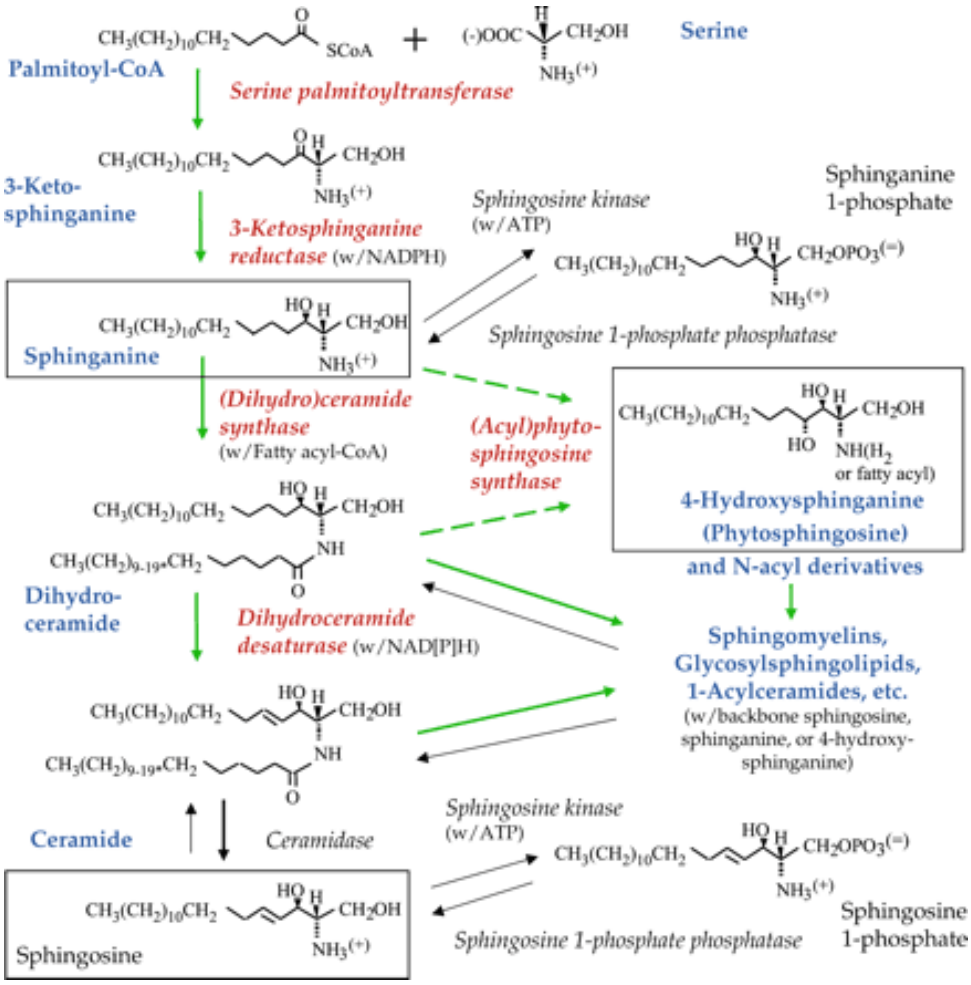

Fig. 1.2 *De novo* biosynthetic pathway for sphingoid bases and complex sphingolipids (2). The color coding distinguishes the biosynthetic enzymes (with common names in *red* and *green arrows* for the reactions catalyzed) and intermediates (in *blue*) from additional reactions that occur with these intermediates (in *black*). The *dashed line* for (*N*-acyl)phytosphingosine synthesis reflects that in yeast, where this has been best characterized.

1.1.2 Functions of sphingolipids

Most sphingolipids (SM, GSL) are membrane constituents and found in different subcellular compartments but some are present in biological fluids. So has a role in regulating the cell cycle and apoptosis (7). Ceramide mediates many cell-stress responses,

including the regulation of apoptosis (8), cell senescence (9), and autophagy (10), whereas S1P has crucial roles in cell survival, cell migration and inflammation (11). Complex sphingolipids (glycosphingolipids and sphingomyelins) affect cell behavior by associating with membrane microdomains that contain receptors, transporters, and other signal transducers such as Src family kinases, small G-proteins (e.g., RhoA, Ras), and focal adhesion kinase (12, 13). The above is not a complete list of sphingolipid functions and the implications of sphingolipids in biological processes are discovered more and more every year.

1.2 Biochemical and genetic characteristics of SPT

1.2.1 Early history of SPT

Following over a decade of speculation about how serine and palmitic acid might serve as the precursors for the sphingoid base backbones of sphingolipids, Braun and Snell (14) and Stoffel et al. (15) demonstrated that serine and palmitoyl-CoA could be condensed to form 3-keto-Sa that was rapidly reduced to Sa if NADPH was also present, thereby establishing the first steps of the *de novo* biosynthetic pathway for sphingolipids. In subsequent decades, some of the properties of SPT were elucidated (16), such as a requirement for pyridoxal 5'-phosphate, a predominate localization of SPT activity in the endoplasmic reticulum (ER), the apparent kinetic properties, and various aspects of its regulation; however, the difficulty of purifying this membrane-associated enzyme until relatively recently (17) and the lack of knowledge about its gene(s) was a serious impediment to progress.

1.2.2 Genes of serine palmitoyltransferase (SPT)

Sphingolipid biosynthesis is initiated by condensation of L-serine with palmitoyl-CoA by serine palmitoyltransferase (SPT); therefore, this is a critical enzyme for this pathway. In mammalian cells, SPT is thought to be a membrane bound heterodimer comprised of two subunits, SPT1 and SPT2, with molecular weights of 53 kDa and 63 kDa, respectively (17, 18), but recently, an additional subunit, SPT3, has also been found in some cells and tissues (19). In the early 1990's, Lester, Dickson, and their co-workers isolated mutant strains of *S. cerevisiae* that require an external supply of phytosphingosine for growth and for the synthesis of complex sphingolipids, and showed that the mutant strains are defective in SPT activity (20). Mutations that caused complete loss of SPT activity were shown to fall into two genetic complementation groups, *Lcb1* and *Lcb2*, and their wild-type alleles (*LCB1* and *LCB2*) were isolated by functional rescue experiments (20-22). With the availability of the yeast genes for SPT, identification of the mammalian homologs soon followed for human, mouse, and CHO cells (23-25). There is ~40% identity between yeast and mammalian SPT proteins, and ~95% identity among the mammalian proteins. As for many genes, the nomenclature for the mammalian SPT genes initially followed that of the microbial genes (e.g., LCB) but was later renamed *SPTLC* for the human genomic homologs of the yeast *LCB* genes respectively).

In the human genome, *SPTLC1* comprises 15 exons spanning ~85 kbp on chromosome 9q21-q22 region; *SPTLC2* comprises 12 exons spanning ~110 kbp on chromosome

14q24.3-q31 region and *SPTLC3* is composed of 12 exons on chromosome 20 p12.1–12.3. The predicted MW of human SPT1, SPT2 and SPT3 are 53 kDa, 63 kDa and 63kDa, respectively, and polypeptides of this approximate size are seen on Western blots of human and mouse cells using protein specific antibodies (17, 19, 23). The SPT1 and SPT2 subunits have ~20% identity and have a single highly hydrophobic domain in the amino-terminal region, which probably represents a transmembrane domain without cleavable signal sequences (23, 24). SPT3 subunit has an identity to SPT2 subunit of 68%.

1.3 SPT-associated proteins

Dunn and co-workers have shown that an additional 10-kDa peptide, the product of the *Tsc3* gene, is associated with the SPT1/SPT2 complex in the yeast *S. cerevisiae* (26). Tsc3p is not essential for activity, but is required for optimum activity of SPT in yeast. No mammalian homolog of *Tsc3* has been found so far even by computer search of sequence databases or upon affinity purification of SPT from CHO cells (17). Inuzuka et al.(27) described a class of endoplasmic proteins (termed Serinc1 to 5) in yeast and mammalian cells that increase the synthesis of both phosphatidylserine and sphingolipids. Overexpression of Serinc1 in COS cells doubled SPT activity, therefore, Serinc may interact with SPT to facilitate serine utilization.

Using proteomic technologies (tandem-affinity purification and mass spectrometry) to discover protein-protein interactions, a substantial number of proteins have been identified as potential LCB2-associated proteins in *Saccharomyces cerevisiae* (28). These proteins are involved in various biological processes such as vesicle transport,

nuclear import and export, among others. A genome-wide yeast two-hybrid analysis in *Drosophila* (29) has suggested that SPT2 may interact with 13 proteins, which include a proton transporter, organic cation transporter, hsc-70, and ribosomal proteins, among others.

1.4 Structure and mechanism of the SPT reaction

SPT has significant structural and mechanistic similarities to members of a subfamily of PLP-dependent enzymes that includes 5-aminolevulinic acid synthase, 2-amino-3-ketobutyrate ligase, and 8-amino-7-oxononanoate synthase. These enzymes catalyze condensation of amino acids and the CoA thioesters of carboxylic acids to produce α-oxoamines, therefore, have been referred to as the PLP-dependent α-oxoamine synthase (POAS) family. However, the eukaryotic SPT's are the only members of this family that have been identified to date to be membrane bound and heterodimeric--all other members are soluble homodimers. In contrast to eukaryotic SPT, *Sphingomonas paucimobilis* produces a soluble SPT that is ~30% identical to both mammalian SPT1 and SPT2 at the amino acid level, but is a homodimer of a 45-kDa protein (30). POAS members share a conserved motif around the lysine that is responsible for formation of a Schiff's base with pyridoxal 5'-phosphate (PLP)(T[FL][GTS]**K**[SAG][FLV]G). This motif is present in SPT2 and SPT3 and not in SPT1. PLP is moderately tightly bound by SPT with an apparent Km of approximately 0.1 μM for the mammalian enzyme (31).

It has long been noted (32) that the involvement of PLP in removing the carboxyl group of serine during the condensation of serine and palmitoyl-CoA allows two mechanisms to be postulated: formation of PLP-stabilized carbanion by decarboxylation of the substrate L-serine, followed by acylation, or formation of a carbanion by removing the α-hydrogen atom of L-serine, followed by acylation and decarboxylation (shown in Fig. 1). Krisnangkura and Sweeley (33) provided strong evidence for the latter mechanism by demonstrating that the α-hydrogen atom of serine is replaced by a proton from H_2O during the reaction, which has also been found for the condensation reactions catalyzed by 5-aminolevulinic acid synthase (34) and other enzymes of this family. In addition, the structures of several potent SPT inhibitors (*i.e.*, sphingofungins and myriocin) resemble that for a potential transient state intermediate with the carboxyl group of L-serine still present, which would be found in latter pathway (as shown in the insert in Fig. 1).

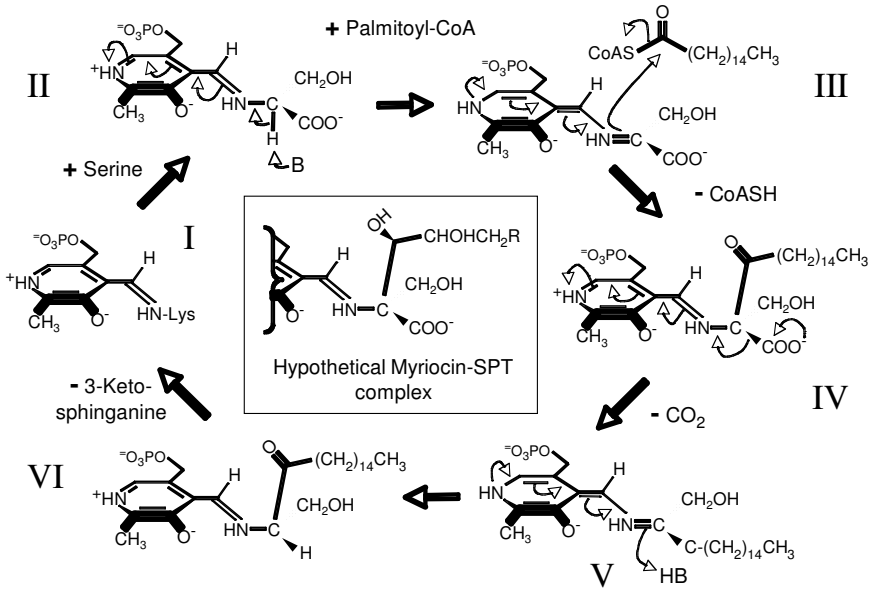

Fig. 1.3 Suggested catalytic pathway of serine palmitoyltransferase (SPT) and rationale for inhibition by myriocin-like compounds (insert)
Starting with the internal aldimine of pyridoxal 5'-phosphate (PLP) with an active site lysine (I), Serine is bound by SPT as an external PLP aldimine (II), deprotonated at the α-carbon and condensed with palmitoyl-CoA (III) (possibly through this quinonoid intermediate), followed by decarboxylation of the doubly β,γ-unsaturated intermediate IV, proton abstraction (V) and release of the produce 3-ketosphinganine (VI). The insert illustrates the similarities between the presumed aldimine of myriocin with SPT and catalytic intermediate IV.

1.4.1 Substrate selectivity of SPT

SPT strictly utilizes l-serine as its amino acid substrate; however, D-serine is a competitive inhibitor with an IC50 of ~0.3 mM, which is similar to the Km for l-serine (17). SPT is also highly selective for the co-substrate fatty acyl-CoA with the mammalian enzyme (17, 31) utilizing palmitoyl-CoA (C16:0) > pentadecanoyl- and heptadecanoyl- CoA's (C15:0 and C17:0) >> stearoyl-CoA (C18:0) and essentially no unsaturated species except palmitelaidic acid (t16:1), which has an uncommon trans- versus cis- double bond. This selectivity, combined with the abundance of palmitoyl-

CoA (and scarcity of C15:0 and C17:0 fatty acids in most species except ruminants) probably accounts for the extremely high 18-carbon-chain-length specificity of most sphingoid bases in mammalian sphingolipids. Indeed, in species where other chain lengths are found, such as *Drosophila* which contain 14-carbon sphingoid bases, or *Sphingomonas* which displays very little sphingoid base specificity, this is reflected in differences in the fatty acyl-CoA selectivity of the SPT from these species (35, 36). A question that remains to be answered is why atypically long sphingoid bases (with 20-carbon atoms) are found in mammalian gangliosides (1, 37) and especially in hippocampus (38); otherwise, these types of sphingoid bases have mainly been observed in yeast under certain stages of growth and stress, and are thought to have roles in cell signaling (39).

These kinetic properties of mammalian SPT, which were measured in vitro and are subject to numerous complications inherent in assaying lipid metabolizing enzymes under artificial conditions, have nonetheless been closely replicated in studies of intact LM cells (40) and hepatocytes (41) where the cellular concentrations of serine and palmitate were varied. Physiologic concentrations of serine are known to fluctuate above and below the Km for SPT (40), which might interfere with sphingolipid metabolism and explain why cells have the recently discovered Serinc (for serine incorporating) proteins to facilitate utilization of this precursor (27). It has also been noted (42) that since D-serine is a strong competitive inhibitor for L-serine, and substantial quantities of D-serine are present in discrete areas of the brain and some other tissues, D-serine might affect *de novo* sphingolipid synthesis in these cells (also providing, perhaps, one of the rationales

for the Serinc proteins). Indeed, serine homeostasis is itself highly complex and part of the one-carbon-metabolism system that includes the biosynthesis and turnover of glycine and methionine, methylation of proteins, lipids and nucleic acids, and many other important regulatory pathways. Recently it was found that alanine could be used as an SPT substrate to form 1-deoxysphinganine (1-deoxy-Sa) in fumonisin B1 treated cells suggesting that under certain circumstances SPT might not strictly require serine as its substrate in vivo (43). The mechanism for SPT substrate selection is not clear yet. These issues illustrate the fundamental questions that have not yet been answered about how *de novo* sphingoid base biosynthesis is coordinated with other metabolic pathways, which one hopes is at last becoming feasible to address with the types of systems models that have been developed for the metabolic pathway in yeast (44-46).

1.4.2 Inhibitors of SPT

A fairly high number of naturally occurring inhibitors of SPT have been discovered and many can be rationalized due to their structural similarity to reaction intermediates, such as myriocin shown in the insert of Fig. 1. These include sphingofungins, lipoxamycin (neoenactin M1), myriocin (ISP-1/thermozymocidin) and sulfamisterin, which are potent (i.e., with IC50 in the nanomolar range) and, as far as has been determined to date, high selective for fungal and mammalian SPT (47-50). Viridiofungins (51) are also potent inhibitors of mammalian SPT, but also inhibit squalene synthase. As expected for an enzyme that utilizes pyridoxal 5'-phosphate, SPT is also inhibited by compounds such as l-Cycloserine and β-chloro-l-alanine in intact cells, however, this is usually not desirable because these compounds affect too many other metabolic pathways as well.

1.4.3 Kinetic and spectroscopic studies of the mechanism of SPT

Because the SPT from *Sphingomonas paucimobilis* is a soluble homodimer (30), it has been much more extensively characterized than the membrane-bound SPT's (35, 52). The purified recombinant SPT has an absorption spectrum with maxima at 426 and 338 nm, which was interpreted as the aldimine (species "I" in Fig. 1) and enolimine tautomer, respectively, of PLP with the active site lysine. Ikushiro et al. also reported that addition of L-serine caused an increase in 426 nm absorption indicative of formation of the external aldimine intermediate (species "II"), however, absorption at ~500 nm was not detected by rapid mixing or static methods, which suggests that the quinonoid intermediate (species "III") does not accumulate. As noted by these authors, this does not necessarily preclude the existence of intermediate "III", but it may not form until addition of palmitoyl-CoA. The absorption and CD spectra of the SPT-myriocin complex were also consistent with the formation of an external aldimine, as hypothesized in Fig. 1. Interestingly, addition of sphinganine or sphingosine also altered the spectrum, although in-depth studies were precluded by the low solubility of these compounds. This may indicate that interaction between SPT and its product (and/or downstream products) might affect activity.

1.5 Regulation of SPT

SPT activity and mRNA have been found in very mammalian tissue and cell type and are especially abundant in organs such as kidney, lung and liver (23, 53). In addition, SPT activity depends on the developmental stage of tissues (54) and is affected by

environmental factors such as diet in several tissues (55, 56). Although surprisingly little is known about SPT regulation—and SPT is sometimes erroneously referred to as a "housekeeping enzyme", a growing number of animal studies and investigations with cells in culture are documenting transcriptional and post-transcriptional regulation of SPT activity.

1.5.1 Transcriptional and post-transcriptional regulation in response to extracellular stimuli

Many of the factors that have been reported to increase SPT mRNA and activity are summarized in Table 1. A large fraction of the stimuli are inflammatory, toxic or some other form of stress. Intraperitoneal administration of endotoxin to Syrian hamsters increased SPT activity 2- to 3-fold in the liver, spleen, and kidney with a concomitant increase in *SPT2/LCB2* mRNA (57). Similar changes were observed upon administration of interleukin 1ß (IL-1), an inflammatory cytokine. Irradiation of keratinocytes with ultraviolet A (UVA) upregulated SPT activity as well as mRNA (58); ultraviolet light B (UVB) also affects SPT mRNA in epidermal cells (59). SPT activity in epidermal cells appears to be up-regulated in response to barrier requirements of skin (60). These results, along with the observation that inflammation and UVB stimuli also enhance the synthesis of other lipid types, including fatty acids and cholesterol (61, 62), raises the possibility that a lipogenic signaling pathway(s) is involved in transcriptional control of SPT genes. Consistent with this possibility, both *SPT1* and *SPT2* mRNA are increased when cultured human keratinocytes are treated with nicotinamide, which also enhances fatty acid and cholesterol synthesis (63). The expression of *SPT1* mRNA is also up-regulated in islets

of leptin-receptor-deficient obese *fa/fa* rats, compared to the levels in control islets, and this up-regulation is suggested to be a response to an increase in intracellular fatty acid (64). A recent study showed that high fat diet led to a substantial increase of SPT in *vitro activity* and the SPT1 protein amount in ldlr-/- mice (65).

Cytotoxic accumulation of palmitate induces apoptosis accompanied by an elevation of the intracellular ceramide level in various cell types, including the hematopoietic LyD9 cell line, *fa/fa* pancreas islets, astrocytes, and CHO cells (66). For most cell types, enhanced *de novo* synthesis of ceramide via SPT is required for palmitate-induced apoptosis (64, 66-68), whereas palmitate-induced apoptosis of CHO cells is suggested to occur through a ceramide-independent, but reactive oxygen species-dependent, pathway (67). Palmitate-induced enhancement of SPT activity in primary astrocytes is prevented by exposure of cells to an activator of AMP-activated protein kinase (AMPK) (68). The AMPK cascade acts as a metabolic sensor that monitors cellular AMP and ATP levels, and once activated, down-regulates various ATP-consuming anabolic pathways including fatty acid and cholesterol synthesis. The AMPK cascade might also participate in the regulation of sphingolipid synthesis.

Certain types of apoptotic stimuli appear to increase SPT activity with little or no change in mRNA amount, hence, may act post-transcriptionally (Table 1). Upon treatment with retinoic acid, mouse teratocarcinoma PCC7-Mz1 cells undergo apoptosis, but a fraction begins to differentiate in a manner mimicking the early steps of neuronal development. Retinoic acid treatment of PCC7-Mz1 stem cells induces accumulation of ceramide

accompanied by an increase in SPT activity without any increases in *SPT1* and *SPT2* mRNA (69). Likewise, treatment of Molt-4 human leukemia cells with the chemotherapy agent etoposide elevates both SPT activity and intracellular ceramide without increasing *SPT* mRNA (70). During cannabinoid-induced apoptosis, both SPT activity and intracellular ceramide increase 4 to 6 fold without major changes in *SPT* mRNA or protein in a subline of the rat glioma C6 cells. When these cells have been treated also with inhibitors of *de novo* sphingolipid synthesis to block the increase in ceramide, there is usually also a decrease in apoptosis in response to these stimuli (69, 70) which suggests that the elevation in ceramide is a mediator of, rather than merely a consequence of, the pro-apoptotic effects of these agents. *De novo* sphingolipid biosynthesis (and SPT activity) is also rapidly up-regulated in Molt-4 cells during heat shock (71), and heat shock is well known to affect—and to be influenced by--sphingolipid biosynthesis in yeast (72).

1.5.2 Regulation of SPT for homeostasis of cellular sphingolipid amounts

Little is known about what controls the sphingolipid amounts of cells. A plausible feedback regulator is sphingosine (or perhaps sphinganine) 1-phosphate because addition of sphingosine or an analog that accumulates in the cells as the phosphate metabolite to cultured mouse cerebellum cells significantly decreases SPT activity (which does not appear to be due to direct inhibition of SPT by the sphingoid base because SPT activity is not reduced when microsomes are incubated directly with sphingoid bases) (73, 74). Similarly, accumulation of S1P and Sa1P by treating primary cultured cerebellum neurons with high concentrations of a dihydroceramide desaturase inhibitor, GT11,

reduced SPT activity by about 90% without changing SPT mRNA amount, which could reflect feedback inhibition of SPT (75). Puzzlingly, depression of *de novo* sphingolipid synthesis by exogenous ceramide or its analogs seems not to be accompanied by any inhibition of the activities of anabolic enzymes, including SPT (76, 77). It is clear that more studies are required to elucidate the mechanisms underlying the regulation of cell sphingolipid homeostasis via *de novo* synthesis versus recycling of endogenous and exogenous sphingoid bases.

Table 1.1 Stimuli/conditions that up-regulate SPT activity in mammalian cells

–, no increase; nd, not determined
[a]After stimulation, the levels initially decreased by ~50%, but subsequently increased above unstimulated control levels.
[b]*De novo* sphingolipid synthesis in intact cells was significantly increased.

Stimulus or condition (tissue or cell type)	**Activity**	**mRNA (protein)**		**References**
		SPTLC1 /LCB1	***SPTLC2 /LCB2***	
UVB (mouse epidermis and cultured human keratinocytes)	1.5	1.5[a]	2-3[a] (2)	(59, 62)
UVA (human keratinocytes)	2.5	14	7	(58)
Endotoxin, IL1 (liver, spleen and kidney of Syrian hamster)	2-3	nd	2-4	(57, 78)
Endotoxin, IL1, tumour necrosis factor-α (human HepG cell line)	2-3	nd	2-3	(57)
Leptin receptor mutation (rat pancreas islet)	nd[b]	2-3	nd	(64)
Fatty acids (rat pancreas islet)	nd[b]	1.5-2	nd	(64)
Palmitic acid (rat astrocytes)	1.3	nd	nd (1.4)	(68)
Nicotineamide (cultured human keratinocytes)	1.2	1.8	1.8	(63)
Etoposide (human leukemia Molt-4 cell line)	2-3	–	–	(70)

Table 1.1 continued

Retinoic acid (mouse teratocarcinoma PCC7-Mz1 cell line)	3	–	–	(69)
Resveratrol (human breast cancer cells)	1.5	–	–	(79)
D^9-Tetrahydrocannabinol (a subline of the rat glioma C6 line)	6	1.4 (1.8)	1.1	(80)
Activation of angiotensin II type 2 receptor (a subline of the rat pheochromocytoma PC12 cell line)	2	nd	nd	(81)
N-(4-hydroxyphenyl)retinamide (human neuroblastoma CHLA-90 cell line)	2	nd	nd	(82)
Hexachlorobenzene (rat liver)	1.5-2[a]	nd	nd	(83)
Apolipoprotein E knockout (mouse liver)	2	nd	–	(84)

1.6 Significance of studying SPT and sphingolipid *de novo* synthesis

1.6.1 SPT is essential for survival

In addition to being essential for yeast (20), SPT activity (or exogenous addition of sphingoid bases) has been shown to be required for survival of a temperature-sensitive Chinese hamster ovary (CHO) cell mutant (strain SPB-1) with a thermolabile SPT was isolated after selection by in situ colony assay (85). Knockout of SPT in fruit flies results in embryonic lethality (86), whereas when the SPT deficiency is partial, mutant flies grow into adults with abnormalities which can be rescued by feeding with sphingosine. Attempts to produce homozygous knockout mice were also unsuccessful due to embryonic lethality (87), although heterozygotes were healthy and had lower SPT mRNA,

protein, and activity in some tissues (e.g., liver). Thus, all of the studies to date demonstrate that sphingolipids are essential for survival of the organisms in which they are produced (i.e., from fungi to invertebrates and mammals).

1.6.2 SPT in hereditary sensory neuropathy type I (HSN1)

HSN1 is a dominantly inherited disease involving the progressive degeneration of lower limb sensory and autonomic neurons. HSN1 is a genetically heterogeneous disease, and at least three gene variants are reported. It has recently been revealed that the genetic defect in the HSN1 families linked to the chromosome 9q22 locus is associated with missense mutations in the human SPTLC1 gene, which alter a specific amino acid residue (Cys133 or Val144) in the SPT1 subunit.

Expression of SPT1/LCB1 mutants having the HSN1 mutations has been shown to inhibit SPT activity and sphingolipid synthesis in CHO cells and yeast. The mutated SPT1 proteins remained capable of forming a complex with the SPT2 subunit, but the complex was enzymatically inactive, which suggests that the mutant SPT1 may have a dominant negative-like phenotype. However, the consequences of the mutations may be more complex because despite the reduction in SPT activity, the rates of sphingolipid biosynthesis, cell proliferation, and death in HSN1 cells were not changed (88).
The amino acid sequence around Cys133 and Val144 in SPT1/LCB1 is highly conserved from yeast to mammals. Although the crystallographic analysis of a mammalian SPT has not been conducted, the tertiary structures of other enzymes in this family reveals that the catalytic site is formed at the interface between the subunits, hence, both Cys133 and

Val144 of SPT1 are predicted to be spatially close to the PLP-binding site of SPT2. Presumably, the amino acid sequence around Cys133 and Val144 in SPT1 is involved in the formation of the catalytic site, and the HSN1 mutant types of SPT1 are unable to contribute to the formation of the active catalytic site. It remains unclear why mutations in a protein widely expressed in all tissues trigger pathology that is highly restricted to specific subsets of cells within a tissue.

1.6.3 Roles of SPT in other biological processes and diseases

SPT is the initial enzyme of a complex metabolic pathway that produces thousands, and potentially tens of thousands, of different molecular species of sphingolipids. While the endproduct complex sphingolipids are known--or in most cases presumed on teleologic grounds--to have cell functions, the turnover products (e.g., ceramide) and biosynthetic intermediates (e.g., sphinganine) have also been shown to be highly bioactive and to participate in both the etiology and sometimes suppression/treatment of disease. Hence, SPT is an interesting candidate as a drug target. Recent experiments showed that SPT activity increased along with development stages of rat brains and declined in hypoxic-ischemic brains, which suggests that SPT plays an important role in neuro system myelination (89). Some existing drugs have already been suggested to act at least in part via increasing SPT activity. N-(4-Hydroxyphenyl)retinamide (4HPR or fenretinide) is a chemotherapy drug undergoing human clinical trials. At first, it was reported to elevate ceramide in numerous human cancer cell lines (90, 91) by coordinate activation of SPT and (dihydro)ceramide synthase (82). Most recently, it was found that sphinganine and

dihydroceramide but not ceramide were elevated in 4HPR treated cancer cells (92). The anti-proliferative effect of a selective COX-2 inhibitor, celecoxib, is through increasing *de novo* synthesis of sphinganine and dihydroceramide (DHCer) (93). A dietary factor, resveratrol, is antiproliferative and proapoptotic, and its effects correlate with an increase in endogenous ceramide that has been suggested to involve activation of SPT and neutral sphingomyelinase (79). In Molt-4 human leukemia cells, the chemotherapy agent etoposide increases ceramide due to upregulation of SPT activity (70). γ-Tocopherol, the predominant form of vitamin E in diets, induces apoptosis of LNCap cells and addition of myriocin to inhibit SPT protects cells from γ-tocopherol–induced apoptosis (94). Increases in ceramide have also been proposed to mediate the tamoxifen-dependent accumulation of autophagic vacuoles in MCF-7 cells (95) .

Investigators have for several decades contemplated provocative associations between sphingolipid metabolism and atherosclerosis, however, recent studies of atherosclerotic lesion development in apoE-deficient mice have provided a link between SPT inhibition and this disease. Hojjati et al. have reported that treatment of apoE-deficient mice with myriocin decreases plasma sphingomyelin, ceramide, and sphingosine-1-phosphate and reduces atherosclerotic lesion area (96). Manipulation of *de novo* sphingolipid biosynthesis may have benefits for multiple pathologies associated with advanced age because a link is also surfacing between sphingolipids, lipid rafts, and their components (cholesterol) in the processing of β–amyloid precursor protein (APP). The secretion of soluble APPα and generation of C-terminal fragment cleaved at α-site dramatically increased via activation of MAPK/ERK pathway in Chinese hamster ovary cells treated

with myriocin and in a mutant, LY-B strain defective in the SPT1 protein (97). This indicates modulation of sphingolipid metabolism may able to influence the pathogenesis of Alzheimer's disease by affecting APP cleavage. These examples actually highlight just a few of the promising indications that SPT is a potential pharmaceutical target for prevention and treatment of disease.

1.7 Objectives of the study

The main goal of this work is to study the classic and novel functions of SPT. If SPT activity is increased by overexpression of SPT1 and SPT2 subunits what are the molecular and biological consequences of it. We also want to know the subcellular localizations of endogenous SPT and if SPT play the same role in the different locations. It is also our interest to know if SPT isoforms exist and if they are responsible for the synthesis of sphingoid bases with different chain lengths.

CHAPTER 2

Consequences of increasing the expression of SPT in a cell model system

2.1 Introduction

SPTLC genes have been expressed in mammalian cell lines before (18, 23). However, because of method limitation its molecular consequences and the effect on *de novo* synthesis of sphingolipids have not been evaluated. Previous study showed that HEK293 cells express *SPTLC1* and *SPTLC2* but not *SPTLC3* (19). HEK293 cells stably expressing *SPTLC1* and *SPTLC2* (SPT1/2 cells) were generated and used for our study. A method for quantification of sphingolipid *de novo* synthesis has been developed by our lab. Uniformly labeled [^{13}C] palmitate was used to label the sphingoid base backbone and fatty acid (including longer chain fatty acids by elongation of the [^{13}C] palmitate) followed by LC ESI-MS/MS analysis. Using this method, the *de novo* synthesis of sphingolipid was compared in SPT1/2 cells and HEK293 cells and sphingolipid amount was not only quantified for each sphingolipid species but also for each of its subspecies with different fatty acyl chain lengths. Our analyses confirmed that overexpression of *SPTLC1* and *SPTLC2* in HEK293 cells increased the flux through the *de novo* pathway and most *de novo* species were elevated except for sphingomyelin. The subspecies with various chain lengths were quantified and among them C18 subspecies has the highest fold elevation in SPT1/2 cells. Newly synthesized sphingolipids that have very low amount in HEK293 cells, such as Sa, 1-deoxySa and dihydro-species, are highly elevated in SPT1/2 cells.

2.2 Materials and methods

2.2.1 Materials

The HEK293 cells were obtained from the American Type Culture Collection (Manassas, VA). All tissue culture plastic ware was obtained from Corning (Corning, NY). Fetal bovine serum was supplied by Hyclone (Logan, Utah). The affinity purified polyclonal rabbit anti-human primary antibodies raised against SPT1 peptides have been previously described (98). The epitope sequences that were used to generate the antibody are "KLQERSDLTVKEKEE" (aa 45-59) and "EQEIEDQKNPRKAR" (aa 223-236). C6-NBD-SM and C6-NBD-Cer are from Avanti Polar Lipids (Alabaster, AL). Protease inhibitor cocktail was obtained from Roche (Indianapolis, IN). The internal standard cocktail (catalog number LM-6002) was provided by Avanti Polar Lipids (Alabaster, AL) in sealed ampoules and certified (99) to be > 95% pure and within 10% of the specified amount (250 μM); it was comprised of the 17-carbon chain length sphingoid base analogs: C17-sphingosine, (2S,3R,4E)-2-aminoheptadec-4-ene-1,3-diol (d17:1-So); C17-sphinganine, (2S,3R)-2-aminoheptadecane-1,3-diol (d17:0-Sa); C17-sphingosine 1-phosphate, heptadecasphing-4-enine-1-phosphate (d17:1-S1P); and C17-sphinganine 1-phosphate, heptadecasphinganine-1-phosphate (d17:0-Sa1P); and the C12-fatty acid analogs of the more complex sphingolipids C12-Cer, N-(dodecanoyl)-sphing-4-enine (d18:1/C12:0-Cer); C12-Cer 1-phosphate, N-(dodecanoyl)-sphing-4-enine-1-phosphate (d18:1/C12:0-Cer1P); C12-sphingomyelin, N-(dodecanoyl)-sphing-4-enine-1-

phosphocholine (d18:1/C12:0-SM); C12-glucosylceramide, N-(dodecanoyl)-1-β-glucosyl-sphing-4-eine (d18:1/C12:0-GlcCer); and C12-lactosylceramide, N-(dodecanoyl)1-β-lactosyl-sphing-4-eine (d18:1/C12:0-LacCer); as well as one very-long-chain Cer analog, C25-Cer, N-(pentacosanoyl)-sphing-4-enine (d18:1/C25:0-Cer). U-[^{13}C]-palmitate (98%) was purchased from Cambridge Isotope (Andover, MA). The HPLC grade solvents (acetonitrile, # EM-AX0145; chloroform, # EM-CX1050; hexane, # JT9304-33; and methanol, # EM-MX0475, as well as formic acid (ACS grade, # EM-FX0440-7), were obtained from VWR (West Chester, PA), and acetic acid (ACS grade, # A38C-212) was obtained from Fischer (Pittsburg, PA).

2.2.2 Cell culture

HEK293 cells and SPT1/2 cells were grown in DMEM / F12 medium (1:1) (Gibco BRL, MD) supplemented with 10 % fetal bovine serum (FBS), penicillin (100 U / ml) and streptomycin (100 µg /ml) at 37 °C in a humidified 5 % CO_2 atmosphere.

2.2.3 Generation of SPT1 and SPT2 over-expressing cell lines

SPTLC1 and *SPTLC2* were cloned from human monocytes. Briefly, total RNA from cells treated for 4 hours with 1µM dexamethosone was isolated using the RNeasy RNA isolation kit (Qiagen, Valencia, CA). The SPT gene-specific RNA was reverse transcribed and PCR amplified using Superscript One-Step RT-PCR System (Invitrogen, Carlsbad, CA). The following oligos were used as amplification primers: *SPTLC1* 5'-CCGGAATTCATGGCGACCGCCACGGAGCAG, *SPTLC1* 3'-

CCGGAATTCGACTCTGCCTAGAGCAGGAC, *SPTLC2* 5'-CCGCTCGAGATGCGGCCGGAGCCCGGAGGCTG, *SPTLC2* 3'-CTAGTCTAGAGGCTCAGTCTTCTGTTTGTTC. The SPT1 gene was cloned into pcDNA3.1NEO and SPT2 was cloned into pcDNA3.1ZEO. The expression plasmids were transfected separately or co-transfected into HEK293 cells using Superfect (Qiagen, Valencia, CA) according to the manufacture's directions. 50 μg of plasmid DNA was mixed with 30 μl of the Superfect reagent in 500 μl serum-free media (DMEM, 2 mM L-glutamine) and incubated at room temperature for 15 minutes. The liposomes were added to 5 ml of serum-containing media (DMEM, 10% FBS, 2 mM L-glutamine, 10 Units/ml Penicillin, 10 μg/ml Streptomycin) and incubated on 5 x 10^6 HEK293 cells for 2 hours at 37°C, 5% CO_2. The cells were washed and the serum-containing media was replaced. 400 μg/ml geneticin or 200 μg/ml zeocin were added to the culture media 48 hours after transfection to select for cells stably expressing SPT1 or SPT2, respectively. The co-transfection was selected in media containing both geneticin and zeocin. The media was changed every 4 days. After 2 weeks, surviving colonies were selected and grown in individual wells of a 6-well plate. Three colonies for each transfection, *SPTLC1*, *SPTLC2*, *SPTLC1/SPTLC2*, pcDNA 3.1 NEO vector control and pcDNA3.1Zeo vector control, were selected and checked by RT-PCR for the transfected gene transcript and by Western blot for recombinant protein expression. The highest expressing cell line for each gene transfection and vector controls were selected for further study.

2.2.4 Western blotting

50 μg of microsomal membrane protein were loaded on a 10 % SDS-PAGE gel (BIO RAD, Hercules, CA). For Western blotting, the gel was transferred to nitrocellulose membrane using Tris-glycine buffer with 20 % methanol, as the transfer medium, for 1 hour at 100 volts (constant), in a transfer unit (BIO RAD, Hercules, CA). After blocking overnight at 4 ^{o}C with 5% milk/TBST (Tris buffered saline with 0.05 % Tween 20) the membrane was incubated with rabbit anti-SPT1 serum diluted in 5% milk/TBST for 2 hours and then with a AP-conjugated secondary antibody and its substrate using a ECF Western blotting kit (GE Healthcare, Piscataway, NJ).

2.2.5 *In vitro* SPT activity assay

SPT activity was assayed as previously described (31). Data of specific activity for SPT represent results from two or more assays conducted under the same conditions. Values are presented as mean with standard deviation of all acquired values.

2.2.6 [^{13}C]-palmitate isotope labeling

Uniformly labeled [^{13}C]-palmitate was mixed with fatty acid-free bovine serum albumin (BSA) at 1:1 molar ratio to make 1mM solution which was further diluted into 0.1mM with complete cell culture medium just before use and filter sterilized. Twenty-four hours before the experiment cells were seeded in 100-mm Petri dishes in complete growth medium. Just before treatment, medium was removed from the petri dish and [^{13}C]-palmitate/BSA medium mixture was applied to the cells for a certain period.

2.2.7 Lipid extraction

The method has been described before (100, 101). The collected cells were centrifuged at 2500rpm for 5min and the supernatant was removed. 0.5 ml of methanol and then 0.25 ml chloroform with internal standards were added. Samples were sonicated and incubated overnight at 48^{o}C in heating block. After cooling down 75 µl of 1 M KOH in methanol was added and the sample was sonicated and incubated 2 h at 37^{o}C. The sample was centrifuged and 400 µl of supernatant was transfered to a new glass tube for ms/ms analysis of sphingoid bases. The remaining sample was neutralized with 3 µl of glacial acetic acid and 1 ml chloroform and 2 ml water were added. After sonication and centrifuge the lower layer was carefully removed to a new glass test tube with a pasteur pipette, leaving the interface (w/some water). The solvent and water were removed from all the above samples using a speed vac.

2.2.8 Liquid Chromatography Electrospray Tandem Mass Spectrometry of Sphingolipids

The method has been described previously (100, 101). All data was collected using a Perkin Elmer Series 200 MicroPump system coupled to a PE Sciex API 3000 triple quadrupole mass spectrometer equipped with a turbo ion-spray source. Free sphingoid bases were separated by reverse phase HPLC using a binary solvent system and a Supelco 2.1mm i.d. x 5 cm Discovery C18 column and a flow rate of 1mL/min. Mobile

phase A consisted of $CH_3OH/H_2O/HCOOH$ (58:41:1) (v,v,v) with 5 mM ammonium formate. Mobile phase B consisted of $CH_3OH/HCOOH$ (99:1) (v,v) with 5 mM ammonium formate. Before every run, the column was equilibrated for 0.4 min with 60:40 (A/B) prior to injection. After sample injection (50 µL by a Perkin Elmer Series 200 autosampler), the column was eluted with 60:40 A/B for 0.5 min, followed by a 1.8 min linear gradient to 100% B, which was held for 5.3 min and followed by a 0.5 min re-equilibration with 60:40 A/B before the next run.

The complex sphingolipids (Cer, CMH, SM) were separated by normal phase HPLC using a binary solvent system and a Supelco 2.1mm i.d. x 5 cm LC-NH_2 column at a flow rate of 1.5 mL/min. Mobile phase A consisted of $CH_3CN/CH_3OH/CH_3COOH$ (97:2:1) (v,v,v) with 5 mM ammonium acetate. Mobile phase B consisted of $CH_3OH/H_2O/CH_3(CH_2)_3OH/CH_3COOH$ (64:15:20:1) (v,v,v,v) with 5 mM ammonium acetate. Before every run, the column was equilibrated for 0.5 min at 98:2 A/B prior to injection. After sample injection, the column was eluted with 98:2 A/B for 1.1 min, followed by a 0.2 min linear gradient to 82% A, which was held for 0.4 min, and then followed by a 0.8 min linear gradient to 100% B. The column was then re-equilibrated at 98:2 A/B for 0.5 min.

In the API 3000 triple quadrupole mass spectrometer, dry ultra high-purity N_2 was used as the nebulizing gas at a flow rate of 6 liters/min. The ionspray needle was held at 5500 V, and the orifice and ring voltages were kept low (30-40 V and 180-220 V, respectively) to prevent collisional decomposition of molecular ions prior to entry into the first

quadrupole, and the N_2 Turbo Ion Spray gas temperature was 500 °C. N_2 was used to collisionally induce dissociations in Q2, which was offset from Q1 by 30-40 V. Q3 was then set to pass molecularly distinctive product ions. A multiple reaction monitoring (MRM) method was created by setting Q1 and Q3 to pass the precursor and product ions of the most abundant sphingolipid molecular species. For example, for Cer, these transitions occur at *m/z* 538.7/264.4, 566.5/264.4, 594.6/264.4, 622.7/ 264.4, 648.7/264.4, 650.7/264.4, which correspond to Cer with a d18:1 sphingoid base and 16:0, 18:0, 20:0, 22:0, 24:1, and 24:0 N-acyl chain, respectively. The dwell time was 25 ms for each transition. Quantitation was achieved by spiking the samples prior to extraction with the synthetic internal standards.

Prior to selecting MRM pairs for each cell type, the variation in fatty-acyl chain length was determined, which allowed MRM transitions to be tailored for the major N-acyl species. This was usually accomplished by precursor ion scans of *m/z* 184.4, the structure specific fragmentation indicative of SM. SM were chosen because they are typically abundant and are indicative of both sphingosine (So) and sphinganine (Sa) based species. For example, in HEK293 cells, the major SM species are 16:0, 18:0, and 24:1.

2.2.9 Measuring cell growth rate and doubling time

HEK293 and SPT1/2 cells were seeded at 4.4 x 10^5 / 100 mm-dish. Samples were duplicated for each treatment. Cell number was measured every 24 hours. Medium was

removed from the dish and cells were washed by 10 ml of PBS, trypsinized for 3 min at 37^{o}C and resuspended in 6 ml of complete medium. After centrifuge at 1.3 rpm for 5 min, the cell pellet was resuspended in complete medium and applied for cell counting by a hemocytometer. Cells entered exponential phase 24 hours after seeding. The cell growth line was drawn according to the time (x-axis) and the natural logarithm of cell number (y-axis). The cell doubling time (x) was derived from the following equations:

$N_{(t)}$: The number of cells at time t N_0: the number of cells at time 0 t: cell-growing time

$$N_{(t)} = N_0 \cdot 2^{t/x}$$

$$\ln N_{(t)} = \ln N_0 + t/x \cdot \ln 2$$

$$\ln N_{(t)} = (\ln 2 /x) \cdot t + \ln N_0$$

$$\ln 2/ x = \text{slope}$$

$$x = \ln 2 / \text{slope}$$

Thus, the cell doubling time can be calculated from the slope of the growth curve.

2.2.10 In vitro sphingomyelinase activity assay

The methods for nSMase assay and aSMase assay have been thoroughly described before (102) and the modified part is described as below. Cells were collected in the lysis buffer as described (102) plus protease inhibitor cocktail (Roche, Indianapolis, IN). For our experiment, instead of using radiolabeled SM as a substrate NBD fluorescence labeled SM (C6-NBD-SM) was used at 2 nmol per 100 µl reaction. Each reaction was triplicated and stopped by adding 1.4 ml of HPLC solvent which is composed of 90% methanol and 10% aqueous phase (5 mM K_2HPO_4). The sample was centrifuged at 2500 rpm for 8 min

and 1.2 ml of the supernatant was transferred to a glass HPLC sample tube. C6-NBD-SM and C6-NBD-Cer were diluted separately or together in the HPLC solvent as a standard. For each analysis 100 μl of each sample was injected into the HPLC machine and the isocratic flow rate of the solvent is 2 ml / min. BCA protein assay (Pierce, Rockford, IL) was used to determine the protein concentrations.

2.2.11 In situ sphingomyelinase activity assay

NBD-C6-SM was dissolved in ethanol to make 5mM solution. Fatty acid free BSA was dissolved in PBS to make 2mM stock solution. The two solutions were mixed at 1:1 molar ratio and sonicated. Then the NBD-C6-SM/BSA complex was diluted to 5 μM working solution in complete cell culture medium and filter sterilized. Twenty-four hours before the experiment cells were seeded in 60-mm dishes in complete growth medium. Just before treatment, the old medium was replaced with the medium containing NBD-C6-SM/BSA.

2.3 Results

2.3.1 Sphingolipid *de novo* synthesis pathway

The *de novo* synthesis of sphingolipid starts from condensation of serine and palmitoyl-CoA by SPT into 3-keto-Sa which is quickly reduced to Sa. Then Sa is acylated by a family of (dihydro)ceramide synthases (CerS) using different fatty acyl-CoAs to form the

corresponding DHCer subspecies (Fig 2.1). In mammals, six genes that encode CerS have been recently cloned (103-106). Individual ceramide synthase isoforms show substrate preference for specific chain length fatty acyl CoAs, thus generating distinct ceramides with distinct acyl-chain lengths. For example, CerS1 shows significant preference for stearyl-CoA (C18:0), whereas CerS5 and CerS6 preferentially catalyze the acylation of Sa with myristoyl- (C14:0) and palmitoyl- CoAs (C16:0) (103, 107). Then the different DHCer are reduced to the Cer by (dihydro)ceramide reductase (DES) and both DHCer and Cer are converted to complex sphingolipid (SM, DHSM, CMH, DHCMH) by adding different head groups.

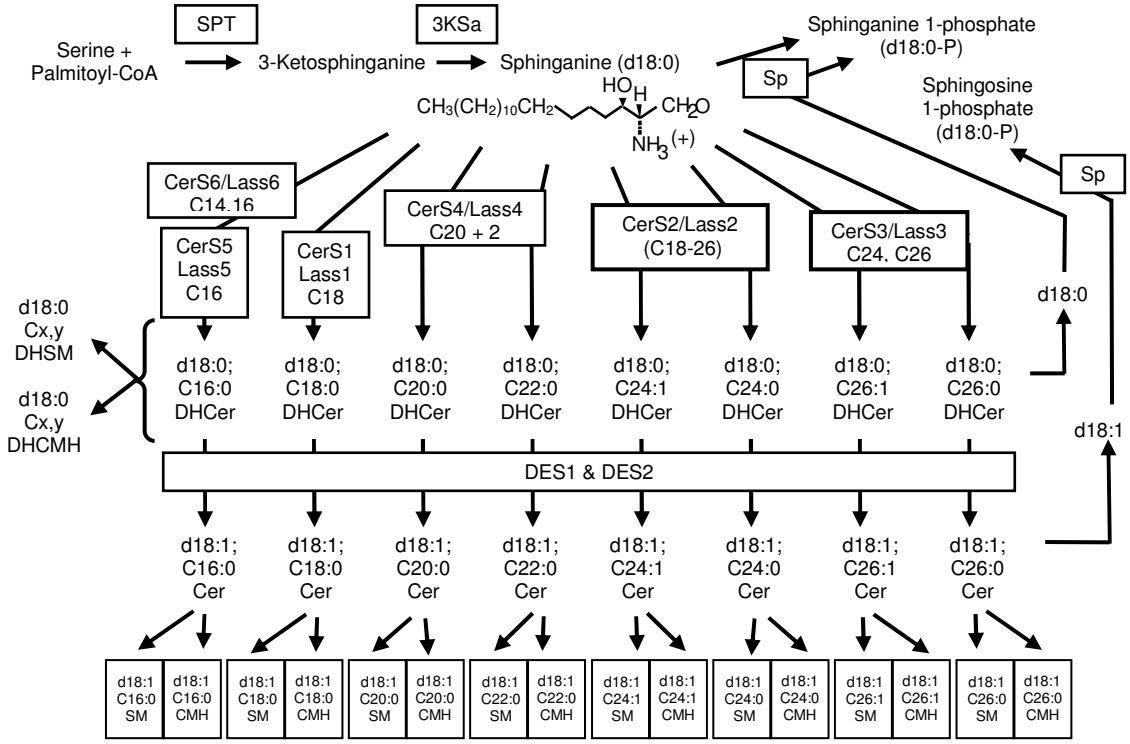

Fig 2.1. Diagram of sphingolipid *de novo* biosynthesis pathway. D18:0 stands for sphingoid base backbone with 18-carbon chain and 0 unsaturated bond. C16:0 stands for fatty acyl side chain with 16 carbons and 0 unsaturated bond.

2.3.2 Generation of functional HEK293/*SPTLC1*/*SPTLC2* stable cell line

Since SPT is the first as well as the key enzyme in the *de novo* synthesis it is interesting to know the impact of increasing SPT activity on the pathway. To explore this issue a SPT overexpression cell model was constructed. The *SPTLC1* and *SPTLC2* cDNA were cloned from human monocytes and inserted into pcDNA3.1NEO and pcDNA3.1ZEO separately. The expression plasmids were transfected separately or co-transfected into HEK 293 cells. Antibiotic selection was used to generate cells stably expressing *SPTLC1* or *SPTLC2* or *SPTLC1/SPTLC2*. For convenience we call these cells SPT1, SPT2 and SPT1/2 cells separately. Using quantitative real-time PCR analysis the significant elevation of *SPTLC1* and/or *SPTLC2* mRNA were detected in these cell lines (data not shown). When total cell lysate was applied for SDS-PAGE followed by Western blotting using anti-SPT1 or anti-SPT2 antibody the protein amount of SPT1 and/or SPT2 increased significantly in the stable transfected cells comparing with wild type as well as empty vector transfected HEK293 cells (Fig. 2.2).

The above results showed that overexpression of SPT1 and SPT2 was successful and then the next question was if the overexpressed proteins were functional. Previous studies showed that SPT activity was mainly from the microsome fraction (108). Microsome fractions were isolated from the same set of cells as those used for Western blotting for *in vitro* SPT enzyme activity assay. There was no significant change of SPT activity in SPT1 stable cells while a 3.5-fold SPT activity change was observed in SPT2 stable cells which is consistent with the previous finding that SPT2 is the catalytically active subunit

of the SPT enzyme (23) (Fig. 2.2). Co-expression of *SPTLC1* and *SPTLC2* caused SPT activity to increase 5-fold suggesting a synergistic effect of the two subunits, (18). The high SPT activity made the SPT1/2 stable cells a useful model in studying sphingolipid *de novo* synthesis and it is interesting to know the molecular consequences of it.

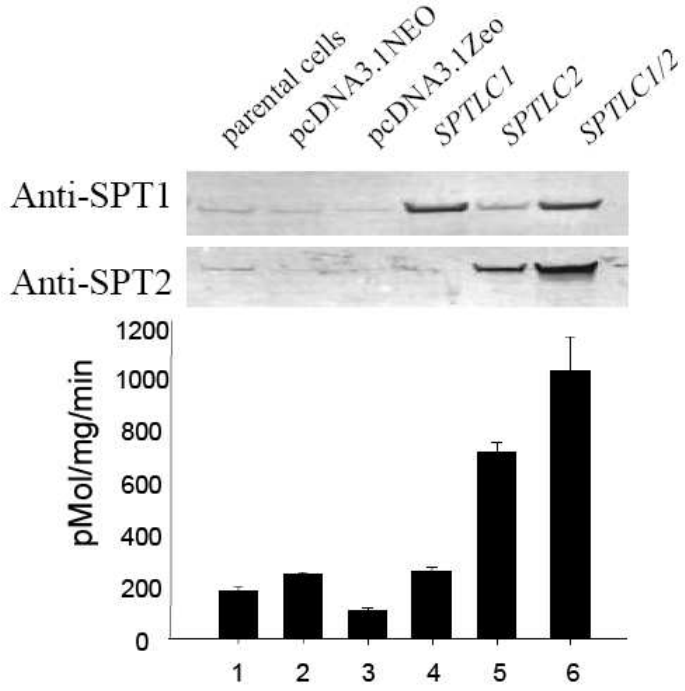

Fig. 2.2 Characterization of *SPTLC* transfected cell lines.
50 µg of microsomal membrane protein from untransfected HEK293 cells (Lane 1), cells tranfected with vector controls (pcDNA31.NEO, lane 2 and pcDNA3.1Zeo lane 3), *SPTLC1* transfected cells (Lane 4), *SPTLC2* tranfected cells (Lane 5), or cells co-transfected with *SPTLC1* and *SPTLC2* (lane 6) was applied for Western blotting (upper two panels) and SPT enzyme activity assay (lower bar graph). The nitrocellulose membrane was probed with either anti-SPT1 antibodies (upper panel) or anti-SPT2 antibodies (lower panel). The enzyme activity assay data represent the mean of three independent experiments.

2.3.3 An *in situ* SPT activity assay was developed using stable isotope labeling and LC ESI-MS/MS

To explore the *de novo* synthesis change inside the cells an in situ assay using stable isotope labeling was developed. Uniformly [^{13}C] labeled palmitate was used as a tracer to follow the synthesis of sphingolipids. After taken up by a cell it can be converted to [^{13}C]-palmitoyl CoA which is condensed with serine by SPT to form the sphingolipid base backbone (3-ketoSa and Sa). [^{13}C]-palmitoyl CoA can also be used to acylate a base backbone by (dihydro)ceramide synthase to form DHCer. If a sphingolipid molecule is labeled only at the base backbone we call it base labeling. If it is labeled only at fatty acyl chain we call it fatty acid labeling. If it is labeled at both the backbone and the fatty acyl chain we call it dual labeling. Using tandem MS the different labelings can be differentiated. Only the dual labeling and base labeling are considered from *de novo* because they are synthesized directly from serine and [^{13}C]-palmitate by SPT while the fatty acid labeling may not be generated from that because the unlabeled base backbone may come from broken down of complex sphingolipids. The details of this method are described in "methods".

2.3.4 The dynamics of *de novo* synthesis of sphingoid bases in SPT1/2 cells versus HEK293 cells

Both SPT1/2 cells and HEK293 cells were treated with [^{13}C]-palmitate and collected every hour for 6 h. Then lipids were extracted from the cell pellets, went through a reverse phase C18 column and then analyzed by ESI MS/MS. The first product in the sphingolipid *de novo* synthesis pathway is 3-ketosphinganine produced by SPT but its amount is below the detection limit for both cell lines, which is consistent with previous

studies that it is rapidly reduced to Sa and there is no accumulation of it inside the cells. Both [^{13}C] labeled and [^{12}C] Sa (unlabeled) were rapidly accumulated in SPT1/2 cells, reached their peaks at about the same level after 2 h of [^{13}C]-palmitate treatment and then both dropped down and leveled off (Fig. 2.3 up left panel). While in HEK293 cells [^{13}C] Sa was under the detection limit and [^{12}C] Sa was lower than that in SPT1/2 cells. Furthermore, both labeled and unlabeled Sa did not show any increase after [^{13}C]-palmitate treatment (Fig. 2.3 up left). However, due to the fact that the downstream products of Sa increased in HEK293 cells after [^{13}C]-palmitate treatment (Fig. 2.4) the absence of Sa increase in these cells may be caused by fast conversion of Sa to complex sphingolipids.

Sa can be converted to either dihydroceramide (DHCer) by dihydroceramide synthase or phosphorylated by sphingosine kinase to form Sa1P. Sa1P was not detectable in HEK293 cells but significantly increased overtime in SPT1/2 cells (Fig. 2.3 up right). Another abundant sphingoid base backbone is So which is more abundant than Sa in both HEK293 cells and SPT1/2 cells at any time point measured. Like Sa, the amount of [^{13}C] labeled or unlabeled So was much higher in SPT1/2 cells than in HEK293 cells (Fig. 2.3 bottom left). However, the dynamic pattern of this sphingoid base is quite different from that of Sa. The unlabeled So was at least 4 fold higher than the labeled form in SPT1/2 cells during the first 6 h of [^{13}C]-palmitate treatment. There was no increase of either labeled or unlabeled So in SPT1/2 cells during the first hour of [^{13}C]-palmitate treatment. Similar observation was seen for its phosphorylated product, S1P (Fig. 2.3 bottom right). These observations are consistent with the fact that So is derived exclusively from the

turnover of GSL, SM or Cer and, unlike Sa, cannot be generated through *de novo* synthesis. S1P in turn is also a product of sphingolipid breakdown. Thus unlike [^{13}C]-labeled Sa and Sa1P [^{13}C]-labeled So and S1P are affected much less by the overexpression of SPT and do not represent the dynamics of *de novo* synthesis.

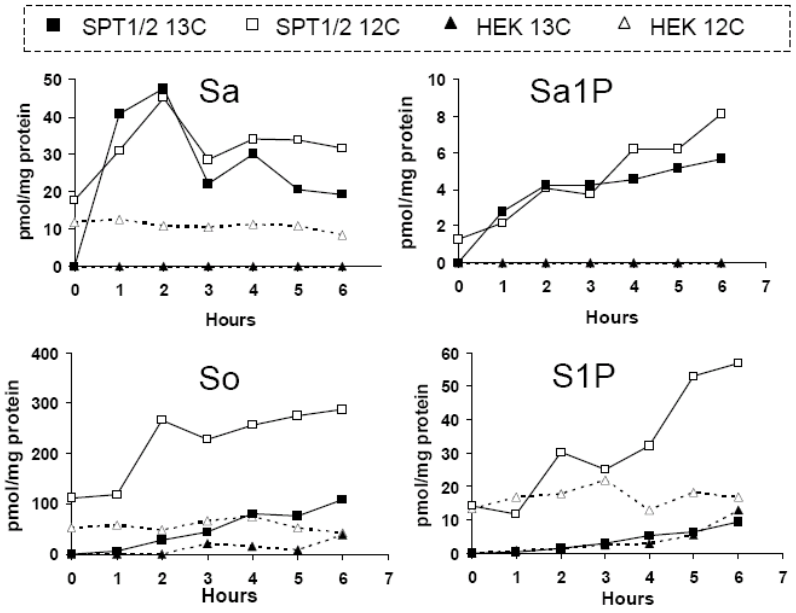

Fig. 2.3 The dynamics of sphingoid bases in HEK293 cells and SPT1/2 cells after [^{13}C]-Palmitate treatment. Lipids were extracted from HEK293 cells and SPT1/2 cells treated with 0.1 mM ^{13}C-Pal for different periods of time (0~6 h) and analyzed for sphingoid bases by ESI-MS/MS. Both labeled (^{13}C) and unlabeled (^{12}C) sphinganine (Sa, up left), sphinganine-1-phosphate (Sa1P, up right), sphingosine (So, bottom left) and sphingosine-1-phosphate (S1P, bottom right) were measured.

2.3.5 The dynamics of *de novo* synthesis of complex sphingolipids in SPT1/2 cells versus HEK293 cells

To quantify *de novo* synthesized complex sphingolipids, the sum of dual labeling and base labeling was used, which represents majority of the *de novo* synthesis. The first

complex sphingolipid along the biosynthesis pathway is dihydroceramide (DHCer) which is formed by acylation of Sa backbone by (dihydro)ceramide synthase. [^{13}C] labeled DHCer in SPT1/2 cells rapidly increased during the first 2 h with [^{13}C]-palmitate treatment, leveled off from 2 to 4 h and then dropped down about 25% (Fig. 2.4A). While in HEK 293 cells it increased slowly overtime and to a much less extent during the first 6 h after [^{13}C]-palmitate treatment (Fig. 2.4A). Two hours after treatment, DHCer in SPT1/2 cells is 40 fold higher than that in HEK293 cells. DHCer can be reduced to Cer or converted to more complex sphingolipids such as DHCMH and DHSM. Both DHCMH and DHSM were significantly increased overtime in a very similar pattern in SPT1/2 cells and the increase in HEK 293 cells is 3~5 fold less (Fig. 2.4B, 2.4C).

The *de novo* synthesis of Cer was increased in a similar pattern as those of DHCer in SPT1/2 cells and in HEK 293 cells (Fig. 2.4D). An increase of [^{13}C]-labeled CMH over time was observed in both cell lines after treatment and was progressively faster in SPT1/2 cells than in HEK293 cells with a 2 to 5 fold increase from 3 h to 6 h(Fig. 2.4E). SM *de novo* synthesis was also increased over time in both cell lines, however, to our surprise, unlike other sphingolipids its synthesis rate was higher in HEK293 cells than that in the SPT1/2 stable cells (Fig. 2.4F). A further investigation on this phenomenon will be described below.

Thus by comparing SPT1/2 cells with HEK293 cells, after 3 h of [^{13}C]-palmitate treatment, among all the *de novo* synthesized complex sphingolipids the most significant elevation was seen in DHSM (58 fold), DHCer (25 fold) and a less elevation was seen in

DHCMH (6 fold), Cer(5.6 fold) and CMH (2 fold) while a decrease was seen in SM. A time dependent increase followed by a decrease was seen in DHCer and Cer in SPT1/2 cells after 4 h of treatment while other species continuously elevated over time. As Sa started dropping down as early as 2 hours after treatment (Fig. 2.3) these data together suggest that either substrate depletion or feedback inhibition happened through the pathway.

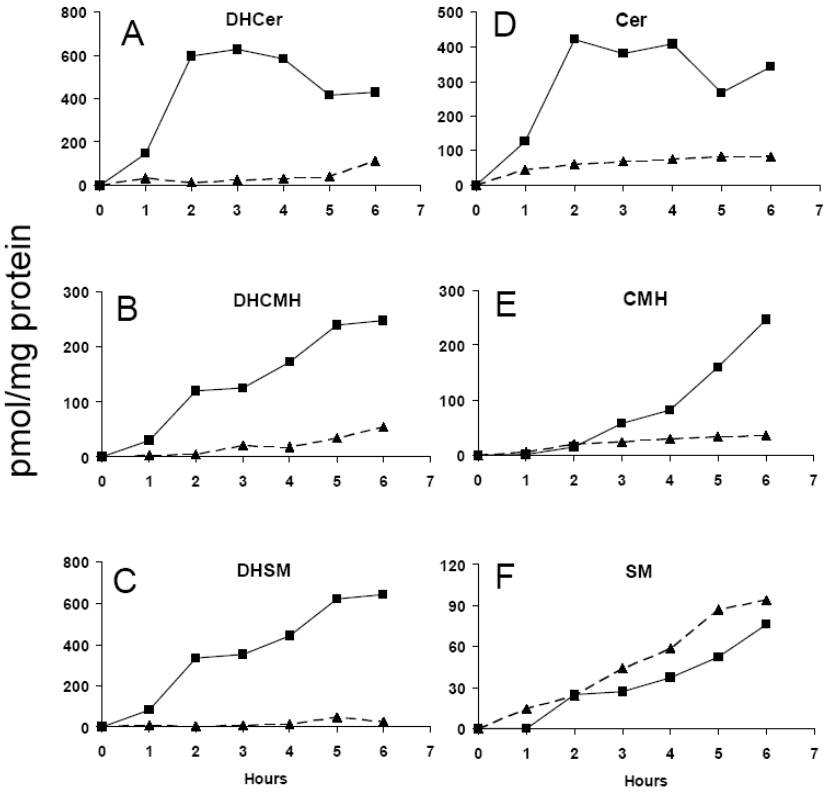

Fig. 2.4 The dynamics of *de novo* synthesis of complex sphingolipid in HEK293 cells and SPT1/2 cells after ^{13}C-palmitate treatment
HEK293 cells (dashed line) and SPT1/2 cells (solid line) were treated with 0.1 mM ^{13}C-palmitate for various periods of time. Lipid extractions from those cells were applied for LC-MS/MS analysis of DHCer (A), DHCMH (B), DHSM (C), Cer (D), CMH (E) and SM (F). At each time point the quantified number for each complex sphingolipid is a sum of the total ^{13}C dual labeled subspecies and the total ^{13}C base labeled subspecies.

In HEK293 cells *de novo* synthesized sphingolipid is higher than its corresponding dihydro-species while it is the opposite in SPT1/2 cells when the dual and base labeled DHCer and Cer (after 3 h of treatment) are compared in the two types of cells (Fig. 2.5). This observation is consistent with the above Sa data that [^{13}C]-Sa is highly elevated in SPT1/2 cells but not HEK293 cells (Fig. 2.3). Together these results show that overexpression of SPT in SPT1/2 cells caused a flux of downstream molecules which exceeded the capabilities of the downstream enzymes. For example, the *de novo* synthesized Sa exceeded the capacity of (dihydro)ceramide synthase and DHCer exceeded the capacity of (dihydro)ceramide desaturase.

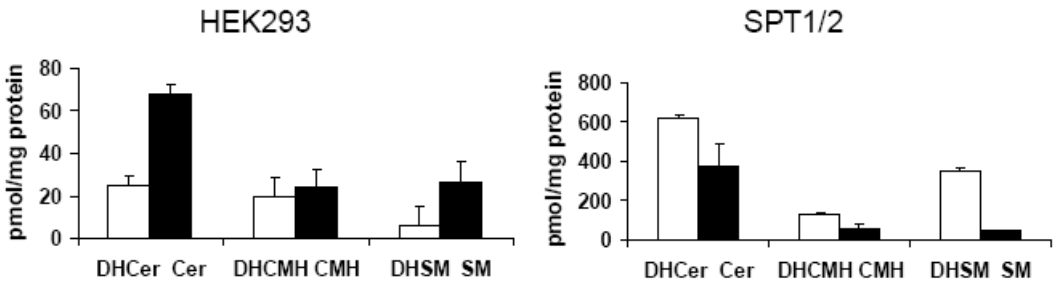

Fig. 2.5 *De novo* synthesized dihydro-sphingolipids and their desaturated species are compared in HEK293 cells and SPT1/2 cells.
Each species was quantified by a sum of ^{13}C dual and ^{13}C base labeling after 3 hours of ^{13}C-palmitate treatment using LC-MS/MS analysis.

2.3.6 The distribution of *de novo* synthesized sphingolipids with varying acyl-chain lengths in SPT1/2 cells versus HEK293 cells

Most sphingolipids are built upon So or Sa backbone and can have various lengths of fatty acyl-chains. C16, C18, C20, C22, C24, C24:1, C26 and C26:1 are the most common

fatty acids that have been found to be incorporated into the sphingoid base backbone. These different subspecies of sphingolipids are first generated by acylation of Sa or So using different ceramide synthases (CerS) which prefer certain types of fatty acyl-CoA (103-106). For example, CerS1 prefers stearyl-CoA (C18) and CerS5/6 prefers palmitoyl-CoA (C16) (Fig. 2.1). To compare the sphingolipid subspecies with varying fatty acyl chain lengths the sum of dual labeling and base labeling was used. Majority of [^{13}C] labeled subspecies of each complex sphingolipid with different fatty acyl chain lengths were increased in SPT1/2 cells while those of SM decreased comparing with HEK293 cells (Fig. 2.6). The chain length distribution for each kind of sphingolipid is similar between SPT1/2 cells and HEK293 cells.

Among all the subspecies of DHCer, Cer, DHSM and SM, those with C16 fatty acyl-chain (palmitate) are the most abundant in both HEK293 cells and SPT1/2 cells (Fig. 2.6). The subspecies component of DHCMH and CMH is different from that of other complex sphingolipids and C16 subspecies is not the dominant species in both cell lines (Fig. 2.6 middle panel). Comparing the subspecies increases between HEK293 cells and SPT cells the elevation of C18 subspecies is higher than others (Fig. 2.6). Examination of fatty acyl-CoA showed that the amounts of labeled and unlabeled C18 acyl-CoA were comparable in both cells (data not shown). We also found that the Lass1 gene which encodes CerS1 was increased in SPT1/2 cells by quantitative PCR analysis (data not shown) suggesting that elevation of SPT activity may affect the gene expression of downstream enzymes.

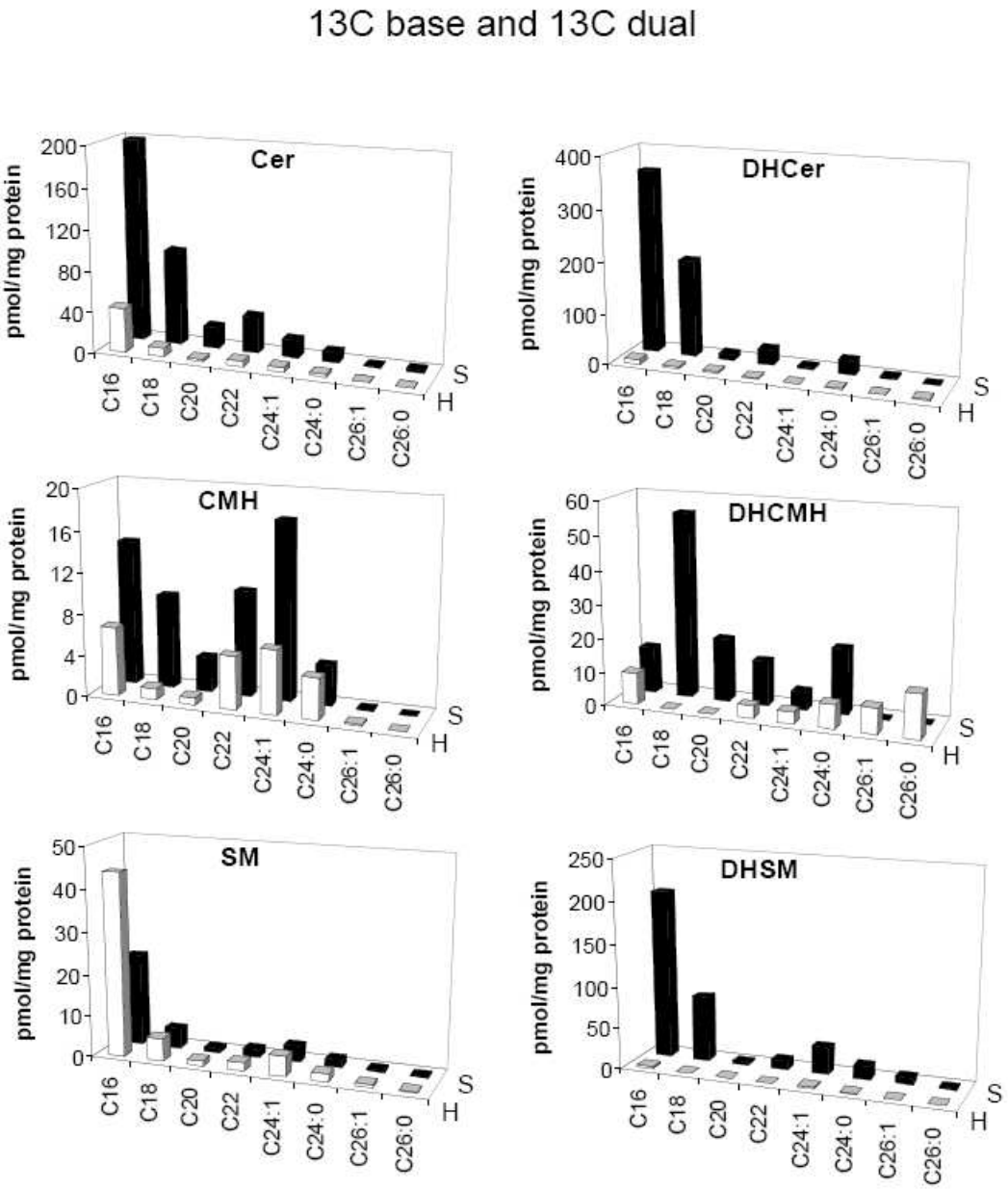

Fig. 2.6 Comparison of *de novo* sphingolipids with different fatty acyl chains in HEK293 cells and SPT1/2 cells.
Lipids were extracted from HEK293 cells (white bars) and SPT1/2 cells (black bars) treated with 0.1 mM ^{13}C-Pal for 3 h and analyzed by ESI-MS/MS. The number showed in the figure is a sum of ^{13}C dual label and ^{13}C base label, which represents the *de novo* synthesis. The x axis is the fatty acyl chain lengths and from the left to the right are C16, C18, C20, C22, C24:1, C24, C26:1, C26.

2.3.7 Elevation of novel sphingolipid species in SPT1/2 cells

SPT prefers serine as its substrate, however, recently sphingoid bases generated from alanine and glycine were also identified in mammalian cells and they are quite abundant in cells treated with Fumonisin B1, a ceramide synthase inhibitor (43). Condensation of alanine and palmitoyl-CoA by SPT generates 1-deoxy sphinganine (1-deoxySa) and its N-acylated form is 1-deoxy dihydroceramide (1-deoxy-DHCer). Condensation of glycine and palmitoyl-CoA produces 1-desoxymethyl sphinganine (1-desoxMeSa) and its N-acylated form is 1-desoxMe-DHCer. Using [^{13}C]-palmitate method we found 1-deoxy-Sa was dramatically elevated in SPT1/2 cells comparing with HEK293 cells (Fig. 2.7A). Among the [^{13}C] labeled sphingoid bases 1-deoxySa was lower than So but much higher than other species. While, in HEK293 cells, 1-deoxySa was at the same level as all other species except for So (Fig. 2.7A). Both the [^{13}C] base labeling and dual labeling showed that 1-deoxy-DHCer and 1-desoxMe-DHCer were significantly increased in SPT1/2 cells comparing with HEK293 cells (Fig. 2.7B). It was very impressive that the amount of 1-deoxy-DHCer was comparable to that of Cer in SPT1/2 cells. Unlike DHCer which has C16 acyl-chain as its dominant subspecies, for 1-deoxy-DHCer and 1-desoxMe-DHCer C18 subspecies was the most abundant.

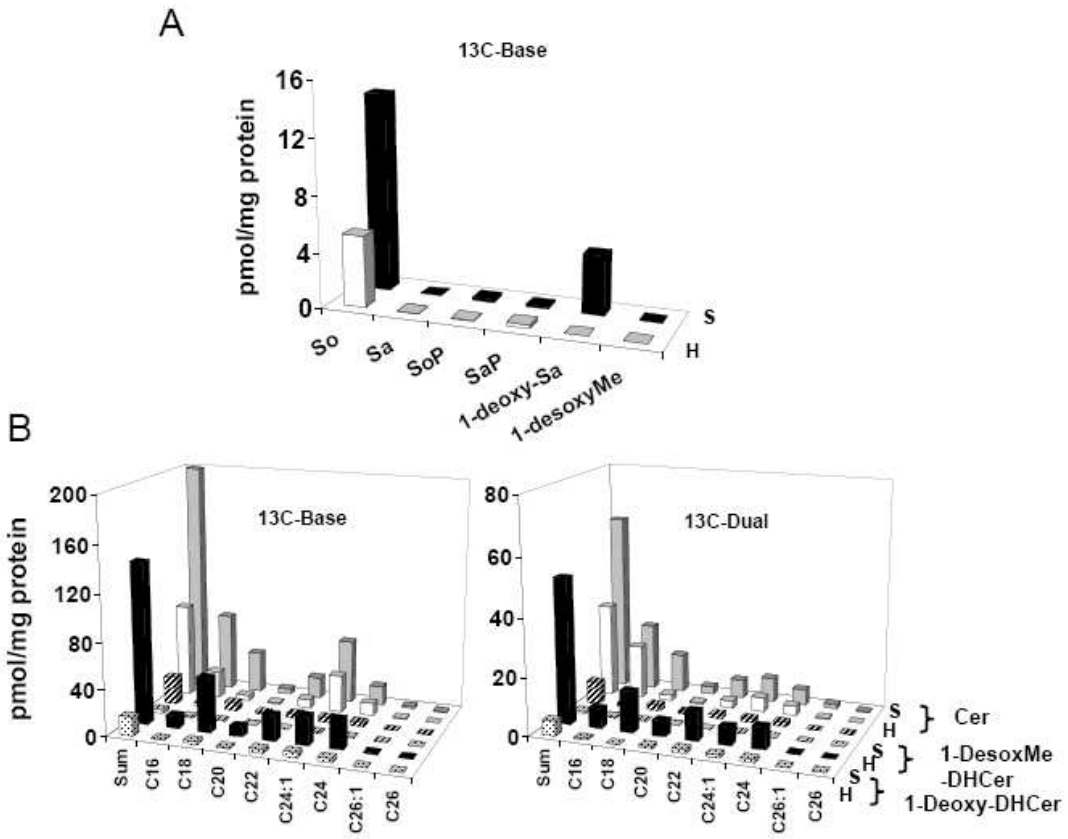

Fig. 2.7 Quantification of novel sphingolipid species after ^{13}C-pamitate labeling. A. 13C labeled sphingoid bases were measured in HEK293 cells (H, white bars) and SPT1/2 cells (S, black bars). B. Quantification of N-acylated forms of the novel sphingoid bases. 1-deoxy-DHCer and 1-desoxMe-DHCer with different chain lengths were measured in HEK293 cells and SPT1/2 cells and compared with Cer. From the left to the right are the sum of all subspecies, C16, C18, C20, C22, C24:1, C24, C26:1, C26. The left panel is ^{13}C-base labeling and the right panel is ^{13}C-dual labeling.

2.3.8 The sphingolipid change at the steady state of SPT1/2 cells vs. HEK293 cells

The above data showed the *de novo* synthesis change of sphingolipids in SPT1/2 cells versus HEK293 cells. To explore the effect of SPT overexpression in the steady state the

SPT1/2 cells without any treatment (0 hour) were analyzed (Fig. 2.8A). Quantification of all the unlabeled sphingolipids species showed that they increased in SPT1/2 cells except for SM and DHSM and the greatest increase was seen in Cer and DHCer. Comparing with the *de novo* synthesized sphingolipids data (Fig. 2.4, 2.5) the elevation of sphingolipids in the steady state of SPT1/2 cells was much less and even reversed such as DHSM. The amount of SM was much lower in SPT1/2 cells.

The proportions of complex sphingolipids were compared in HEK293cells and SPT1/2 cells (Fig. 2.8B). From the most abundant to the least abundant species for HEK293 cells they are SM (65%), CMH (17%), DHSM (8%), Cer (6%), DHCer (3%) and DHCMH (1%) while those for SPT1/2 cells are SM (34%), Cer (28%), CMH (20%), DHCer (11%), DHSM (5%), DHCMH (2%). The proportion of Cer and DHCer dramatically increased in SPT1/2 cells while that of SM went down. Therefore, elevation of SPT activity not only increased the absolute value of sphingolipids but also changed the cellular component of the sphingolipids.

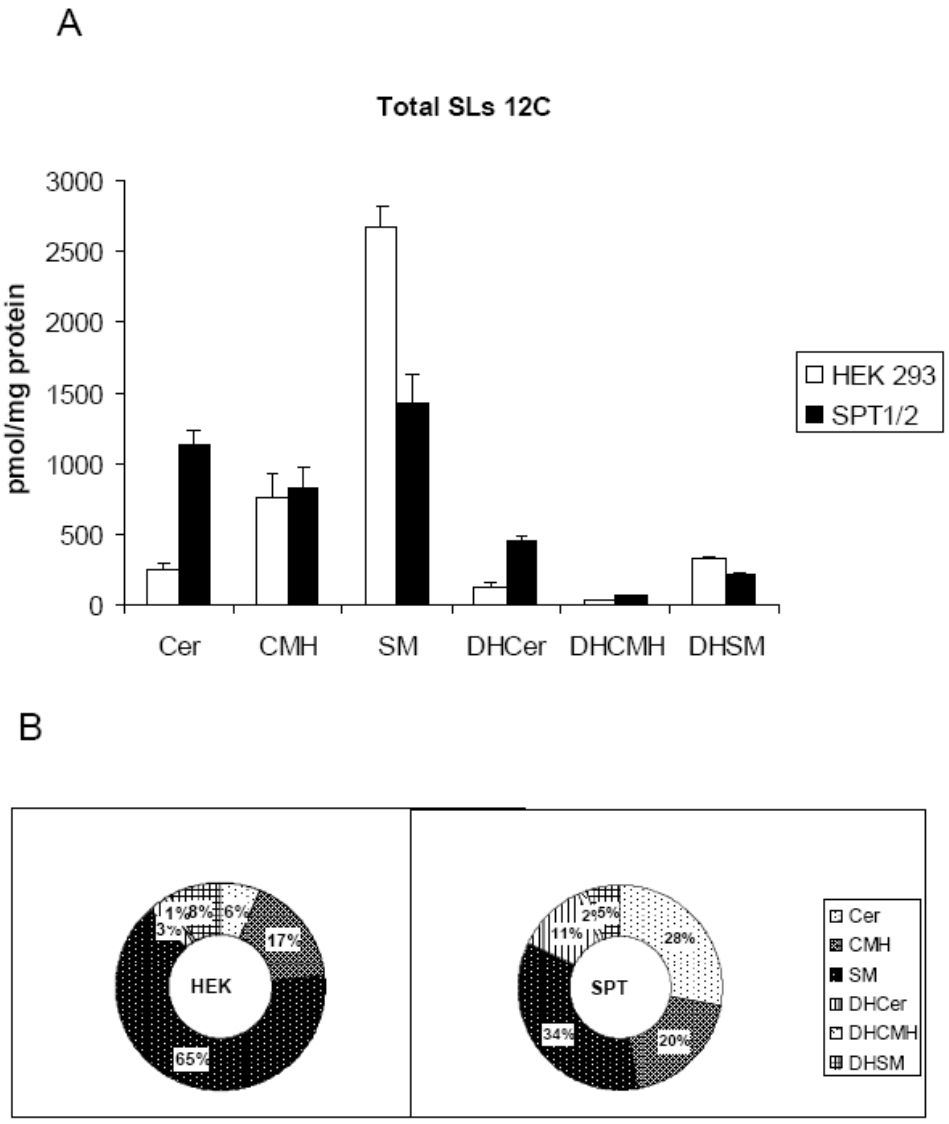

Fig. 2.8 Comparison of sphingolipid components in HEK293 cells and SPT1/2 cells without [^{13}C]-palmitate treatment.
Total amount of each complex sphingolipid was quantified in HEK293 cells (white bars) and SPT1/2 cells (black bars) without treatment (A). The distribution of sphingolipid species was compared in HEK293 cells and SPT1/2 cells without treatment (B).

2.3.9 The fast growth rate of SPT1/2 cells is partially due to SPT overexpression

Overexpression of *SPTLC* genes caused an elevation of lethal Cer which has been found to induce cell cycle arrest and apoptosis (3), however, the cells did not die and grow even faster than the untransfected HEK293 cells. The cell doubling time of SPT1/2 cells and HEK293 cells was measured as described in the methods part and it is 14.9 hours for SPT1/2 cells and 22.3 hours for HEK293 cells. Since SPT1/2 cells were generated through antibiotic selection it is not clear if the fast growth rate is due to SPT overexpression or to the selection force. To answer this question, the growth rate was measured when the excess SPT activity was inhibited by a SPT specific inhibitor, ISP-1. ISP-1 was used at 0.1 μM at which the SPT activity in SPT1/2 cells was decreased to the same level as that in HEK293 cells as measured by LC-MS/MS described in chapter 2. SPT1/2 cells and HEK293 cells were seeded at very low density in complete growth medium. Cell numbers were counted everyday for 3 days and growth curves were drawn from 24 hours to 72 hours when the growth of the cells entered exponential phase (Fig 2.9). ISP-1 treatment slowed down the growth of SPT1/2 cells. The growth rate of the treated SPT1/2 cells is between that of untreated SPT1/2 and HEK293 cells with a cell doubling time of 18.6 hours, which suggests that the fast growth rate of SPT1/2 cells is partially due to the overexpression of SPT.

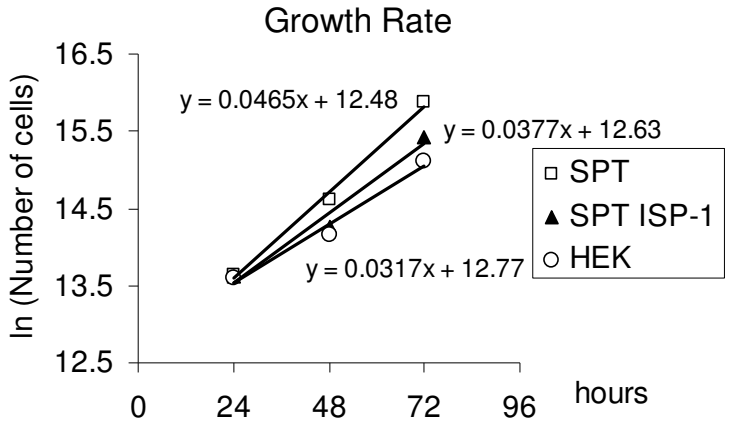

Fig. 2.9 Growth curves for HEK293 cells, SPT1/2 cells and SPT1/2 cells treated with 0.1 μM ISP-1.
Cells were seeded at low density in 100 mm-dishes and a group of SPT1/2 cells were treated with 0.1 μM ISP-1. Cell numbers were counted everyday and growth medium was replaced for the remaining cells. Fresh ISP-1 was added to the treated cells in the fresh medium everyday. Growth rates of HEK293 cells (circle), SPT1/2 cells (square) and SPT1/2 cells were plotted against cell growing hours and natural logrithm of the number of cell.

2.3.10 An open question for the decrease of SM in SPT1/2 cells

An interesting phenomenon about SPT1/2 cells is that unlike other sphingolipid species the amount of [^{13}C] labeled SM is lower than that in HEK293 cells. On the dynamic chart (Fig. 2.4) [^{13}C]-SM is lower in SPT1/2 cells throughout all the 6 hours. Is this because that the sphingomyelinase activity is higher in SPT1/2 cells? To answer this question the activity of both acidic and neutral SMase was measured *in vitro* for HEK293 and SPT1/2 cells. NBD fluorescent-labeled SM was used as a substrate and after reaction the samples were analyzed by HPLC. As shown in figure 8, the aSMase activity is slightly but significantly higher in SPT1/2 cells than in HEK293 cells while the activity of nSMase in SPT1/2 cells is only about 50% of that in HEK293 cells (Fig. 2.10).

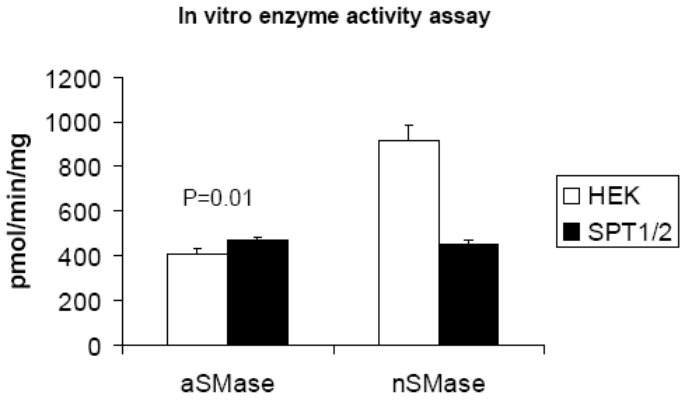

Fig. 2.10 Comparison of sphingomyelinase activity in HEK293 cells and SPT1/2 cells.
Enzyme activities of acidic sphingomyelinase and neutral sphingomelinase were measured in vitro using cell lysates of HEK293 cells and SPT1/2 cells. C6-NBD-SM was used as a substrate and after reaction the product was analyzed by HPLC. The data represents the mean of two independent experiments.

It seems that the *in vitro* degradation of SM is faster in SPT1/2 cells than in HEK293 cells. To confirm this result *in vivo* both HEK293 cells and SPT1/2 cells were incubated in medium containing C6-NBD-SM for 7 hours and then the cells were collected and extracted in methanol at 37^{o}C for one hour. After centrifugation the supernatant was applied for HPLC analysis. All the NBD fluorescent signals were measured, normalized by protein amount and the percentage of SM signal over total NBD signal was calculated. The remaining SM was 8% in HEK293 cells and 15% in SPT1/2 cells after 7 hours of NBD-SM treatment, which is consistent with the *in vitro* assay result and suggests that SM degradation is faster in HEK293 cells than in SPT1/2 cells. The decrease of SM in SPT1/2 cells is not clear and will be discussed below.

2.4 Discussion

Previously overexpression of SPT has been done in mammalian cells (18, 23) however the impact of it on the *de novo* pathway has not been fully investigated. We used a *SPTLC1/SPTLC2* overexpression cell model (SPT1/2 cells) to study the impact of SPT on the *de novo* sphingolipid synthesis. Our study showed changes of downstream molecules at each step. Overexpressing SPT activity increased the flux through the pathway and the elevation of up stream molecules exceeded the capacity of the down stream enzymes, which caused the flux slowing down gradually through the pathway. Futhermore, sphingolipid subspecies with different fatty acyl chain lengthes were measured and significant elevations were seen in SPT1/2 cells compared with HEK293 cells. The higher fold elevation of C18 subspecies and evidence of CerS1 mRNA increase in SPT1/2 cells (Ying Liu, unpublished data) suggest that CerS1 may be regulated by SPT and contribute more in the *de novo* synthesis than other ceramide synthases.

In the past, studies have focused on So, Cer and their derivatives which were potent bioactive lipids involved in cell growth, death, senescence, adhesion, migration, inflammation, angiogenesis and intracellular trafficking (3, 109, 110). Recently, Sa, dihydro-sphingolipids and their derivatives which usually exist at a very low level inside the cells have been found to be bioactive (92, 93, 111). *De novo* synthesized sphinganine and dihydro sphingolipids have been found to play a role in 4HPR induced cancer cell apoptosis (92). *De novo* generated Sa and DHCer were increased in celecoxib, a COX-2 specific inhibitor, treated tumor cells and may contribute to the anti-proliferative effects of celecoxib (93). L-threo-sphinganine, a synthetic stereoisomer, induces autophagy in solid tumor cells (111). So far few studies have analyzed those species, furthermore,

traditional thin layer chromatography method cannot differentiate dihydro-species with the desaturated species, which might have masked the effect of dihydro-species in some studies.

Some novel *de novo* synthesized sphingolipids, such as 1-deoxySa which only exist at a low level in certain mammalian cells, were also identified in [^{13}C]-pamitate treated SPT1/2 cells and surprisingly the amount of 1-deoxyDHCer was comparable to Cer. These observations suggest that the highly expressed SPT and the exogenous [^{13}C]-palmitate might cause a fast consumption of the introcellular serine and thus alanine and glycine which have structural similarity to serine were used as a substrate. Recently it was reported that 1-deoxySa (spisulosine) isolated in sea *mollusc Spisula polynyma* induced prostate tumor cell death by *de novo* synthesis of Cer (112). Our result suggests that mammalian SPT can generate 1-deoxySa under certain circumstances. It would be interesting to know what the targets of the novel compound are.

The *de novo* synthesis of all other sphingolipids increased in SPT1/2 cells while that of SM decreased. This is not caused by elevated degradation of SM as seen in the above data or by impairment in SM synthesis because the synthesis of DHSM which uses the same SM synthase is dramatically increased in SPT1/2 cells (Fig. 5C, 6). We noticed that the ratio of DHCer to Cer is higher in SPT1/2 cells than that in HEK293 cells after palmitate treatment. Since the DHCer and Cer share the same transporter, CERT, from ER to Golgi (113, 114) is it possible that DHCer and Cer might compete for the binding site of CERT? One might argue that CMH and DHCMH (mainly GlcCer) are also

synthesized in Golgi and why they do not compete for each other. This is probably caused by a different transportation mechanism which is not clear yet and might involve vesicle transportation (115).

It is interesting that SPT1/2 cells did not show any cytotoxicity with the accumulation of cytotoxic sphingolipid molecules as Cer. The cells grow fast and show a morphology change comparing with the HEK293 cells. No toxicity was observed in SPT1/2 cells even after 36 hours of [^{13}C]-palmitate treatment. How the SPT1/2 cells handle the large amount of sphingolipids is still an interesting question.

2.5 Conclusions

Overexpression of *SPTLC1* and *SPTLC2* in HEK293 cells (SPT1/2 cells) elevated SPT enzyme activity.

The dynamics of *de novo* synthesis of sphingolipids was measured in both HEK293 cells and SPT1/2 cells after cells were treated with [^{13}C]-palmitate.

The *de novo* synthesized sphinglipids were increased more rapidly and significantly in SPT1/2 cells than in HEK293 cells except for SM.

Sphingolipid subspecies with different fatty acyl-chains were compared in the two cell types and C18 subspecies were elevated more than other subspecies in SPT1/2 cells.

The amount of each dihydro-species was lower than that of its desaturated form in HEK293 cells but higher in SPT1/2 cells.

The slow increase of SM in SPT1/2 cells is not caused by increased SM degradation and might relate to the substrate pool change.

SPT used not only serine but also alanine and glycine as its substrate to synthesize novel sphingolipid species *in vivo*.

Overexpression of SPT caused accumulation of cytotoxic sphingolipids but the cells did not die and instead they grow faster.

CHAPTER 3

SPT1 is present in ER, nucleus and focal adhesions, and functions in cell morphology

3.1 Introduction

Sphingolipids are a complex family of compounds that play important roles in membrane structure, biological recognition, cell adhesion, and cell regulation as participants in signaling, membrane trafficking, autophagy and other processes (3-5, 13, 109). In some cases, complex sphingolipids (glycosphingolipids and sphingomyelins) affect cell behavior by associating with membrane microdomains that contain receptors, transporters, and other signal transducers such as Src family kinases, small G-proteins (e.g., RhoA, Ras), and focal adhesion kinase (13). In other cases, the lipid backbones and related metabolites (e.g., ceramide, ceramide 1-phosphate, sphingosine 1-phosphate, and sphingosine) serve as first and second messengers (3, 109, 110) for behaviors such as cell migration and the associated actin stress fiber formation and focal adhesion formation (116-118). These are often orchestrated by changes in the membrane dynamics of the pertinent sphingolipids as well as their trafficking, metabolic remodeling and *de novo* sphingolipid biosynthesis (3).

Sphingolipid biosynthesis is initiated by condensation of L-serine with palmitoyl-CoA by SPT. In mammalian cells, SPT is thought to be a membrane bound heterodimer

comprised of two subunits, SPT1 and SPT2, with molecular weights of 53 kDa and 63 kDa, respectively (17, 18), but in some cells, an additional subunit, SPT3, has also been noted (19). SPT is often described as an enzyme of the endoplasmic reticulum (ER) because enzymatic activity has been found primarily in microsomes (31, 108), and hemaglutinin (HA)-tagged SPT1 has been localized to the ER when expressed in Chinese hamster ovary cells (18). Nonetheless, immunohistochemical analyses of different tissues and cells using the antibodies for SPT1 have found cross-reacting species in not only the cytoplasm (i.e., ER at this resolution) but also the nucleus (98, 119) and focal adhesions (120). Furthermore, a recent study (121) has detected an interaction of SPT1 with ABCA1.

This study establishes that SPT1 is, indeed, found in these surprising locations using siRNA suppression of SPT to confirm the specificity of the antibody staining, which also results in cell rounding and detachment. SPT1 is not only colocalized with vinculin by immunofluorescence staining but also coimmunoprecipitated with vinculin in HEK293 cells. The localization of SPT1 with focal adhesions is seen in growing but not confluent cells in culture, and reappears when cell migration is induced by a scratch-wound healing assay. Thus, these studies have found that SPT1 has cell functions beyond its already known catalysis of the first step of *de novo* sphingolipid biosynthesis in the endoplasmic reticulum.

3.2 Materials and methods

3.2.1 Materials

The affinity purified polyclonal rabbit anti-human primary antibodies raised against SPT1 peptides have been previously described (98). Anti-BiP antibody was from StressGen, Inc. (Victoria, BC, Canada). Anti-vinculin antibody was from Sigma Aldrich (Saint Louis, MO) and anti-ABCA1 antibody was from Novus Biologicals. The secondary antibodies were Alexa Fluor-conjugated goat anti-rabbit and anti-mouse obtained from Molecular Probes, Inc. (Eugene, OR). The nucleic acid dye Hoechst 33342 (Invitrogen, Carlsbad, CA). SPT1 epitope peptides were from Abgent (San Diego, CA).

3.2.2 Cells and cell culture

The HEK293, HEK293T and HeLa cells were obtained from the American Type Culture Collection (Manassas, VA). HEK293 cells were grown in DMEM/F12 medium (1:1) (Gibco BRL, MD) supplemented with 10% fetal bovine serum (FBS), penicillin (100 U / ml) and streptomycin (100 µg /ml) at 37 °C in a humidified 5 % CO_2 atmosphere. HeLa cells and HEK293T cells were grown in Dulbecco's minimum essential medium (DMEM; Gibco BRL, MD) with the same supplements.

3.2.3 DNA constructs

SPTLC1 cDNA was obtained from Origene. To generate N-terminal GFP-tagged SPT1 the *SPTLC1* gene was amplified by using the following primers: 5'-ATGGCGACCGCCACGGAGCAGTGG-3' and 5'-

GCCTAGAGCAGGACGGCCTGGGCT-3'. The PCR fragment corresponding to the coding sequence (CDS) of *SPTLC1* was cloned into pEGFP-C2/*SmaI* (Clontech, Mountain View, CA) resulting in pEGFP-C2-SPT1.

For C-terminal GFP-tagged SPT1, *SPTLC1* gene was first amplified using the primers: 5'-ATGGCGACCGCCACGGAGCAGTGG-3' and 5'-GAGCAGGACGGCCTGGGCTACCTC-3'. The PCR fragment of *SPTLC1* was then subcloned into the pUC18 cloning vector. It was next digested from the pUC18 vector by using *BamH*I and *EcoR*I restriction enzymes and subcloned into the same sites in pEGFP-N1 to generate pEGFP-N1-*SPTLC1*.

To create small peptide-tagged SPT1, pCMV-MAT-FLAG vector was used (Sigma Aldrich, Saint Louis, MO). *SPTLC1* was first amplified by the following primers: 5'-ATGGCGACCGCCACGGAGCAGTGG-3' and 5'-TAAGCGTAATCTGGAACATCGTATGGGTAGAGCAGGACGGCCTGGGCTACCTC-3', the latter contains a HA sequence. The PCR fragment corresponding to the CDS of *SPTLC1* was then cloned into pCMV-MAT-FLAG/EcoRV resulting in pCMVMAT-FLAG-*SPTLC1*-HA.

To construct internal tagged SPT1, the 5'-end of *SPTLC1* gene was first amplified by 5'-GGATCCGCCACCATGGCGACCGCCACGGAGCAGTG-3' and 5'-GATATCAGCGTAATCTGGAACATCGTATGGGTAAGCGTAATCTGGAACATCGTATGGGTAAGCGTAATCTGGAACATCGTATGGGTATCCATTCACCACAGTTTTGTGGCTTG-3'. The forward primer contains BamHI site and the reverse primer has

three HA sequences. The 3'-end of *SPTLC1* was amplified by the following primers: 5'-CATACGATGTTCCAGATTACGCTGATATCAAAGAATGTATAAACTTCGCCTCATTTAATTTTC-3' and 5'-CTAGAGCAGGACGGCCTGGGC-3'. The forward primer has an overlap sequence with the previous reverse primer. The overlap extension was completed by using the same forward primer from the first pair and the same reverse primer from the second pair to amplify *SPTLC1* gene from the beginning to the end. Then the amplified CDS was cleaved by BamHI and inserted into pcDNA 3.1 vector (Invitrogen, Carlsbad, CA).

All of the above have been sequenced to confirm the fidelity of the constructs.

3.2.4 Generation of *SPTLC1* and *SPTLC2* over-expressing cell line

HEK293 cells stably overexpressing *SPTLC1/SPTLC2* were generated as described in Chapter 2.

3.2.5 Immunofluorescence confocal microscopy

Cells were cultured on collagen (BD, San Jose, CA) coated glass coverslips (VWR, Inc., West Chester, PA) in a 24-well plate and fixed with 4 % formaldehyde in PBS at room temperature for 15 min. Fixed cells were permeabilized with 0.1 % Triton X-100 for 5 min, blocked in 10 % fetal calf serum in PBS (serum-PBS) for 30 min and then subjected to indirect immunofluorescence staining. Cells were incubated for 1 h at room

temperature, with primary antibody diluted in PBS-serum, then the cells were washed 3 times with PBS-serum for 5 min each, and incubated for 1 h at room temperature with Alexa Fluor-conjugated secondary antibody. Nucleic acids and actin were stained by incubating fixed cells with PBS containing 1 μg/ml Hoechst 33342 dye and rhodamine phalloidin (Invitrogen, Carlsbad, CA). Stained cells were rinsed in PBS and mounted in Fluoromount G (Southern Biotechnology Associates, Inc., Bermingham, AL) before observing under a Zeiss LSM 510 inverted laser scanning confocal microscope (Heidelberg, Germany) equipped with a Zeiss Plan-Apochromat 43 x oil immersion objective lens, and controllers for setting the band excitation and emission of wavelengths in the green, red and blue regions. Slides were scanned in "line mode" and then singled at an average of 16 scans to eliminate background noise. Images were collected with the resident Zeiss confocal microscope software.

3.2.6 Western blotting

Equal amounts of protein (30 μg) from each fraction and 50 μg of total cell lysate were loaded on a 12 % SDS-PAGE gel (Pierce, Rockford, IL). For Western blotting, the gel was transferred to the nitrocellulose membrane using a Tris-glycine buffer with 20 % methanol as the transfer medium, for 1 h at 100 volts (constant), in a transfer unit (BIO RAD, Hercules, CA). The blot was blocked overnight at 4 ^{o}C with SuperBlock blocking buffer (Pierce, Rockford, IL). The membrane was then incubated with rabbit anti-SPT1 serum diluted in SuperBlock and incubated for 2 h at room temperature. The membrane was rinsed three times in Tris buffered saline with 0.05 % Tween 20 (TBST) and

incubated for 1 h at room temperature, with a peroxidase-conjugated secondary antibody (Pierce, Rockford, IL). Finally, the membrane was rinsed in TBST and incubated in Supersignal West Pico chemiluminiscent reagent (Pierce, Rockford, IL).

3.2.7 Peptide competition assay

The SPT1 epitope peptides KLQERSDLTVKEKEEC (45~59 aa) and KEQEIEDQKNPRKARC (222~236 aa) were synthesized by Abgent (San Diego, CA). Each peptide was dissolved in PBS/10 % serum to a final concentration of 20 μg/ml for the competition experiments. The antibody-peptide mixture was incubated overnight at 4oC and then applied for immunostaining following the standard protocol.

3.2.8 Coimmunoprecipitation

Immunoprecipitation procedure was modified from the standard protocols (122, 123). Cells that were 60% confluent in 100-mm dishes were rinsed with ice-cold PBS and then scraped in 0.6 ml of ice- cold RIPA buffer (50 mM Tris-HCl, pH 7.4; 1% NP-40; 0.25% Na-deoxycholate; 150 mM NaCl; and 1 mM sodium orthovanadate) with protease inhibitor cocktail (Roche, Indianapolis, IN), and the cell lysate was centrifuge at 16,000 x *g* at 4 ^{o}C for 15 min to prepare the supernatant for the co-immunoprecipitation studies. The cell lysate was cleared of proteins that bind non-specifically by mixing 0.5 ml of the supernatant with 50 μl of a 50% protein G-sepharose bead slurry (Sigma Aldrich, Saint Louis, MO) for one hour and then centrifuged at 16,000 x g for 5 min. In another

microcentrifuge tube 50 µl of the 50% protein G-sepharose bead slurry was incubated with the antibody of interest (4 µg of mouse anti-vinculin antibody, Sigma Aldrich, Saint Louis, MO, or mouse anti-V5 antibody, Invitrogen, Carlsbad, CA, as a control) for 2 hours at 4°C and centrifuged at 16,000 x g for 5 sec (the following centrifugations were at the same condition). The antibody-conjugated beads were washed 3 times with 1 ml of ice-cold RIPA buffer and the supernatant was removed. Then the antibody-conjugated beads were mixed with 0.5 ml pre-cleared cell lysate and 0.5 ml of PBS and incubated overnight at 4°C. After 3 times of washing with ice-cold RIPA buffer and one time washing with ice-cold PBS the complex beads were centrifuged down and the precipitated proteins were eluted with 40 µl of laemmli sample buffer (Biorad, Hercules, CA) by boiling at 95°C for 5 min. After centrifugation the supernatant was transferred into a new tube and 25% of it was applied for SDS-PAGE.

3.2.9 siRNA transfection

The day before transfection HEK293 cells were seeded on collagen-coated coverslips in a 24-well plate at 4 x 104 per well. Three different SPTLC1 siRNA probes (Ambion, Austin, TX) targeting to exon 4 or 5 were pooled. The cells were transfected with the SPTLC1 siRNA pool or non-specific control siRNA (Ambion, Austin, TX) at 100 nM using DharmaFECT 1 transfection reagent (Dharmacon, Lafayette, CO). Mock transfection was performed with transfection reagent alone. Cell culture medium was replaced after 48 h of transfection. Cells were fixed for immunofluorescence staining after 72 h of transfection.

3.2.10 Subcellular fractionation

For a crude subcellular fractionation of the siRNA transfected cells, three 100-mm dishes were transfected with each kind of siRNA as above and after 72 h the cells were washed in PBS then scraped from the dishes in hypotonic buffer (20 mM Hepes, pH 7.9, at 4 ^{o}C, 1.5 mM MgCl2, 10 mM KCl, 0.5 mM DTT) plus protease inhibitor cocktail, Complete Mini (Roche, Indianapolis, IN) and homogenized by 30 strokes of a Dounce homogenizer. Nuclei were recovered by centrifugation at 1000 x g for 15 min and washed once using Nuclei Wash Buffer (10 mM Hepes, pH 7.9 at 4 ^{o}C, 0.2 mM MgCl2, 10 mM KCl, 0.5 mM DTT, and protease inhibitor cocktail) and centrifuged as the crude nuclear fraction. The post-nuclear fraction was then centrifuged for 1 h at 100,000 x g, the supernatant was defined as the cytosoluble fraction, and the pellets resuspended in the same buffer as the membrane fraction. All the fractions were stored as aliquots at -80^{o}C (124, 125).

3.2.11 Cell viability assay

The floating cells were collected from three 100-mm dishes 48 h after siRNA transfection, centrifuged, suspended in 0.1 % trypan blue. Both the viable cells and the unviable cells were counted using a hemocytometer.

3.2.12 Lipid extraction and analysis by LC-ESI MS/MS

The method has been described in the previous chapter. Briefly, the cells were collected in PBS and lipids were extracted in methanol/chloroform. The mass spectrometry data were collected using a PE Sciex API 3000 triple quadrupole mass spectrometer equipped with a turbo ion-spray source. As the first step of the analyses, the cells were examined by precursor ion scans for m/z 264.4 and 266.4 through the ceramide and monohexosylceramide range, and by precursor ion scans of m/z 184.4 for sphingomyelins to identify the major subspecies. Then for quantitative analysis, samples that had been spiked with an internal standard cocktail (from Avanti Polar Lipids, Alabaster, AL) were analyzed by LC ESI-MS/MS using a multiple reaction monitoring program built to encompass the subspecies of these sphingolipids found in the extracts (101).

3.2.13 Wound healing assay

HeLa cells were grown on collagen coated glass coverslips until confluent and a pipette tip was used to scratch the plate and the medium was replaced to remove the floating cells (126). Three hours after scratching the cells were fixed and processed for immunofluorescence staining and confocal microscopy.

3.2.14 Transfection of plasmid DNA

The transfection was done according to GeneJuice transfection protocol. The DNA to be transfected should be at a concentration of 0.5–1 μg/μl; if the DNA concentration is lower,

decrease the volume of serum-free medium in the transfection mix to compensate for the larger volume of DNA.

The day before transfection glass coverslips were placed in a 24-well plate. 3×10^4 cells were seeded in complete growth medium per well and incubated at 37°C (5% CO_2) overnight. Cells were 50% confluent before transfection. For each well to be transfected, serum-free medium was placed into a sterile tube. GeneJuice was added drop-wise directly to the serum-free medium and thoroughly mixed by vortexing. The mixture was incubated at room temperature for 5 min. For each well to be transfected, 0.25 μg DNA was added to GeneJuice/serum free medium mixture and mixed by gentle pipetting. The mixture was incubated at room temperature for 10 min and then added drop wise to the cells in complete growth medium. The dish was gently rocked to ensure even distribution. The cells were incubated for 48 h at 37°C (5% CO2).

3.3 Results

3.3.1 Native cell lines display novel subcellular localizations for endogenous SPT1

As has been done before (18), we initially examined SPT localization using SPT1/2 cells, a HEK293 cell line that stably overexpresses *SPTLC1* and *SPTLC2* as described under "materials and methods". As shown in Figure 3.1A, the immunofluorescence produced by the anti-SPT1 antibodies (98, 119) overlapped with BiP, a marker for the ER (127), which agreed with the previous localization of a stably overexpressed SPT1 with epitope

tags at either the N or C terminus (18). However, when untransfected HEK 293 cells were examined, the results (shown in Figure 1B) revealed some immunostaining in the cytoplasm (consistent with SPT1 in the ER), however, a substantial amount of endogenous SPT1 appears to be in the nucleus (based on co-localization with the DNA intercalating dye Hoechst 33342), and as punctate dots at the periphery of the cell at what appear to be the convergence points for actin stress fibers (stained red with phalloidin), which are referred to as focal adhesions (128). The SPT1 immunostaining at the cell periphery clearly co-localized with a focal adhesion marker protein, vinculin, as shown in Figure 1C.

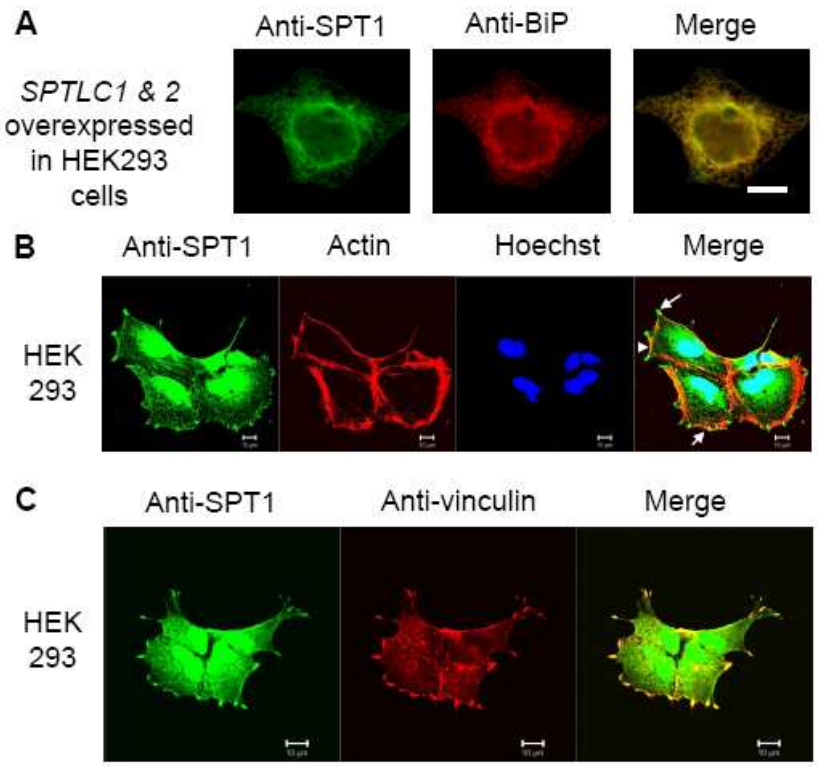

Fig. 3.1 Intracellular localization of SPT1 in *SPTLC1&SPTLC2* overexpressing HEK293 cells and native HEK293 cells by immunofluorescence staining and confocal microscopy.
Cells were grown on glass coverslips for 24 h before collecting for immunostaining. Rabbit anti-SPT1 antibody was used as primary labeling and Alexa Fluor 488 anti-rabbit antibody (green) as secondary labeling. (A) Localization of SPT1 in HEK293/SPTLC1/2 stable cells. SPT1 protein was stained in green and the ER marker protein, Bip, was labeled with Alexa Flour 568 (red). (B) Localization of endogenous SPT1 proteins in HEK293 cells. SPT1 was labeled in green. Actin was labeled by rhodamin phalloidin (red) and the nucleus was by Hoescht 33342 (blue). The arrows point to the focal adhesion localization of SPT1 at the tips of actin stress fibers. (C) Co-localization of SPT1 and vinculin in HEK293 cells. Mouse anti-vinculin antibody was used as a primary labeling followed by Alexa Flour 568 anti-mouse antibody (red). The images were taken by Zeiss confocal microscope. Bar, 10 µm.

These findings were not an anomaly of these HEK cells because the same results were obtained using HEK 293T cells and HeLa cells (Figure 3.2A). In agreement with the original characterization of the antibody (98, 119), immunostaining was not seen with pre-immune serum, as shown in Fig. 2B for HEK 293 cells (similar images for the other

two cell lines are not shown). Furthermore, the majority of the immunostaining was eliminated by incubating the antibody with an excess amount of the peptides that were used in the immunization to prepare this antiserum prior to immunostaining (as illustrated for HeLa cells in Fig. 3.2). The polypeptides that were used to prepare these anti-SPT1 antibodies (as described under "materials and methods") do not appear in any other known proteins, including SPT2 and SPT3, as determined by protein blast analysis; therefore, it is unlikely that these results are due to immuno-cross-reactivity with another protein, although this cannot be asserted conclusively until further analyses are performed (see below).

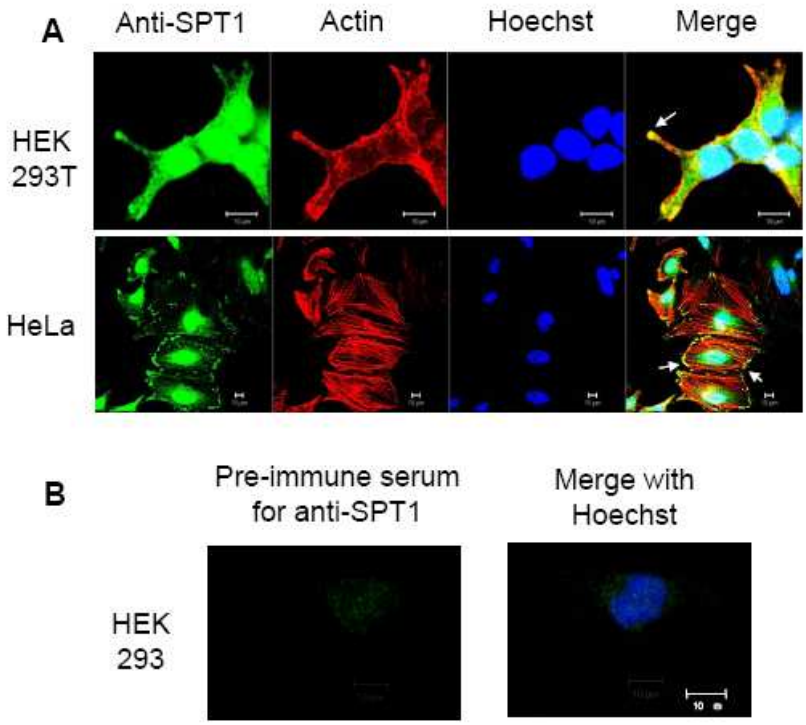

Fig. 3.2 SPT1 staining in HEK293T cells and HeLa cells and the results with pre-immune serum
(A) Confocal image of SPT1 in HEK293T cells and HeLa cells by rabbit anti-SPT1 antibody labeled by Alexa Fluor 488 anti-rabbit antibody (green). Actin was labeled by rhodamin phalloidin (red) and the nucleus was by Hoescht 33342 (blue). (B) Pre-immune serum staining of HEK cells followed by Alexa Fluor 488 secondary labeling. Bar, 10 µm.

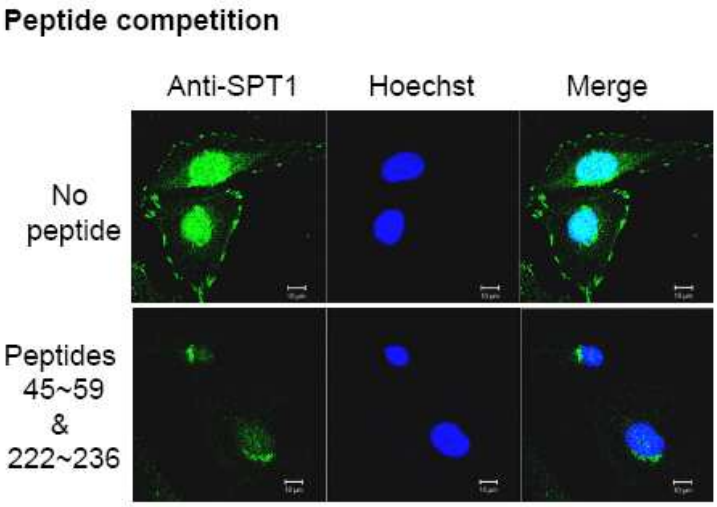

Fig. 3.3 The effect of adding SPT1 polypeptides to block SPT1 binding by the SPT1 antibody
The rabbit anti-SPT1 antibody was incubated with epitope specific peptides (aa 45~59, aa 222~236) in blocking buffer and then applied for primary labeling of HeLa cells followed by Alexa Fluor 488 anti-rabbit antibody. For control, the antibody was incubated with blocking buffer only. Bar, 10 µm.

3.3.2 Coimmunoprecipitation of SPT1 and vinculin in HEK293 cells

To further confirm the focal adhesion localization of SPT1, coimmunoprecipitation was used. Vinculin was precipitated by mouse anti-vinculin antibody conjugated protein G sepharose beads (Fig. 3.4, right lane). Mouse V5 antibody conjugated protein G sepharose beads were used as a nonspecific control and protein G sepharose beads alone were used as a negative control. The precipitate was immunoblotted with anti-vinculin antibody, our rabbit anti-SPT1 antibody, and a commercial rabbit anti-SPT1 antibody (Abnova). As shown in Figure 3.4, vinculin was successfully precipitated (bottom panel) and both anti-SPT1 antibodies detected SPT1 on the membrane (top and middle panels). No band was detected from the precipitate of nonspecific control or the negative control (middle and left lane).

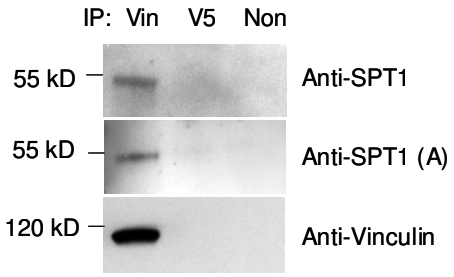

Fig. 3.4 Coimmunoprecipitation of SPT1 and vinculin
Vinculin was precipitated from HEK293 cell lysate using mouse anti-vinculin antibody bound protein G sepharose beads (right lane). Mouse V5 antibody was used as a nonspecific control antibody (middle lane) and protein G sepharose alone was used as negative control (left lane). The immunoprecipitate was applied for SDS-PAGE and immunoblotted with our rabbit anti-SPT1 antibody (top panel), commercial rabbit SPT1 antibody (middle panel) and anti-vinculin antibody (bottom panel).

3.3.3 Confirmation of the novel localization of SPT1 by siRNA silencing of the expression of SPT1

As shown in Figure 3.5, when HEK293T cells were transfected with *si*RNA against *SPTLC1* or a combination of *siSPTLC1* and *siSPTLC2* (i.e., against both subunits of SPT), then immunostained with the anti-SPT1 antibody, there was a substantial decrease in the overall fluorescence of the cells (middle and lower panels of Fig. 3.5A) versus cells treated with a non-specific siRNA control (top panel of Fig. 3.5A). Indeed, fluorescence in the nucleus and focal adhesions appeared to be suppressed the most by *siSPTLC1* and *siSPTLC1/siSPTLC2*; however, the SPT specific siRNAs caused cell rounding, which obscures some of the decrease in SPT1 in the cytoplasm/ER. Western blotting of total cell lysates confirmed that the amount of ~53 kDa SPT1 protein decreased significantly in the *siSPTLC1* and *siSPTLC1*/*siSPTLC2* transfected cells compared with the non-specific siRNA transfected cells (Fig. 3.5B left). Decreases were also seen when the

Western blotting was conducted using crude nuclei and membranes (Fig. 3.5B right), with the nuclear immunostaining appearing to be depleted the most, which is similar to what is seen by confocal microscopy (c.f. middle panels of Fig. 3.5A). Thus, these observations confirm that the SPT1 immunostaining in focal adhesions and the nucleus is due to SPT1 in those regions of the cell.

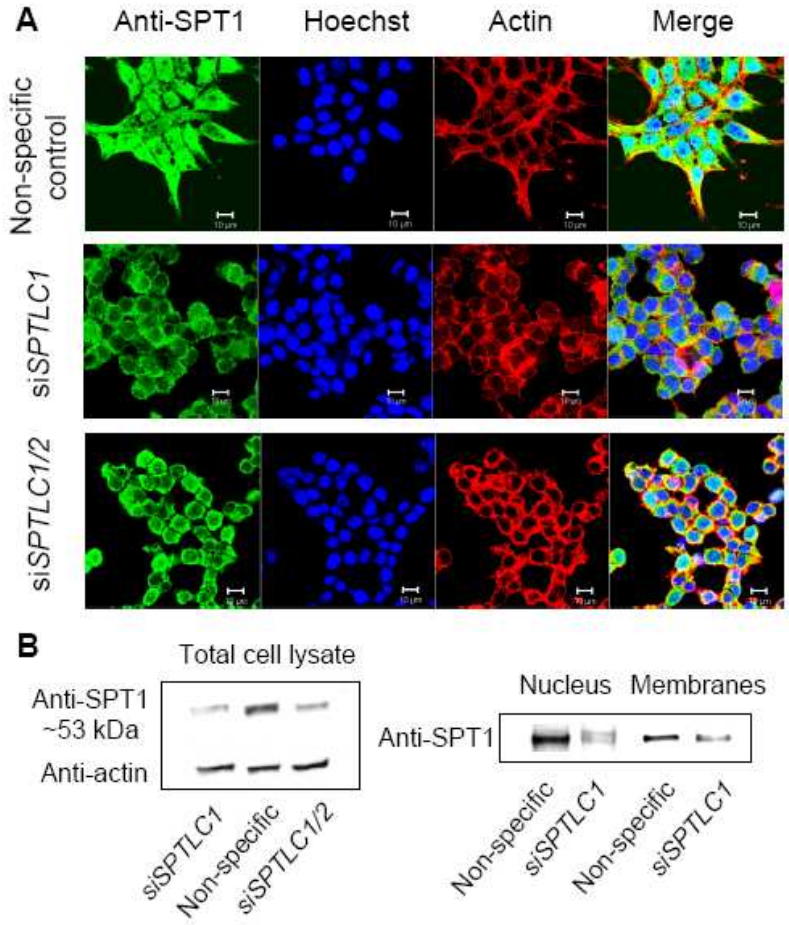

Fig. 3.5 Confocal imaging of SPT1 in HEK293T cells transfected with siRNA to silence *SPTLC1*

(A) HEK293T cells grown on collagen coated coverslips were transfected with non-specific siRNA, *siSPTLC1* and *siSPTLC1/siSPTLC2* separately for 72 h and then fixed for immunofluorescent staining using anti-SPT1 antibody and Alexa Fluor 488 anti-rabbit antibody (green) as well as for actin fibers (phalloidin) and nuclei (Hoechst 3342) (Bar, 10 µm); or (B) analyzed by Western blotting for SPT1 normalized by actin. The right immunoblot is for the nuclear and membrane fractions isolated from HEK293T cells transfected with either non-specific siRNA or *siSPTLC1* as described in experimental procedures.

3.3.4 SPT1 suppression using si*SPTLC1*, but not si*SPTLC2* silencing, induces cell rounding followed by detachment

Suppression of SPT1 by *si*RNA for *SPTLC1* alone, or the combination of *si*RNAs for *SPTLC1* and *SPTLC2,* causes cell rounding as observed by confocal (Figure 3.5) or light microscopy (Figure 3.6A). Since it is not clear whether the changes in morphology are due to loss of SPT1 per se or to its indirect effect on SPT2, which is known to be bound and stabilized by SPT1 (129), the effect of silencing SPT2 alone was evaluated. When HEK293T cells were transfected with *siSPTLC2* alone, there was no noticeable cell rounding (Figure 3.6A), despite the almost complete disappearance of the ~63 kDa SPT2 polypeptide (Figure 3.6B). Therefore, suppression of SPT1 but not SPT2 has this impact on cell morphology.

In addition to causing cell rounding, *siSPTLC1* and the combination of *siSPTLC1 & 2* caused a noticeable increase in the number of cells that had detached from the dish after ~48 h (data not shown). This did not appear to be due to cell death because the floating cells were ~70% viable based on the Trypan blue exclusion assay; however, when the floating cells were collected and replated in new medium minus the *si*RNA(s), they did not survive. These observations suggest that the cell rounding upon suppression of SPT1 facilitates cell detachment and death, presumably due to anoikis after loss of cell-matrix interactions (130).

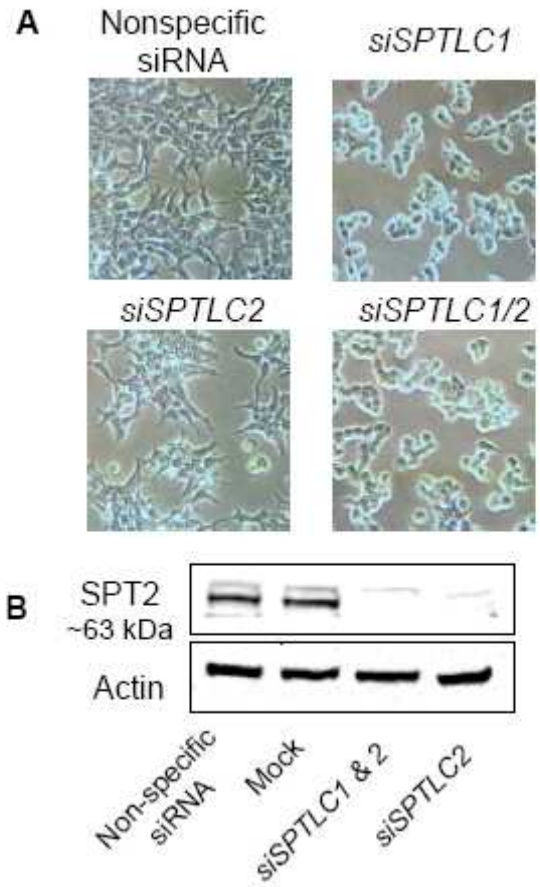

Fig. 3.6 Morphology of HEK293T cells after transfection with control and *SPTLC* siRNAs.
(A) Phase contrast images of HEK293T cells transfected with non-specific siRNA, *siSPTLC1*, *siSPTLC2* and *siSPTLC1/siSPTLC2* separately. (B) The Western blots that show that SPT2 protein has been suppressed by *siSPTLC2* alone and in combination with *siSPTLC1*, with normalization using actin.

3.3.5 The change in cell morphology induced by *siSPTLC1* is not due to reduction of the sphingolipid amounts of the cells

To determine how *si*RNAs for SPT1 and 2 affect the sphingolipid content of the cells, HEK293T cells were treated with transfection reagent alone, non-specific *si*RNA or

siSPTLC1 and/or *2* then analyzed by liquid chromatography-electrospray tandem mass spectrometry (LC-ESI MS/MS) (Fig. 3.7). Compared to the non-specific *si*RNA, *siSPTLC1* did not reduce the amount of total sphingolipids (defined as the major species sphingomyelin + monohexosylceramide + ceramide), but the total sphingolipid content of the *siSPTLC2* treated cells was somewhat lower (~17%, P = 0.06). Ceramides were lower for all of the cells treated with for *siSPTLC1* (13%), *siSPTLC2* (35%) or both (40%), as might be anticipated to occur upon suppression of de novo biosynthesis of ceramide. These findings are consistent with previous findings that when de novo biosynthesis is eliminated, cells can still survive when supplied medium containing serum sphingolipids (129).

Thus, since *siSPTLC2* caused a greater change in the sphingolipid content of the cells than *siSPTLC1* alone, which is the opposite of the effects of these *si*RNAs on cell morphology, it is unlikely that the cell rounding is induced by changes in sphingolipid metabolism versus a reduction in SPT1 per se. Consistent with this conclusion, treatment of HEK293 cells with myriocin, a potent inhibitor of SPT that essentially eliminated de novo sphingolipid biosynthesis, did not change cell morphology for up to 48 h (data not shown).

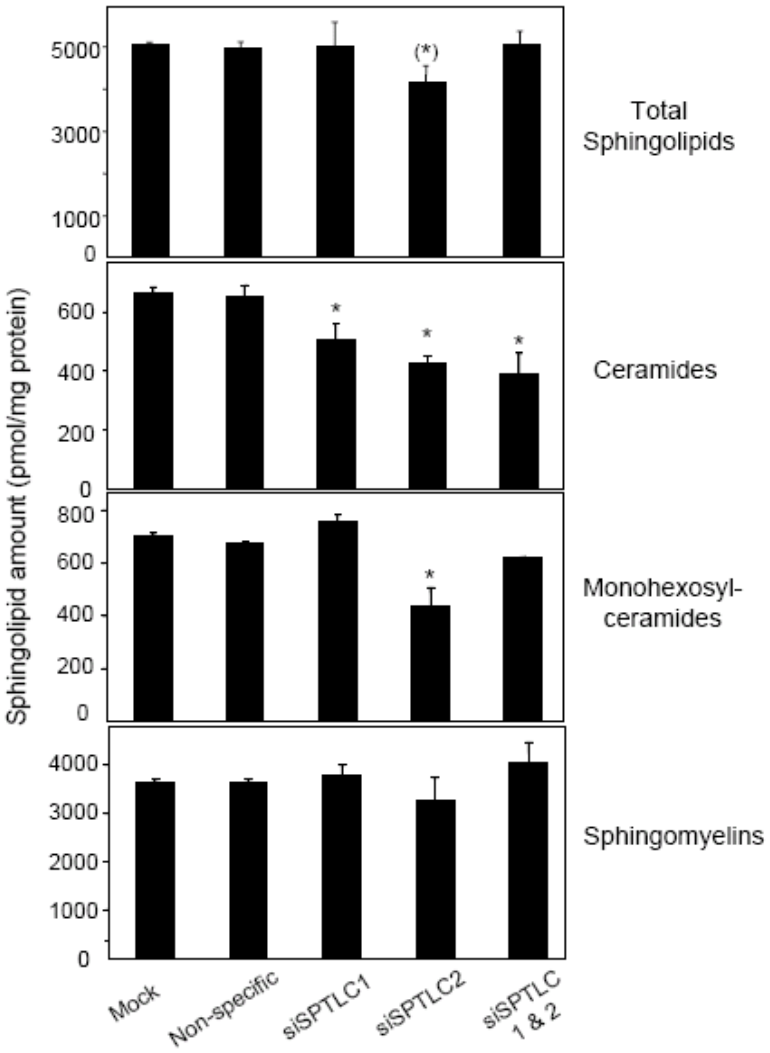

Fig. 3.7 Amounts of ceramide, monohesoxylceramides and sphingomyelins in HEK293T cells after transfection with control vectors or *siSPTLC1* and/or *siSPTLC2*.
HEK293T cells were transfected with non-specific siRNA, *siSPTLC1*, *siSPTLC2* and *siSPTLC1/SPTLC2* separately for 72 h and then collected for lipid extraction and analysis by LC ESI MS/MS. The amounts are given as the mean $\pm$ SD for analysis of 2 dishes.

3.3.6 Appearance of SPT1 in focal adhesions decreases as cells in culture reach confluence and increases with induction of cell migration

As illustrated in Figure 3.8A, the focal adhesion staining of SPT1 disappears when the cells grow to confluence (with little difference in the staining of the nucleus and cytoplasm/ER) compared to cells at lower density (Figure 3.8B). The percentage of cells with focal adhesion staining for SPT1 before confluence (i.e., before the cells are completely surrounded by other cells) was essentially the same for HEK293 cells (95%) and HeLa cells (90%), whereas, neither cell type had any detectable SPT1 with focal adhesions after they were confluent.

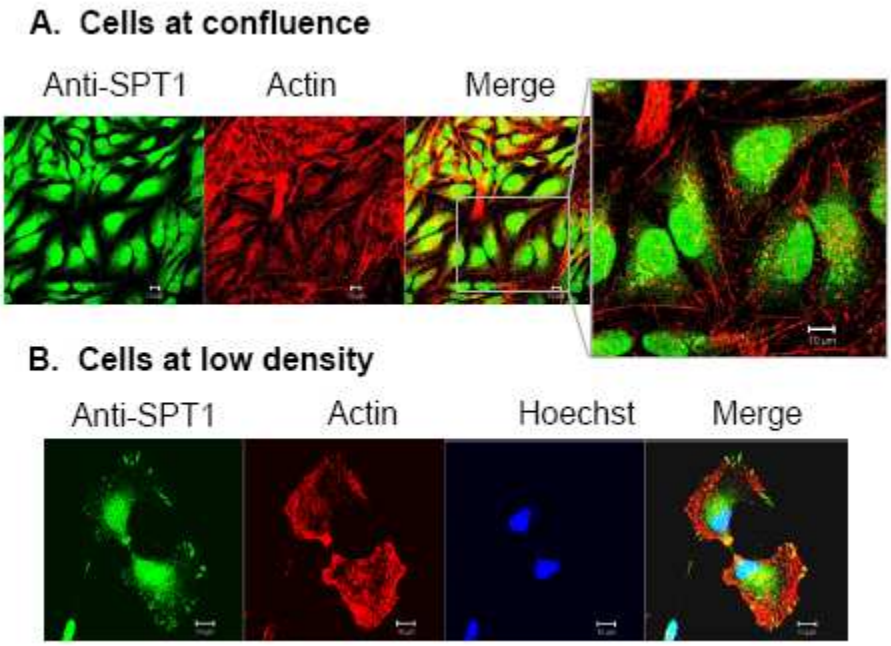

Fig. 3.8 Focal adhesion staining of SPT1 in low density cells and confluent cells. (A) Confocal fluorescence imaging of SPT1 in confluent HeLa cells. HeLa cells were grown on collagen coated coverslips until confluent and then fixed for immunofluorescent stain with anti-SPT1 antibody followed by Alexa Fluor 488 anti-rabbit antibody (note enlarged image). (B) SPT1 in low density cells. Cells were cultured at low density before applied for immunofluorescence staining. The two cells shown here appear to be at a late stage of mitosis. Actin fibers and nuclei were labeled by rhodamine phalloidin and Hoechst 3342 separately. Bar, 10 μm.

The dynamic of SPT1 localization was also examined using the scratch-wound healing assay to induce cell migration (126). HeLa cells were grown to confluence on collagen coated glass coverslips, scratched to produce an open furrow using a pipette tip, and then the cells were incubated for 3 h before being fixed and stained. Confocal imaging of the cells (Fig. 3.9) showed that the focal adhesion staining of SPT1 appears mainly at the tips of actin stress fibers at the migrating edges of the cells along the wound gap (Fig. 3.9), whereas little or none was seen in cell-cell junctions away from the wound edge, nor in any of the confluent cells away from the site of the scratch.

These images provide compelling evidence that the SPT1 in focal adhesions is associated with, and plays a role in, cell morphology and migration.

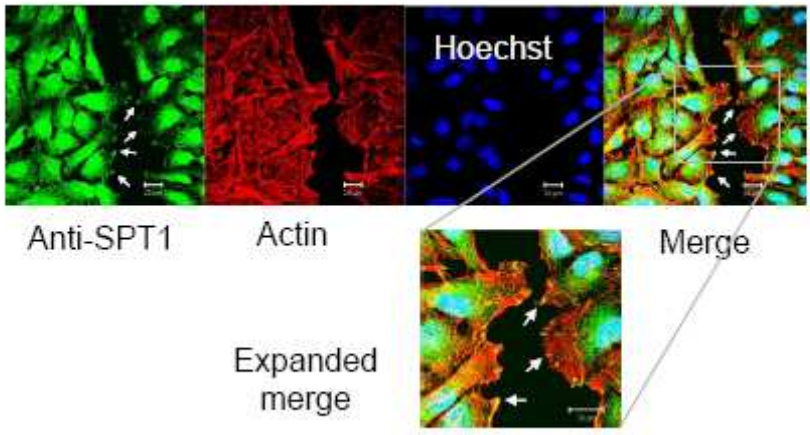

Fig. 3.9 Focal adhesion staining of SPT1 during the scratch wound-healing assay. HeLa cells were grown to confluent on collagen coated glass coverslips, scratched by a pipet tip, and processed for immunofluorescence staining using anti-SPT1 antibody after 3 h. Bar, 10 µm. The bottom image is an enlarged one.

3.3.7 Partial co-localization of ABCA1and SPT1 in the cell periphery

ABCA1 was first identified on plasma membrane and later in multiple subcellular locations. It has recently been reported that SPT1 can be found in ABCA1 immunoprecipitates (121); therefore, the localization of ABCA1 was compared to that of SPT1 in HEK293 cells (Fig. 3.10). Most of the ABCA1 staining appeared to be associated with intracellular membranes (and in a pattern similar to that for SPT1), and a portion (see expanded panel in the lower half of Fig. 3.10 and merge) was also detected in focal adhesion-like assemblies in the same vicinity as SPT1. These results are consistent with the proposal that SPT1 and ABCA1 interact (121), although it is not clear if this is direct or perhaps by binding to the same scaffold protein system, as will be discussed later.

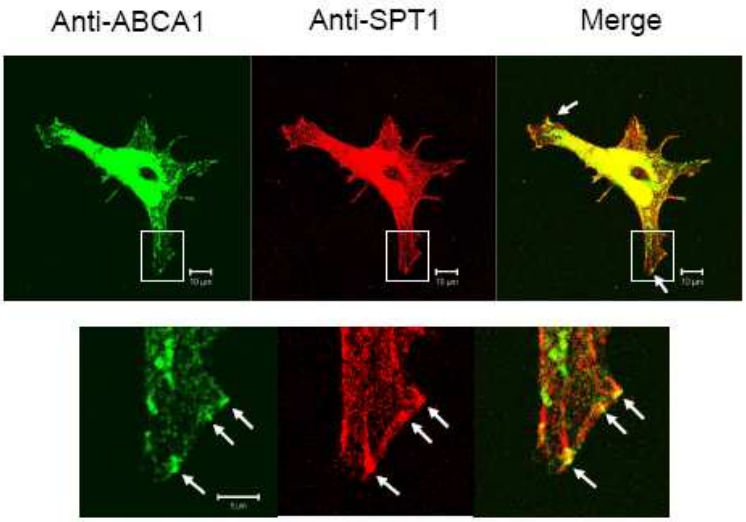

Fig. 3.10 Localization of SPT1 and ABCA1 in HEK cells.
HEK293 cells grown on collagen coated coverslips were stained with rabbit anti-SPT1 antibody and mouse anti-ABCA1 antibody followed by Alexa Fluor 488 anti-rabbit antibody (green) and Alexa Flour 568 anti-mouse antibody (red). The enlarged images show the localization similarity of the two proteins at the leading edge of the cell. Upper panel: bar, 10 µm; lower panel: bar, 5 µm.

3.3.8 Unlike native SPT1, overexpressed SPT1s do not localize in the nucleus nor focal adhesions

As has been seen before with HA-tagged SPT1 in LY-B cells (18), immunostaining of SPT1 in SPT1-overexpressing HEK cells appears to detect SPT1 only in the ER (Fig. 3.1A). This was also seen with SPT1 constructs with other types of epitope tags, including both N- (pEGFP-C2-*SPTLC1*) and C-terminal (pEGFP-N1-*SPTLC1*) GFP-tagged SPT1s (Fig. 3.11A), SPT1 constructs with a smaller amino-terminal MAT-FLAG tag and a carboxyl-terminal HA tag (Fig. 3.11B, which shows the combined construct with detection using an anti-HA antibody, but the individual constructs gave similar results), and an SPT1 recombinant with three HA tags between amino acids 97 and 98 (Fig. 3.11B, lower), which is in a region of the SPT1 polypeptide that is likely to be an external loop based on proposed three-dimensional structures (131, 132) (this construct was made in case an N- or C- terminal tag interferes with the localization of SPT1 in the nucleus and focal adhesions).

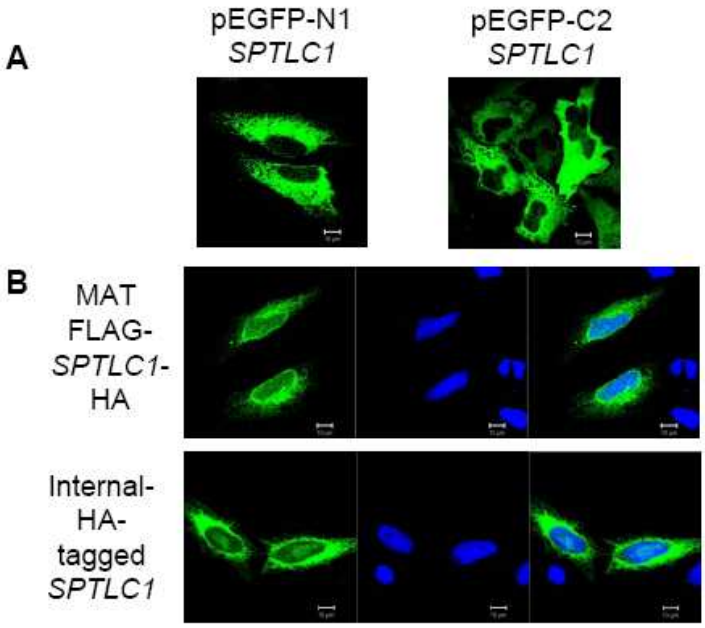

Fig. 3.11 Localization of N-, C- and internally tagged SPT1 in HeLa cells.
(A) Hela cells were grown on collagen coated coverslips, transfected with pEGFP-N1-SPT1 or pEGFP-C2-SPT1 for 24 h, and then fixed for confocal imaging. (B) HeLa cells were transfected with pCMV MAT FLAG-*SPTLC1*-HA or pcDNA-*SPTLC1*-internal HA before immunofluorescence staining using an anti-HA antibody. Bar, 10 µm.

3.4 Discussion

Serine palmitoyltransferase has been long thought to reside in the ER where *de novo* sphingolipid biosynthesis is initiated (115), and these studies have confirmed that at least a portion of the endogenous SPT1, and essentially all of the ectopically expressed SPT1s, have this localization. The more novel contributions of these studies are: i) the establishment that a portion of the endogenous SPT1 is also located in the nucleus and focal adhesions, as had been suggested but not proven earlier (98, 119, 120); and ii) the

demonstration that the localization in focal adhesions is related to, and apparently necessary for, cell migration and maintenance of a normal cell morphology.

The structural basis for the surprising localization of SPT1 with the nucleus and focal adhesions is not known, however, SPT1 is predicted to have multiple PDZ binding motifs (e.g., a Class II motif at $AVLL_{470-473}$, and four Class III domains binding motifs at $VEMV_{11-14}$, $KEEL_{57-60}$, $EELI_{58-61}$ and $PEPL_{66-69}$) using the ELM (Eukaryotic Linear Motif) functional site prediction tool (http://elm.eu.org/) (133) and the UniProtKB/Swiss-Prot identifier for human SPTLC1: O15269. These motifs might interact with PDZ-containing scaffold proteins in the nucleus and plasma membrane because PDZ-containing scaffold proteins are known to assemble multiprotein complexes in such locations to perform specialized local functions such as organization of subcellular structures and signal transduction (134, 135).

Additional evidence for the possibility of such interactions has been provided by the recent report (121) that SPT1 is associated with ABCA1, and our confirmation that at least a portion of both are in the vicinity of focal adhesions (Fig. 3.9). ABCA1 is thought to interact with β-syntrophin/utrophin complexes through syntrophin PDZ domains (136, 137), which could also account for the SPT1 (and ABCA1) in focal adhesions via the binding of utrophin to the actin cytoskeleton and the dystroglycan complex in the plasma membrane (138, 139). The reported interaction of ABCA1 and SPT1 (121) might, therefore, be indirect and mediated by a mutual interaction with β-syntrophin or another protein with multiple PDZ domains.

The physiologic significance of this interaction is not known, but might provide a mechanism to link sphingolipid metabolism and S1P delivery and/or removal from the cell because ABCA1 is the major receptor for HDL (140), the major plasma carriers of S1P (141). S1P can inhibit de novo sphingolipid biosynthesis (74), therefore, perhaps the SPT1 in these atypical localizations is serving as a "sphingoid base status sensor" rather than as a subunit of the catalytically active SPT1-SPT2 dimer (17) or multimer (19). It is interesting that HDL also promote endothelial cell motility (142). The finding that SPT1 is associated with focal adhesions at the migrating edge of cells in the scratch-wound healing assay (Figure 3.8), and that knockdown of SPT1 mRNA caused cell rounding (Figure 3.5 and 3.6) would be consistent with a role for SPT1 in cell adhesion and migration.

The nuclear localization of SPT1 might also be a consequence of interactions with scaffold proteins such as gamma 1-syntrophin that have PDZ motifs and participate in the translocation of other proteins (e.g., DGK-zeta) (143) between the cytoplasm and nucleus. Many focal adhesion proteins have been found in the nucleus, and play a role in signaling from focal adhesion to nucleus (144). In addition, SPT1 has a transcription cofactor motif (LXXLL) that is found in coregulators that shuttle between nucleus and cytoplasm. Considering that new transcriptional coregulators are continually being discovered and these include factors that were not expected to serve such functions (145) and even nuclear receptors that are down-regulated by binding sphingosine (146), these

possibilities should be borne in mind as a potential explanation for the nuclear localization of SPT1.

The finding that all of the SPT1 constructs prepared by us and others (18) produce a recombinant protein that appears only in the ER and not in the nucleus and focal adhesions complicates follow-up investigations into these hypotheses (such as by deletion of the PDZ-binding motifs to determine how this affects localization). There is currently no explanation for this distinction, but it is not unprecedented because neutral sphingomyelinase (nSMase1), for example, has also been found in the nucleus of cells, but the over-expressed enzyme does not appear there (147). Such behavior might be caused by the existence of additional, endogenous isoform(s), such as splice variants, or perhaps co- or post-translational modification(s) that is (are) important for protein folding and/or interaction with binding partners. These are important questions for future study.

3.5 Conclusions

SPT1 was found not only in ER but also in the nucleus and focal adhesions using immunofluorescence confocal microscopy.

SPT1 co-localizes and interacts with a focal adhesion marker protein, vinculin.

siRNA silencing of *SPTLC1* but not *SPTLC2* caused cell morphology change and this phenomenon was not related to the intracellular sphingolipid change.

SPT1 focal adhesion staining disappeared when the cells reached confluence and appeared in migrating cells.

SPT1 colocalized with ABCA1, a lipid transporter to form HDL particles, at focal adhesion like structures.

Overexpressed SPT1 did not get to the nucleus or focal adhesions.

CHAPTER 4

Investigations on *SPTLC1* isoforms

4.1 Introduction

Although all of the studies to date of SPT1 have focused on one transcript, three *SPTLC1* mRNA isoforms are found in the GenBank database. The functions of these isoforms are not yet known, but they might be responsible for biosynthesis of different types of sphingoid bases. The prevalence of sphingoid bases with 18-carbons in most sphingolipids is thought to be due to the specificity of SPT for the co-substrate fatty acyl-CoA, with the mammalian enzyme (17, 31) utilizing palmitoyl-CoA (C16:0) > pentadecanoyl- and heptadecanoyl- CoA's (C15:0 and C17:0) >> stearoyl-CoA (C18:0). However, other chain length sphingoid bases (with 20-carbon atoms) are found in mammalian brain gangliosides (1), and have been selectively localized in hippocampus by imaging mass spectrometry analysis (38). Therefore, it is possible that one of the alternative SPT1 isoforms may be responsible for producing such species. To explore this possibility, the isoform (*SPTLC1L*) originally found in hippocampus was isolated and expressed in LYB cells to explore if it is functional and responsible for the synthesis of sphingolipids with a C20-sphingoid base.

4.2 Materials and methods

4.2.1 Materials

The *SPTLC1L* plasmid pcDNA used in this study was cloned by Dr.Leipelt. SPT1L specific antibody targeting to the C-terminal of the protein was provided by Dr.Ulinger. The epitopes used for immunization are "PRGRTGESC" and "PPATQHAERTQDSR". LYB cells, mutant CHO cells which do not have SPT activity due to SPT1 deficiency, were provided by Dr. Hanada (Japan).

4.2.2 Cell culture

LYB cells were grown in F12 medium (Gibco) with 10% fetal bovine serum. The cell culture condition was the same as described in Chapter 2.

4.2.3 Western blotting

Western blotting was performed as described in Chapter 3.

4.2.4 Transfection of LYB cells

The transfection was performed according to GeneJuice transfection protocol as described in Chapter 3. The day before transfection, 8×10^5 cells were seeded in complete growth medium in 60-mm dishes. 5 μg DNA was added to each dish.

4.2.5 In situ SPT activity assay

This method has been described in Chapter 2. LYB cells were transfected with DNA plasmids for 24 hours and then incubated with 0.1 μM of [^{13}C]-palmitate for 18 hours before collected for lipid extraction and ESI-MS/MS analysis.

4.3 Results and Discussion

4.3.1 Identification of mRNA isoforms of *SPTLC1* in GenBank database

Recent estimates suggest that about 40~60% pre-mRNAs are subject to alternative splicing, which accounts for proteome diversity under various situations (148, 149). Table 4.1 lists the three human SPT1 transcripts that are found in GenBank. The first one, as well as its homologs in mouse and hamster, has been studied previously (17-19, 24) and is thought to be responsible for functional SPT1 protein. The functions of the other two transcripts, if any, have not been reported, so far. They have very high similarity (96.9% and 31.3%) to *SPTLC1* and the 5' sequences of the three transcripts are identical. The second transcript (*SPTLC1S*) encodes a shorter peptide (16 kDa), while the third encodes a longer peptide (57 kDa), so we refer to it as *SPTLC1L*. The mRNA sequences of *SPTLC1* and *SPTLC1L* are identical except that the former one has an extra 32 bp in the middle.

Table 4.1 mRNA isoforms of human *SPTLC1*

Our abbreviation	***SPTLC1***	***SPTLC1S***	***SPTLC1L***
mRNA name from GenBank	Homo sapiens serine palmitoyltransferase, long chain base subunit 1 (SPTLC1), transcript variant 1.	Homo sapiens serine palmitoyltransferase, long chain base subunit 1 (SPTLC1), transcript variant 2.	Homo sapiens serine palmitoyltransferase, long chain base subunit 1.
GenBank No.	NM006415	NM178324	BC068537
Length (bp)	2780	998	2742
Encoding protein size (kDa)	53	16	57

4.3.2 Genomic DNA sequence analysis suggests that the *SPTLC1L and SPTLC1S* mRNA were generated through alternative splicing

The *SPTLC1* gene contains 15 exons. By analyzing *SPTLC1* isoform cDNA sequences and *SPTLC1* genomic DNA sequence, we noticed that both *SPTLC1* isoforms were likely to arise from alternative splicing.

In the case of SPTLC1L, the first 32 nucleotides of exon 15 are missing, therefore, this deletion causes a frame shift which bypasses the original stop codon and makes a stop codon 149 nucleotides downstream (Fig. 4.1). Since in most cases alternative spliced sequences are longer than 50 nucleotides (150), is this short alternative splicing possible? Apparently so because there has been a recent report of very short alternative splicing (< 50 nucleotides), and it has been proposed that such might contribute more to protein-function diversity than has been previously thought (150). Splicing consensus sequences invariantly have GT at the start of the intron and AG at its end (151) and the *SPTLC1*

gene has GT at the beginning of the intron between exon 14 and 15, and AG is not only found at the end of the intron but also at the end of the spliced sequence (Fig. 4.1). Thus, instead of proposing that the 32 nucleotides at the beginning of exon 15 have been spliced out to produce *SPTLC1L,* this might be due to 32 nucleotides of the intron being added to the beginning of exon 15 in *SPTLC1*.

TACAGTGCAT GAACAGAAGT ATTGCATTAA CTCAGGCGCG CTACTTGGAG
AAAGAAGAGA AGTGTCTCCC TCCTCCCAGG TCAGTTGACG ……
…… ATAATTCTTT GTGTCCTTTA CTGTTCTCAG CATTCGGGTT
GTGGTCACGG TGGAACAAAC AGAGGAAGAA CTGGAGAGAG CTGCGTCCAC
CATCAAGGAG GTAGCCCAGG CCGTCCTGCT C**TAG**GCAGAG TCCCGGGACC
ATGGCCTCCT GCCACACAAC ACGCAGAGAG GACTCAAGAC TCCCGCTGGC
CATGGAGTGG CCTGAAAGAG AGCAAGAACA TGTGGATCTT TGATAGGATT
GTTACCAAAT GGTGTCAGTA TGGACCAATT GTG**TGA**CCAT ……

Fig. 4.1 *SPTLC1* genomic sequence where alternative splicing of *SPTLC1L* happens
The sequence contains exon 14 (black letters), an intron between exon 14 and 15 (grey letters) and part of exon 15 (black letters). The alternatively spliced sequence has an underline in it. The "TAG" stop codon for *SPTLC1* and "TGA" stop codon for *SPTLC1L* are in bold letters.

In the case of *SPTLC1S,* the mRNA would be generated by adding part of the intron between exon 5 and exon 6 to the end of exon 5, which generates a premature stop codon "TGA" right after exon 5 and, thus, only contains the first five exons of *SPTLC1* gene(Fig. 4.2). Translation of *SPTLC1S* would produce such a short peptide (16 kDa) that it would seem unlikely to have enzyme activity. However, this alternative splicing might act as a control mechanism adjusting *SPTLC1* expression at mRNA level.

TTCAATAAAG GCAGCAGCTT TAGCATCTCT AAAGAAGTAT GGCGTGGGGA
CTTGTGGACC CAGAGGATTT TATGGCACAT TTGGTAAGTT ……
TTATCTTTCT AGAA**TGA**AGA TGAAGGATCA TTGATTTCCT TGTGTATGGA
TAATCCGGGA ACAGGCCAAC TAAATATTTG ATGAATGTAT GATTTCAAAT
ACAGTGAATT CCCTGGGAGT CATCAAAGAA GACCGGCATT TTATGGTTGT
TTTTATTAAG TGTATATTCT TTGCTCCTGA AAATGTTATT AAATAATTGT
TTAGGCCGGG CATGGTGGCT CATGCCTGTA ATCCCAGCAC TTTCAAAGGC
TGAGGCAGGC AGATCACCTG AGGTCAGGAG TTCAAAACCA GCCTGGCCAA
CATGCTGAAA CCTCGTCTCT ACTAAAAATA CAAAAATTAG CTGGGCGTGG
TGGTGGATAC CTGTAATCCC AGCTACGTGG GAGGCTGAGG TGGGAGAATT
GCTTCAACCT GGGAGGCAGA GGTTGCAGTG AGCCGAGATC ATGCCACTGC
ACTCCAGCCT GGGCAACAGA GCAAGACTGT CTCAAAAATA AATAAATAAA
TAAAATTGTT TAAATGAATT TATTGCTGGA AATAGCATTT ……

Fig. 4.2 *SPTLC1* genomic sequence where alternative splicing of *SPTLC1S* happens
The sequence contains exon 5 (black letters) and an intron between exon 5 and exon 6 (grey letters). Part of this intron (underlined sequence) is added at the end of exon 5, which generates a premature stop codon "TGA" (bold letters) right after exon 5. This splicing produces *SPTLC1S* which only contains the first five exons of *SPTLC1* gene.

We elected to express the longer form, *SPTLC1L,* because its similarity to SPTLC1 in sequence and size makes it likely that it will be able to form a dimer with the other SPT subunits (SPT2 or SPT3) for catalytic activity, and--since it was first identified from brain tissue which is the same place where C20 sphingoid bases were found –perhaps the SPTLC1L-SPT2 heterodimer is responsible for the synthesis of C20 sphingolipids.

4.3.3 The endogenous SPT1L protein was detected by Western blotting

Since the SPTLC1c mRNA sequence is almost identical to SPTLC1 (only lacking the 32 nucleotides in the middle of the sequence), it is difficult to identify this transcript by PCR. However, the frame shift caused by alternative splicing should result in an amino acid

sequence of the isoform that has a unique c-terminal. An anti-SPT1L antibody was generated targeting to this unique sequence [[did you give the sequence? maybe but I don't recall. if not put it here]]] and used for Western blotting of a HEK293 cell lysate (Fig. 4.3). This found that the antibody detects a band slightly above the 55 kDa marker, which is consistent with the predicted molecular weight of SPT1L.

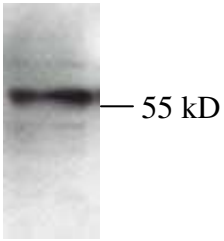

Fig. 4.3 Western blotting of HEK293T cell lysate with anti-SPT1L antibody
30 ug of total cell lysate from HEK293t cells were applied for SDS-PAGE followed by Western blotting using anti-SPT1L antibody.

4.3.4 SPT enzyme activity assay of LYB cells transfected with *SPTLC1L* using [^{13}C]-palmitate as a substrate

To test if the *SPTLC1L* isoform has enzyme activity, it was expressed in LYB cells because LYB cells do not have SPT enzyme activity due to SPT1 deficiency and provide a useful model. LYB cells were transfected with pcDNA-*SPTLC1L* or pcDNA-*SPTLC1* for 24 hours and then incubated overnight in medium containing 0.1 mM [^{13}C]-palmitate (it is possible to use stable-isotope-labeled palmitic acid rather than stearic acid because our lab has found that palmitoyl-CoA can be elongated to stearyl-CoA, so labeled stearyl-CoA is available inside the cells). The cells were collected for lipid extraction and LC ESI-MS/MS analysis, but the studies did not detect any incorporation of ^{13}C into either

C18- or C20-sphingoid bases. To determine if this might be due to an incompatibility between the human *SPTLC1L* and hamster *SPTLC2*, *SPTLC1L* and human *SPTLC2* were co-transfected, but this did result in the production of ^{13}C-labelled sphingolpids. Therefore, it is unclear what the function of this isoform is.

4.4 Possible directions for future research

The lack of SPT activity when SPTLC1L was transfected into LYB cells does not prove that this polypeptide does not function as an SPT subunit. We might not have choosen the right cell line for these studies, and a brain tissue derived cell line might be more successful. It is also possible that the function of SPT1L might require partners and co-transfection of them might be required for SPT activity. Lastly, it is also possible that SPT1L might play a role other than synthesis of sphingolipids, which would be a more difficult outcome to study.

4.5 Conclusions

SPTLC1L and *SPTLC1S* sequences were identified as alternative spliced mRNA isoforms of *SPTLC1*.

The existence of SPT1L peptide in HEK293 cells was confirmed by western blotting using a specific antibody.

Transfection of *SPTLC1L* into LYB cells did not rescue the cells in SPT activity, but the possibility that the SPT1L may have an enzymatic function warrants further study.

OVERALL CONCLUSIONS

Sphingolipid biosynthesis is one of the most complex metabolic processes of mammalian cells, involving hundreds of enzymes, multiple pathways for intra- and extra-cellular trafficking and transport, and dozens (at least) of associated biological functions that are regulated by the types and amounts of sphingolipids that are present. Nonetheless, very little is known on a biochemical level about even the first few steps of the *de novo* sphingolipid biosynthetic pathway. How many polypeptides are involved? Where are they located? What are their functions? What are the consequences of changing their amounts or types? Etc. Therefore, the goal of this thesis was to explore some of these fundamental questions by an overall study of SPT, the first and key enzyme in this pathway, at a gene expression level, a protein level and an *in situ* enzyme activity level.

We found that SPT1 protein was not only in the ER but also in focal adhesions and the nucleus using immunofluorescence confocal microscopy. SPT1 co-localizes and interacts with a focal adhesion marker protein, vinculin. The siRNA silencing of *SPTLC1* but not *SPTLC2* caused cell morphology changes, and this phenomenon does not appear to be related to sphingolipid changes. Furthermore, SPT1 focal adhesion staining disappeared when the cells reached confluence and appeared in migrating cells. It also colocalized with ABCA1, a lipid transporter to form HDL particles, at focal adhesion like structures. Therefore, our results suggest a role of SPT1 in processes beyond just initiation of de novo sphingolipid biosynthesis, including cell morphology and cell migration.

Our interpretation of the sequences of the *SPTLC1* mRNA isoforms in GenBank suggests that they were generated by alternative splicing, and the endogenous expression of at least one, *SPTLC1L,* in HEK293 cells by Western blotting confirms this prediction. The functions of such isoforms are not yet clear, but they may help explain differences in subcellular localization, regulation or other aspects of sphingolipid biology.

Overexpression of *SPTLC1* and *SPTLC2* in HEK293 cells (SPT1/2 cells) elevated SPT enzyme activity. The dynamics of *de novo* synthesis of sphingolipids was measured in both HEK293 cells and SPT1/2 cells after cells were incubated with [^{13}C]-palmitate. The *de novo* synthesized sphingolipids increased more rapidly in SPT1/2 cells than in HEK293 cells except for SM. Sphingolipid subspecies with different fatty acyl-chains were compared in the two cell types and C18 subspecies had the highest fold elevation in SPT1/2 cells. That SM did not increase to the same extent in SPT1/2 cells does not appear to be due to increased SM degradation, but rather, appears to be due to a change in the substrate pool—i.e., elevation of dihydroceramidse. The elevated SPT activity by its stable overexpression evidently increased the flux through the pathway and the amounts of up-stream molecules to the such a high degree that it exceeded the capacity of the down-stream enzymes, such as dihydroceramide desaturase, to accommodate them, thus slowing down the relative production of some of the later products of the pathway.

The finding of elevated amounts of two novel sphingoid base species, the 1-deoxy-sphingoids, in SPT1/2 cells suggests that SPT uses not only serine but also alanine and glycine as its substrate to synthesize these sphingolipids.

Also, it was of interest that overexpression of SPT caused accumulation of cytotoxic sphingolipids (ceramides as well as sphingoid bases) but the cells did not die and instead grow faster. It has been known that sphingolipids participate in various biological responses such as stress response, cell cycle arrest and apoptosis etc. (3) and some chemotherapy drugs, like etoposide and doxorubicin (70, 152), act through increasing intracellular ceramide. Our study of SPT activity *in situ* using [^{13}C]-palmitate labeling allowed us to follow the flux through the pathway, and to find that ceramide elevation can occur without cell killing. Therefore, the elevation of ceramide in cases where it is cytotoxic apparently reflects that it is necessary for cell death, but not necessarily sufficient alone.

Our studies of SPT have revealed that the complexity of this protein is much greater than has been previously appreciated. Not only its classic sphingolipid biosynthesis function was further investigated but also its novel function at novel locations was explored. Our finding of SPT1 in the nucleus and focal adhesions implicate it in cell morphology, migration and signaling. Glycosphingolipids and S1P have been found to be involved in focal adhesion and cell migration (4, 12), but this is the first report that a sphingolipid synthesis enzyme plays a direct role in the processes. SPT1 may become a new model in the family of multi-functioning proteins and provide a clue of regulation of sphingolipid synthesis. More studies are needed to elucidate the molecular structure and connections of SPT1 in these locations.

Future studies should also measure the impact of SPT overexpression on more complex GSL. Analyzing these molecules will be a heavy task, requiring high throughput MS methods and efficient data analysis tools. But once the methods are developed, the *de novo* synthesis of sphingolipids can also be explored in different biological systems. For example, the stem cells would be an interesting object to study because complete knockout of *SPTLC1* or *SPTLC2* is lethal for embryos (87) though sphingolipids can be taken from the serum. And, point mutations of *SPTLC1* cause HSN1 disease, and there may be others that have not yet been found (and it would be interesting to know if the mutations in HSN1 patients affect SPT1 novel functions which we found in this study). Obviously, more work is required to define the mechanisms of regulation of the enzyme and roles of the pathway in specific biological systems.

APPENDIX

Quantification of sphingolipids in HEK293 and SPT1/2 cells after [^{13}C]-palmitate treatment

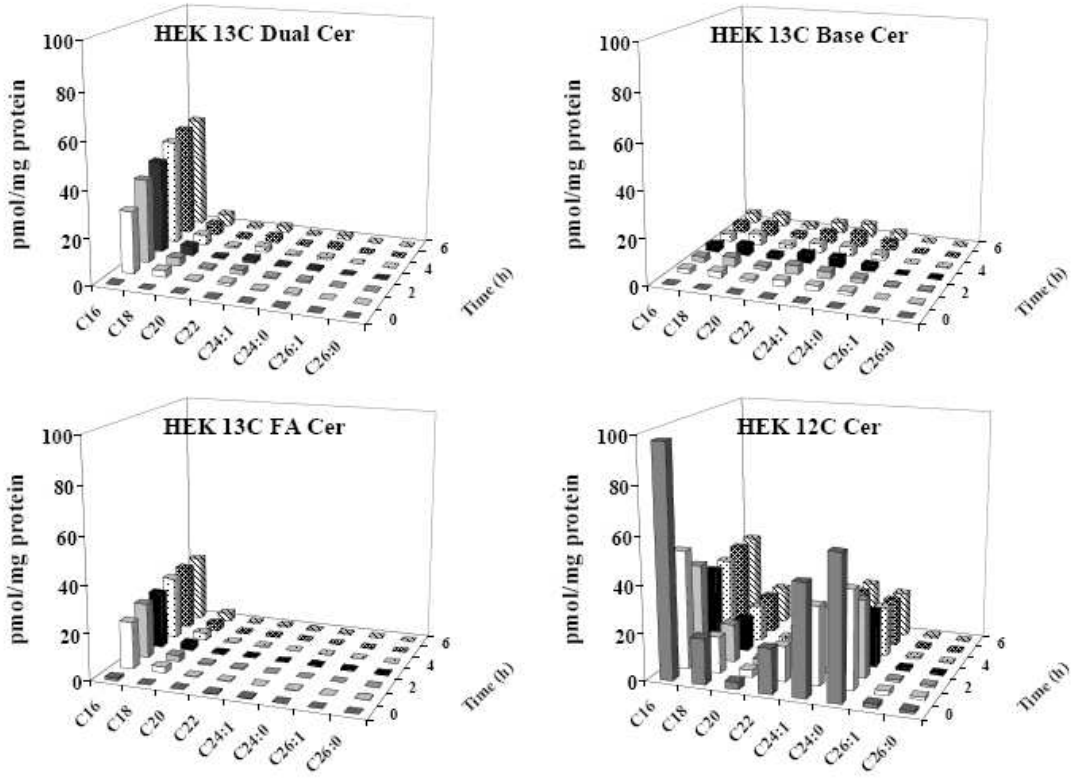

Fig. A.1 Ceramide analysis in HEK293 cells treated with 0.1 mM [^{13}C]-palmitate HEK293 cells were incubated in the complete growth medium containing 0.1 mM ^{13}C-palmitate for 0 to 6 hours. Cells were collected every hour for lipid extraction. Then the samples were analyzed by HPLC and ESI-MS/MS. Ceramide molecules with various fatty acyl chain lengths were quantified. ^{13}C dual labeling (up left), base labeling (up right), fatty acid labeling (bottom left) and unlabeled ceramide (bottom right) are presented in the figure.

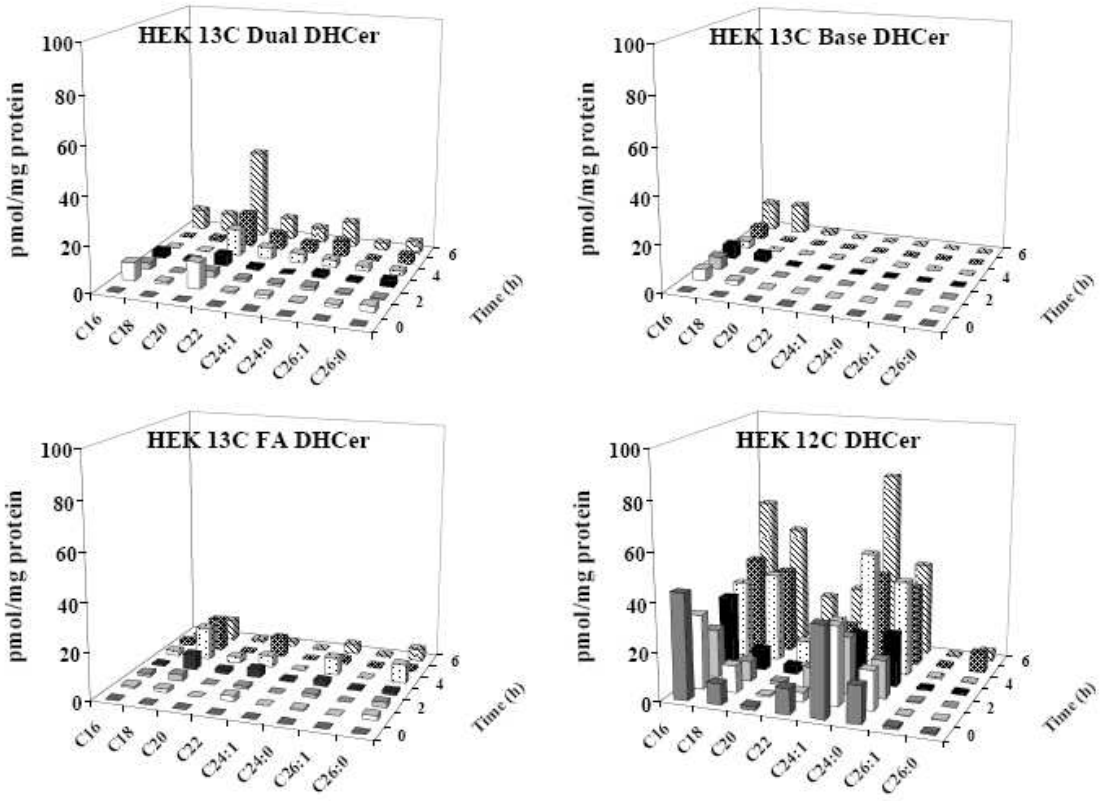

Fig. A.2 DHCer analysis in HEK293 cells treated with 0.1 mM [^{13}C]-palmitate
Same treatment was done as described above. ^{13}C dual labeling (up left), base labeling (up right), fatty acid labeling (bottom left) and unlabeled dihydroceramide (bottom right) are presented in the figure.

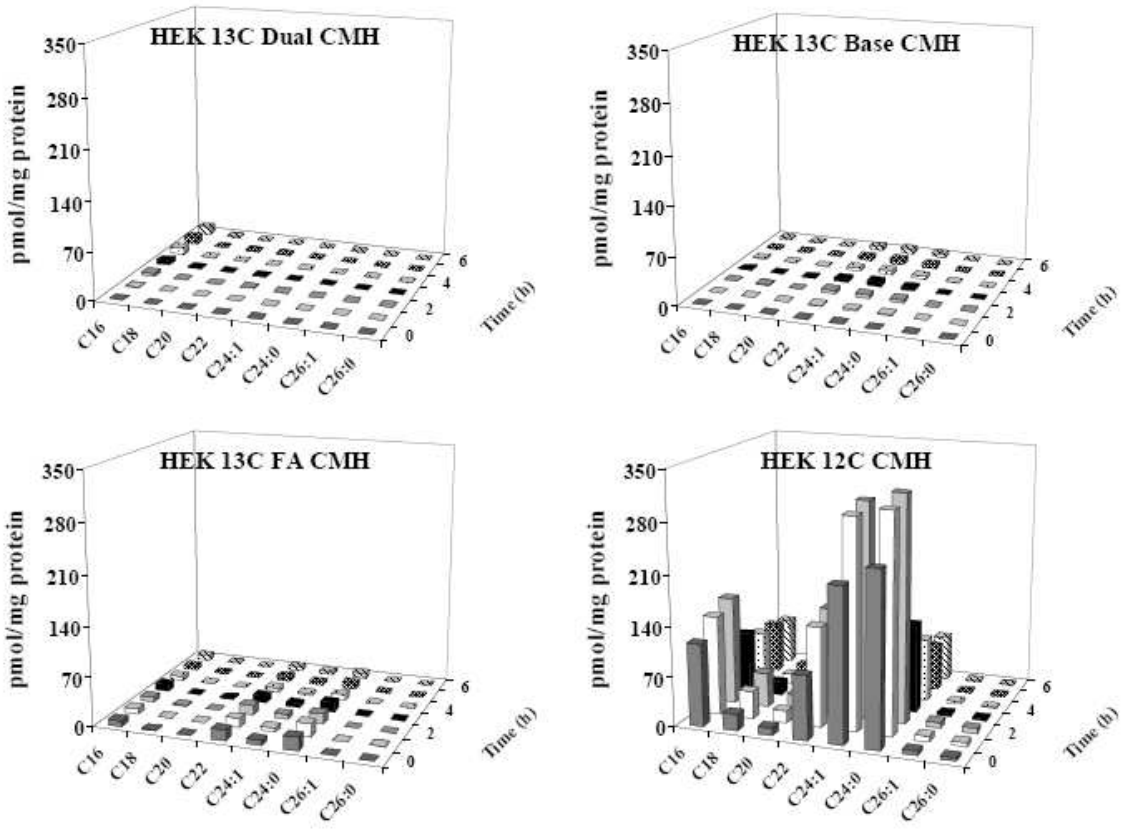

Fig. A.3 CMH analysis in HEK293 cells treated with 0.1 mM [^{13}C]-palmitate
Same treatment was done as above. ^{13}C dual labeling (up left), base labeling (up right), fatty acid labeling (bottom left) and unlabeled CMH (bottom right) are presented in the figure.

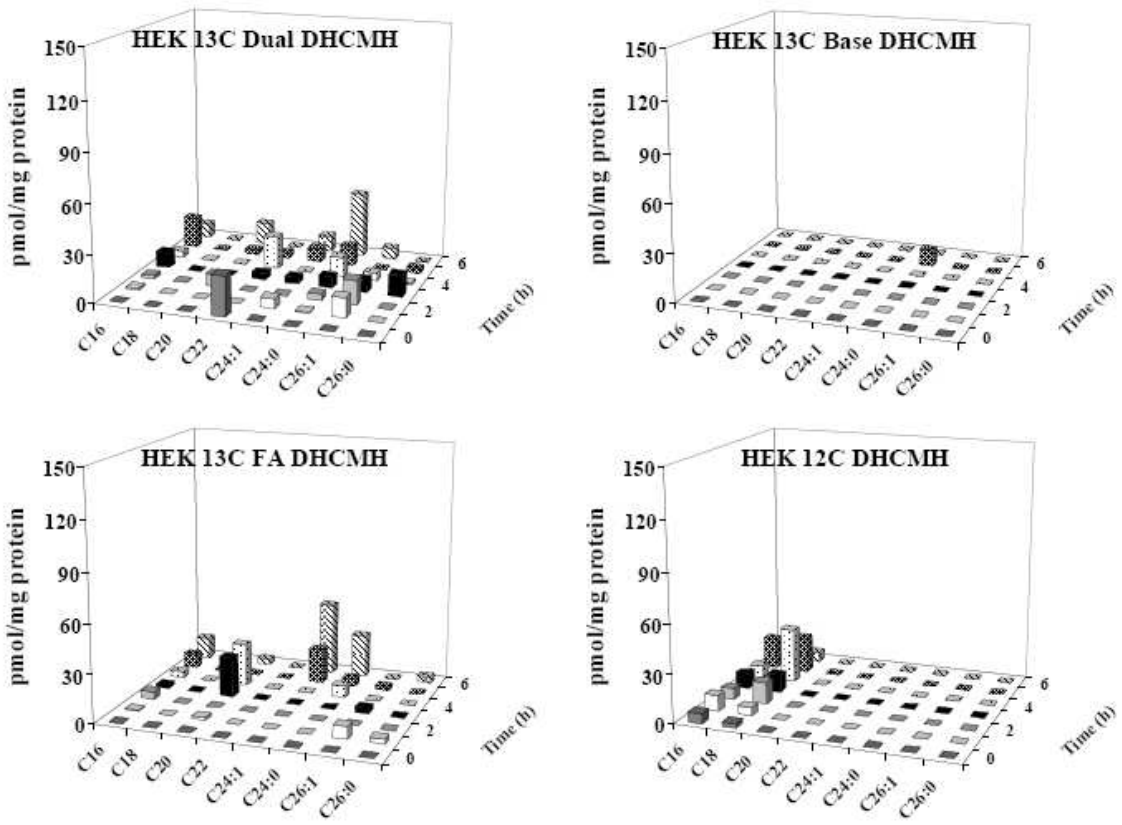

Fig. A.4 DHCMH analysis in HEK293 cells treated with 0.1 mM [^{13}C]-palmitate

Same treatment was done as above. ^{13}C dual labeling (up left), base labeling (up right), fatty acid labeling (bottom left) and unlabeled DHCMH (bottom right) are presented in the figure.

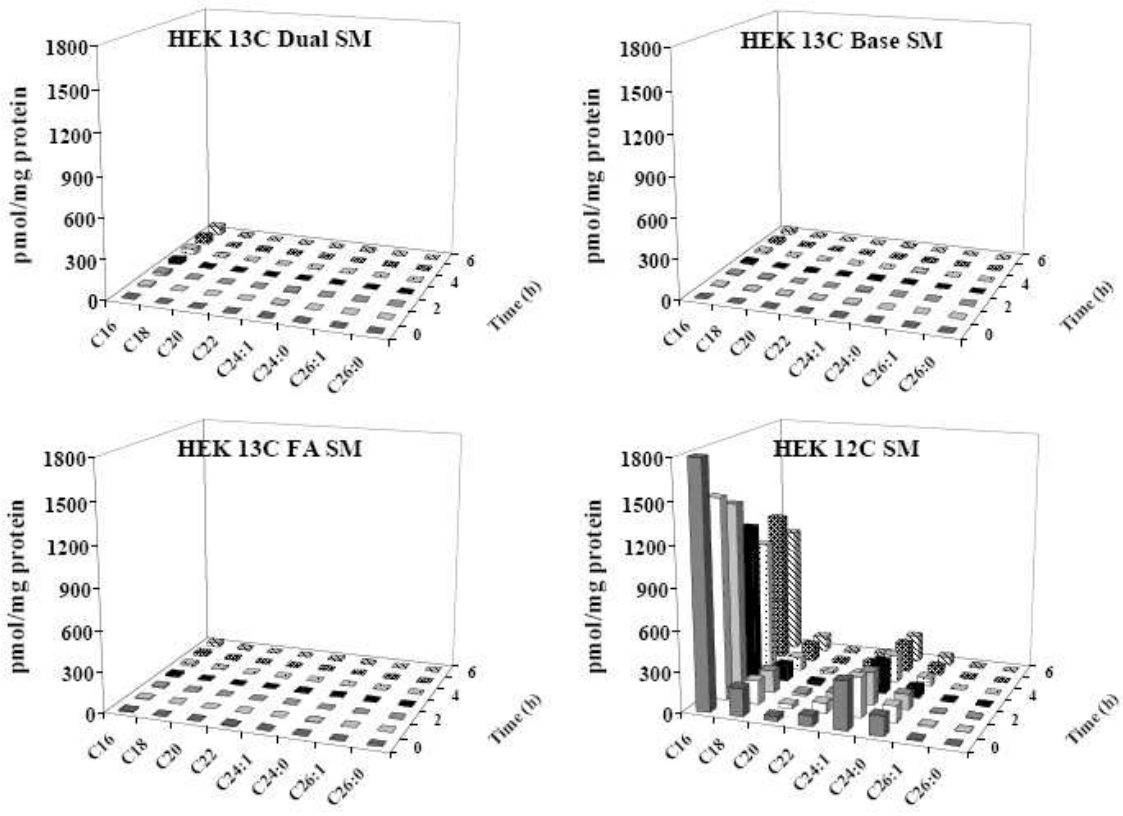

Fig. A.5 SM analysis in HEK293 cells treated with 0.1 mM [^{13}C]-palmitate
Same treatment was done as above. ^{13}C dual labeling (up left), base labeling (up right), fatty acid labeling (bottom left) and unlabeled SM (bottom right) are presented in the figure.

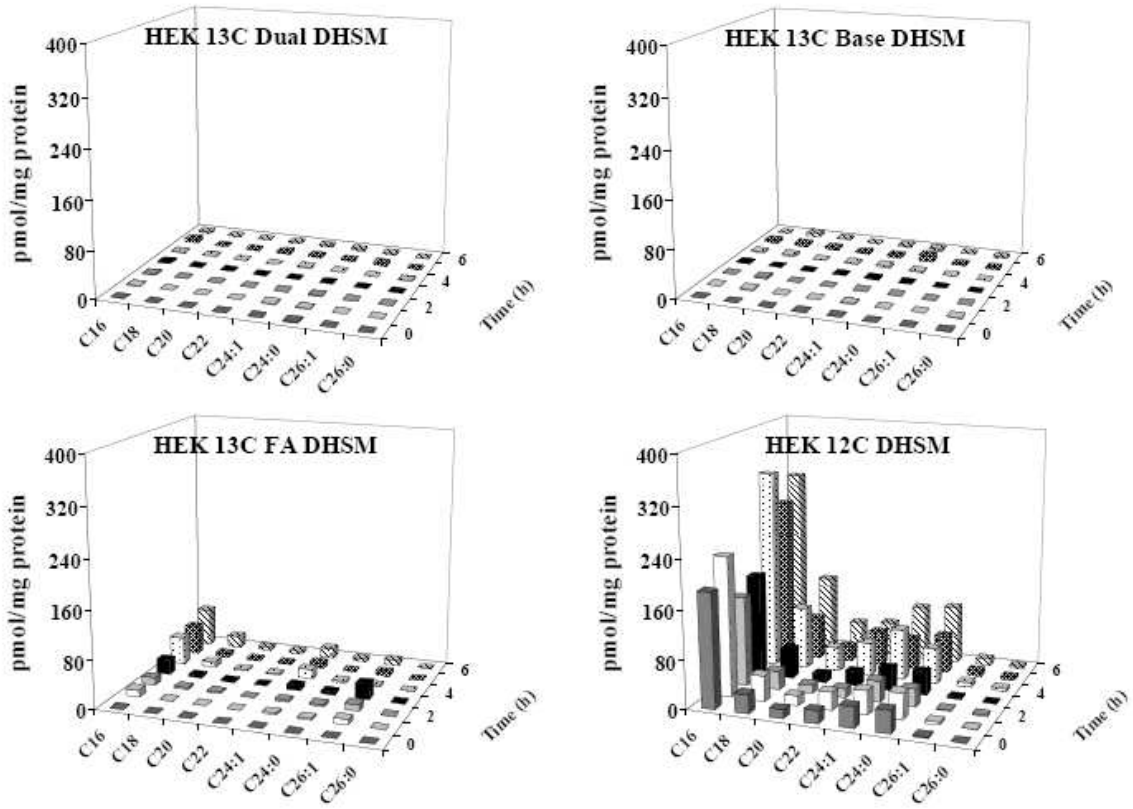

Fig. A.6 DHSM analysis in HEK293 cells treated with 0.1 mM [^{13}C]-palmitate
Same treatment was done as above. ^{13}C dual labeling (up left), base labeling (up right), fatty acid labeling (bottom left) and unlabeled dihydrosphingomyelin (bottom right) are presented in the figure.

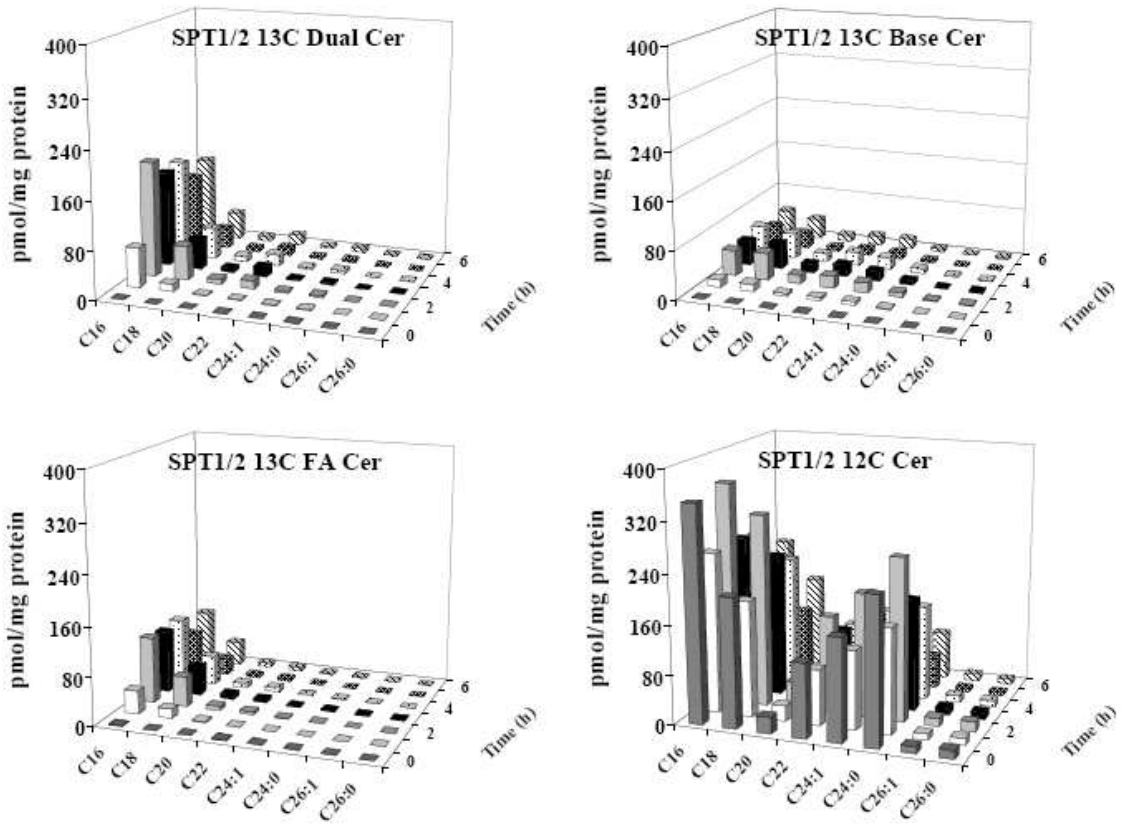

Fig. A.7 Cer analysis in SPT1/2 cells treated with 0.1 mM [^{13}C]-palmitate
Same treatment was done as above in SPT1/2 cells. ^{13}C dual labeling (up left), base labeling (up right), fatty acid labeling (bottom left) and unlabeled ceramide (bottom right) are presented in the figure.

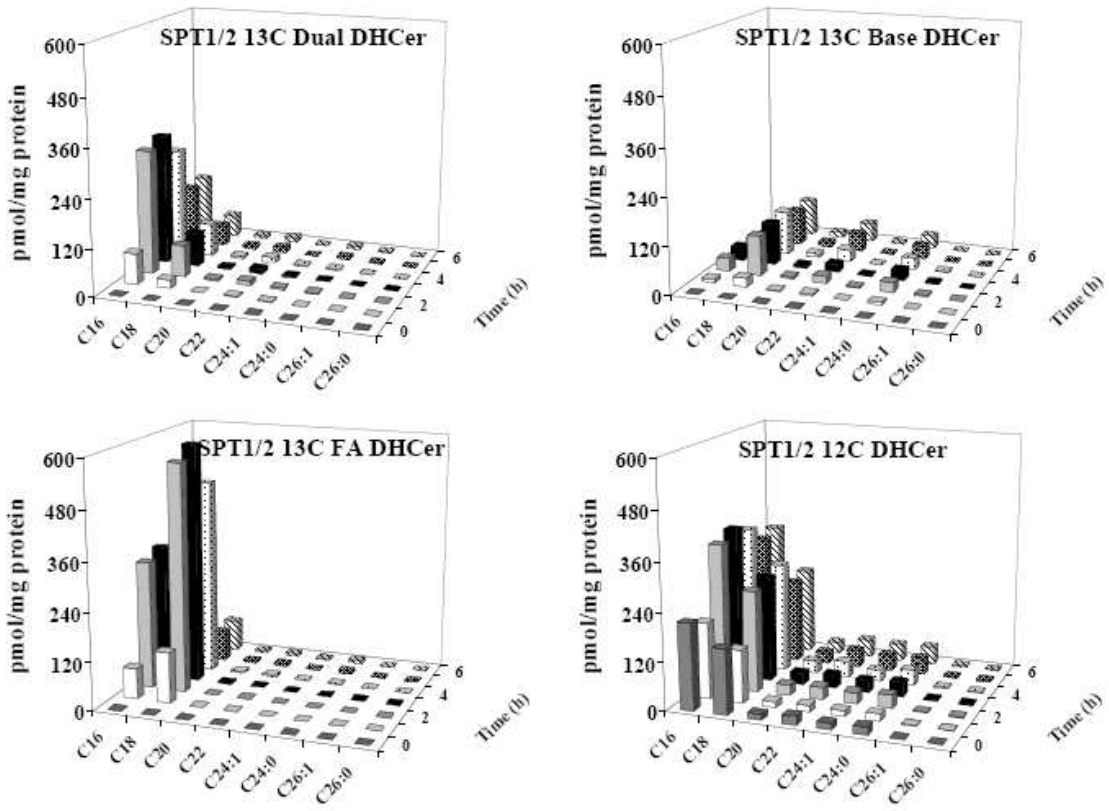

Fig. A.8 DHCer analysis in SPT1/2 cells treated with 0.1 mM [^{13}C]-palmitate
Same treatment was done as above in SPT1/2 cells. ^{13}C dual labeling (up left), base labeling (up right), fatty acid labeling (bottom left) and unlabeled dihydroceramide (bottom right) are presented in the figure.

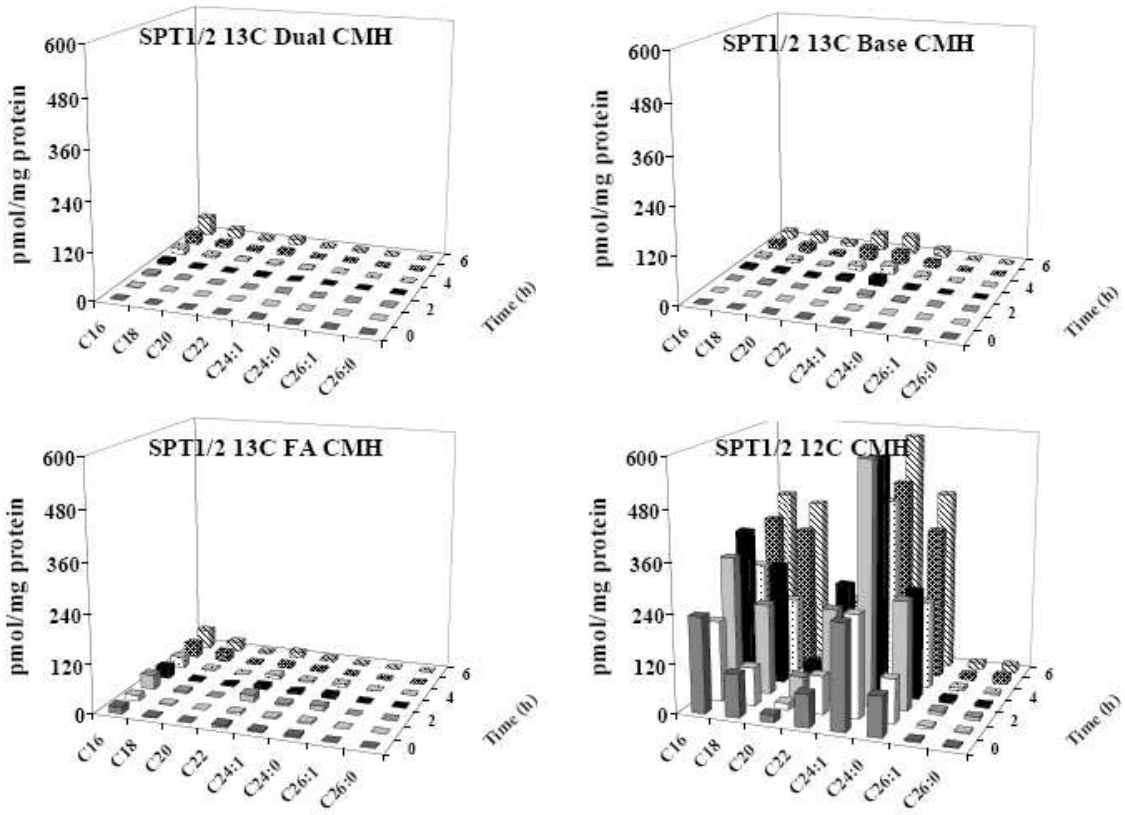

Fig. A.9 CMH analysis in SPT1/2 cells treated with 0.1 mM [^{13}C]-palmitate
Same treatment was done as above in SPT1/2 cells. ^{13}C dual labeling (up left), base labeling (up right), fatty acid labeling (bottom left) and unlabeled ceramide monohexocide (bottom right) are presented in the figure.

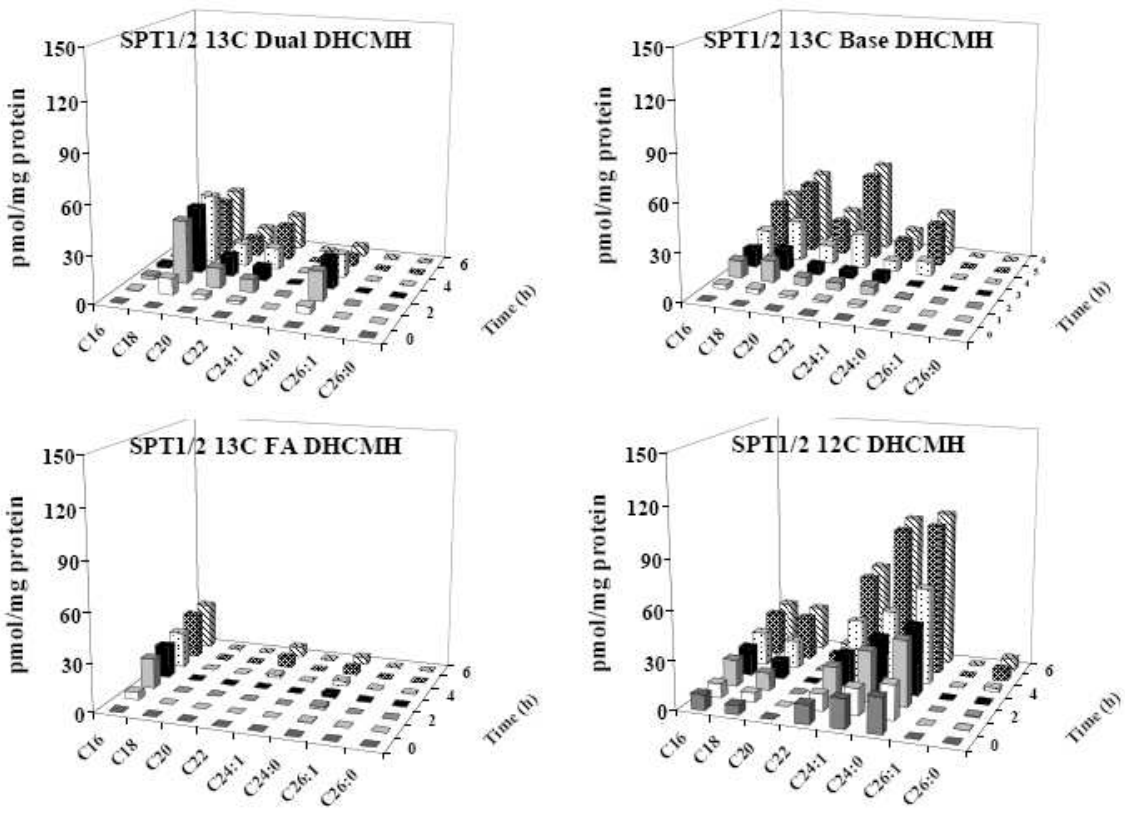

Fig. A.10 DHCMH analysis in SPT1/2 cells treated with 0.1 mM [^{13}C]-palmitate
Same treatment was done as above in SPT1/2 cells. ^{13}C dual labeling (up left), base labeling (up right), fatty acid labeling (bottom left) and unlabeled dihydroceramide monohexocide (bottom right) are presented in the figure.

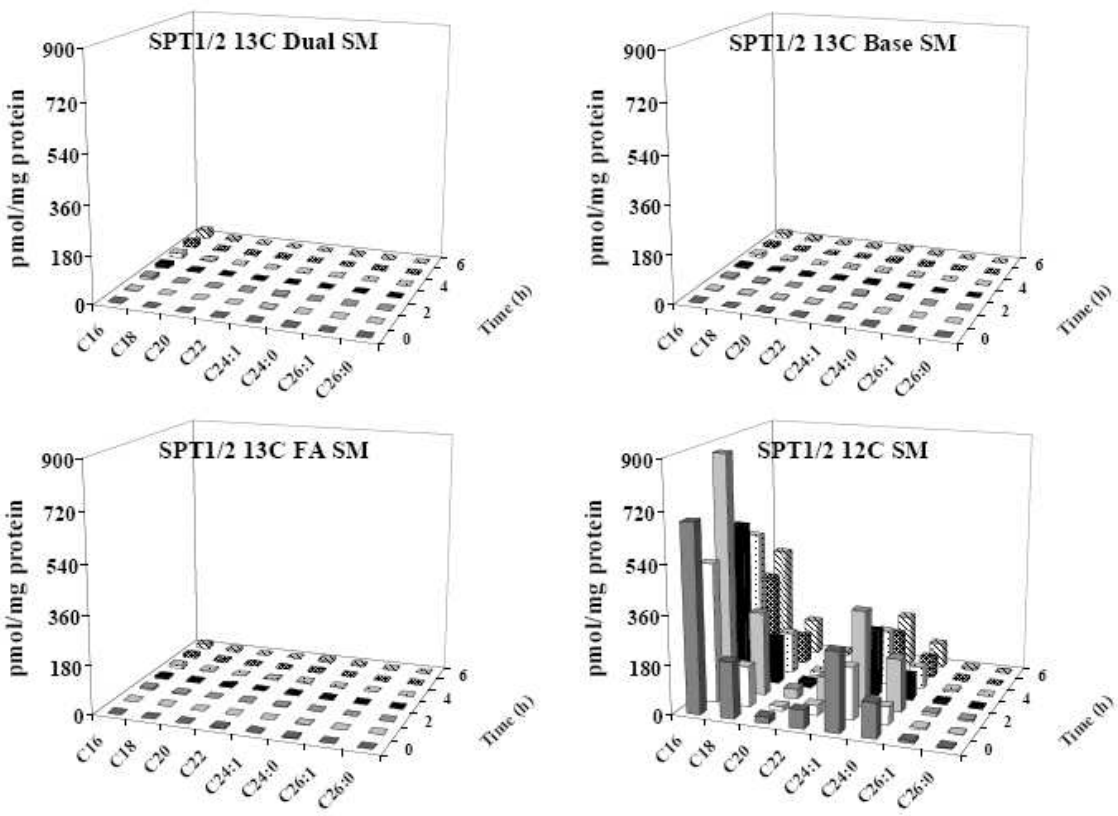

Fig. A.11 SM analysis in SPT1/2 cells treated with 0.1 mM [^{13}C]-palmitate
Same treatment was done as above in SPT1/2 cells. ^{13}C dual labeling (up left), base labeling (up right), fatty acid labeling (bottom left) and unlabeled sphingomyelin (bottom right) are presented in the figure.

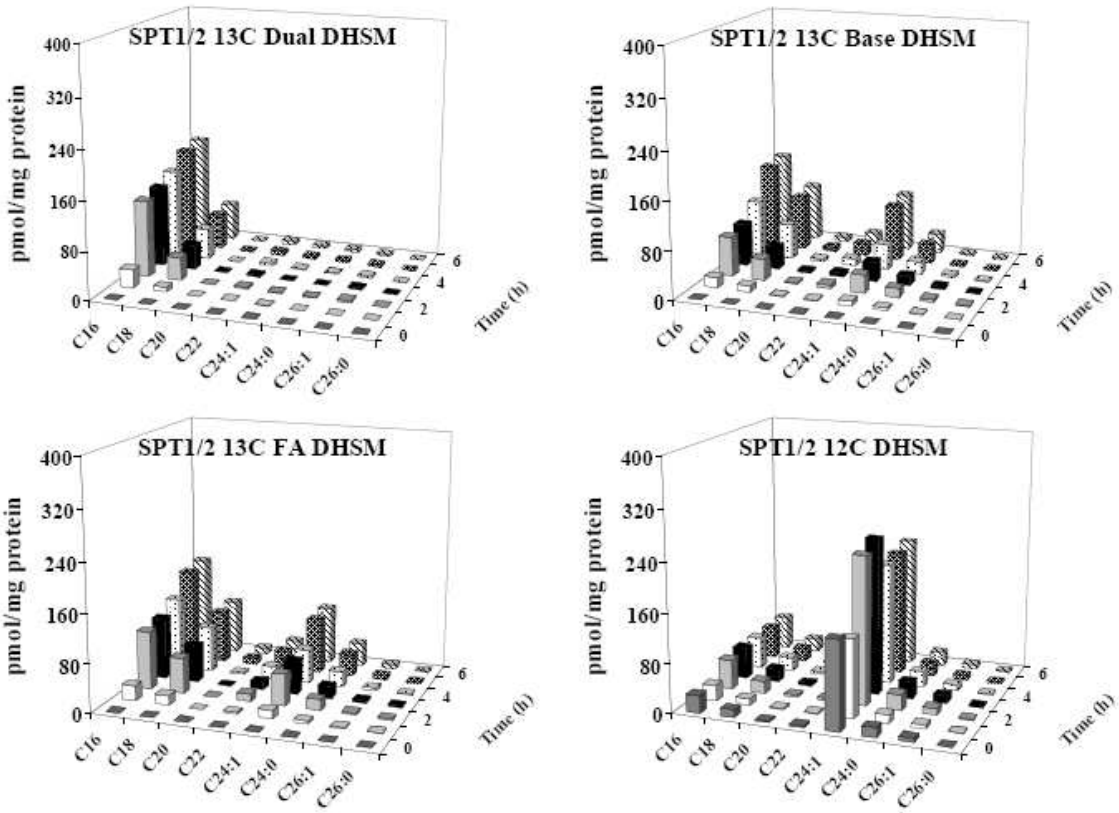

Fig. A.12 DHSM analysis in SPT1/2 cells treated with 0.1 mM [^{13}C]-palmitate
Same treatment was done as above in SPT1/2 cells. ^{13}C dual labeling (up left), base labeling (up right), fatty acid labeling (bottom left) and unlabeled dihydrosphingomyelin (bottom right) are presented in the figure.

REFERENCES

1. Merrill AH, Jr. & Sandhoff, K (2002) in *New Comprehensive Biochemistry: Biochemistry of Lipids,Lipoproteins,and Membranes*, ed. eds VDVJ (Elsevier Science Publ., Amsterdam).

2. Merrill AH, Jr. (2002) *J Biol Chem* **277,** 25843-25846.

3. Hannun YA & Obeid LM (2008) *Nat Rev Mol Cell Biol* **9,** 139-150.

4. Spiegel S & Milstien S (2003) *Nat Rev Mol Cell Biol* **4,** 397-407.

5. Merrill AH, Jr., Wang MD, Park M, & Sullards MC (2007) *Trends Biochem Sci* **32,** 457-468.

6. Wei J, Tokumbo, Y., Liepelt, M., Momin, A., Wang, E., Hanada, K., Merrill, A.H. (2006) in *Sphingolipid Biology*, ed. Hirabayashi Y, Igarashi, Y., Merrill, A.H. (Springer, Tokyo), p. 25~47.

7. Smith ER, Merrill AH, Obeid LM, & Hannun YA (2000) *Methods Enzymol* **312,** 361-373.

8. Obeid LM, Linardic CM, Karolak LA, & Hannun YA (1993) *Science* **259,** 1769-1771.

9. Venable ME, Lee JY, Smyth MJ, Bielawska A, & Obeid LM (1995) *J Biol Chem* **270,** 30701-30708.

10. Zheng W, Kollmeyer J, Symolon H, Momin A, Munter E, Wang E, Kelly S, Allegood JC, Liu Y, Peng Q*, et al.* (2006) *Biochim Biophys Acta* **1758,** 1864-1884.

11. Hla T (2004) *Semin Cell Dev Biol* **15,** 513-520.

12. Hakomori SI (2000) *Glycoconj J* **17,** 143-151.

13. Todeschini AR, Dos Santos JN, Handa K, & Hakomori SI (2008) *Proc Natl Acad Sci U S A* **105,** 1925-1930.

14. Braun PE & Snell EE (1967) *Proc Natl Acad Sci U S A* **58,** 298-303.

15. Stoffel W, LeKim D, & Sticht G (1968) *Hoppe Seylers Z Physiol Chem* **349,** 664-670.

16. Hanada K (2003) *Biochim Biophys Acta* **1632,** 16-30.

17. Hanada K, Hara T, & Nishijima M (2000) *J Biol Chem* **275,** 8409-8415.

18. Yasuda S, Nishijima M, & Hanada K (2003) *J Biol Chem* **278,** 4176-4183.

19. Hornemann T, Richard S, Rutti MF, Wei Y, & von Eckardstein A (2006) *J Biol Chem* **281,** 37275-37281.

20. Pinto WJ, Srinivasan B, Shepherd S, Schmidt A, Dickson RC, & Lester RL (1992) *J Bacteriol* **174,** 2565-2574.

21. Buede R, Rinker-Schaffer C, Pinto WJ, Lester RL, & Dickson RC (1991) *J Bacteriol* **173,** 4325-4332.

22. Nagiec MM, Baltisberger JA, Wells GB, Lester RL, & Dickson RC (1994) *Proc Natl Acad Sci U S A* **91,** 7899-7902.

23. Weiss B & Stoffel W (1997) *Eur J Biochem* **249,** 239-247.

24. Hanada K, Hara T, Nishijima M, Kuge O, Dickson RC, & Nagiec MM (1997) *J Biol Chem* **272,** 32108-32114.

25. Nagiec MM, Lester RL, & Dickson RC (1996) *Gene* **177,** 237-241.

26. Gable K, Slife H, Bacikova D, Monaghan E, & Dunn TM (2000) *J Biol Chem* **275,** 7597-7603.

27. Inuzuka M, Hayakawa M, & Ingi T (2005) *J Biol Chem*.

28. Gavin AC, Bosche M, Krause R, Grandi P, Marzioch M, Bauer A, Schultz J, Rick JM, Michon AM, Cruciat CM*, et al.* (2002) *Nature* **415,** 141-147.

29. Giot L, Bader JS, Brouwer C, Chaudhuri A, Kuang B, Li Y, Hao YL, Ooi CE, Godwin B, Vitols E*, et al.* (2003) *Science* **302,** 1727-1736.

30. Ikushiro H, Hayashi H, & Kagamiyama H (2001) *J Biol Chem* **276,** 18249-18256.

31. Williams RD, Wang E, & Merrill AH, Jr. (1984) *Arch Biochem Biophys* **228,** 282-291.

32. Di Mari SJ, Brady RN, & Snell EE (1971) *Arch Biochem Biophys* **143,** 553-565.

33. Krisnangkura K & Sweeley CC (1976) *J Biol Chem* **251,** 1597-1602.

34. Zaman Z, Jordan PM, & Akhtar M (1973) *Biochem J* **135,** 257-263.

35. Ikushiro H, Hayashi H, & Kagamiyama H (2003) *Biochim Biophys Acta* **1647,** 116-120.

36. Acharya U & Acharya JK (2005) *Cell Mol Life Sci* **62,** 128-142.

37. Sonnino S & Chigorno V (2000) *Biochim Biophys Acta* **1469,** 63-77.

38. Sugiura Y, Shimma S, Konishi Y, Yamada MK, & Setou M (2008) *PLoS ONE* **3,** e3232.

39. Liu K, Zhang X, Sumanasekera C, Lester RL, & Dickson RC (2005) *Biochem Soc Trans* **33,** 1170-1173.

40. Merrill AH, Jr., Wang E, & Mullins RE (1988) *Biochemistry* **27,** 340-345.

41. Messmer TO, Wang E, Stevens VL, & Merrill AH, Jr. (1989) *J Nutr* **119,** 534-538.

42. Hanada K, Hara T, & Nishijima M (2000) *FEBS Lett* **474,** 63-65.

43. Zitomer NC, Mitchell T, Voss KA, Bondy GS, Pruett ST, Garnier-Amblard EC, Liebeskind LS, Park H, Wang E, Sullards MC*, et al.* (2009) *J Biol Chem* **284,** 4786-4795.

44. Alvarez-Vasquez F, Sims KJ, Cowart LA, Okamoto Y, Voit EO, & Hannun YA (2005) *Nature* **433,** 425-430.

45. Cowart LA & Hannun YA (2005) *Biochem Soc Trans* **33,** 1166-1169.

46. Sims KJ, Spassieva SD, Voit EO, & Obeid LM (2004) *Biochem Cell Biol* **82,** 45-61.

47. Yamaji-Hasegawa A, Takahashi A, Tetsuka Y, Senoh Y, & Kobayashi T (2005) *Biochemistry* **44,** 268-277.

48. Zweerink MM, Edison AM, Wells GB, Pinto W, & Lester RL (1992) *J Biol Chem* **267,** 25032-25038.

49. Mandala SM, Frommer BR, Thornton RA, Kurtz MB, Young NM, Cabello MA, Genilloud O, Liesch JM, Smith JL, & Horn WS (1994) *J Antibiot (Tokyo)* **47,** 376-379.

50. Miyake Y, Kozutsumi Y, Nakamura S, Fujita T, & Kawasaki T (1995) *Biochem Biophys Res Commun* **211,** 396-403.

51. Mandala SM, Thornton RA, Frommer BR, Dreikorn S, & Kurtz MB (1997) *J Antibiot (Tokyo)* **50,** 339-343.

52. Ikushiro H, Hayashi H, & Kagamiyama H (2004) *Biochemistry* **43,** 1082-1092.

53. Merrill AH, Jr., Nixon DW, & Williams RD (1985) *J Lipid Res* **26,** 617-622.

54. Longo CA, Tyler D, & Mallampalli RK (1997) *Am J Respir Cell Mol Biol* **16,** 605-612.

55. Geelen MJ & Beynen AC (2000) *Br J Nutr* **83,** 541-547.

56. Rotta LN, Da Silva CG, Perry ML, & Trindade VM (1999) *Ann Nutr Metab* **43,** 152-158.

57. Memon RA, Holleran WM, Moser AH, Seki T, Uchida Y, Fuller J, Shigenaga JK, Grunfeld C, & Feingold KR (1998) *Arterioscler Thromb Vasc Biol* **18,** 1257-1265.

58. Grether-Beck S, Timmer A, Felsner I, Brenden H, Brammertz D, & Krutmann J (2005) *J Invest Dermatol* **125,** 545-553.

59. Farrell AM, Uchida Y, Nagiec MM, Harris IR, Dickson RC, Elias PM, & Holleran WM (1998) *J Lipid Res* **39,** 2031-2038.

60. Holleran WM, Feingold KR, Man MQ, Gao WN, Lee JM, & Elias PM (1991) *J Lipid Res* **32,** 1151-1158.

61. Memon RA, Grunfeld C, Moser AH, & Feingold KR (1993) *Endocrinology* **132,** 2246-2253.

62. Holleran WM, Uchida Y, Halkier-Sorensen L, Haratake A, Hara M, Epstein JH, & Elias PM (1997) *Photodermatol Photoimmunol Photomed* **13,** 117-128.

63. Tanno O, Ota Y, Kitamura N, Katsube T, & Inoue S (2000) *Br J Dermatol* **143,** 524-531.

64. Shimabukuro M, Higa M, Zhou YT, Wang MY, Newgard CB, & Unger RH (1998) *J Biol Chem* **273,** 32487-32490.

65. Deevska GM, Rozenova KA, Giltiay NV, Chambers MA, White J, Boyanovsky BB, Wei J, Daugherty A, Smart EJ, Reid MB*, et al.* (2008) *J Biol Chem.*

66. Paumen MB, Ishida Y, Muramatsu M, Yamamoto M, & Honjo T (1997) *J Biol Chem* **272,** 3324-3329.

67. Listenberger LL, Ory DS, & Schaffer JE (2001) *J Biol Chem* **276,** 14890-14895.

68. Blazquez C, Geelen MJ, Velasco G, & Guzman M (2001) *FEBS Lett* **489,** 149-153.

69. Herget T, Esdar C, Oehrlein SA, Heinrich M, Schutze S, Maelicke A, & van Echten-Deckert G (2000) *J Biol Chem* **275,** 30344-30354.

70. Perry DK, Carton J, Shah AK, Meredith F, Uhlinger DJ, & Hannun YA (2000) *J Biol Chem* **275,** 9078-9084.

71. Jenkins GM, Cowart LA, Signorelli P, Pettus BJ, Chalfant CE, & Hannun YA (2002) *J Biol Chem* **277,** 42572-42578.

72. Friant S, Meier KD, & Riezman H (2003) *Embo J* **22,** 3783-3791.

73. Mandon EC, van Echten G, Birk R, Schmidt RR, & Sandhoff K (1991) *Eur J Biochem* **198,** 667-674.

74. van Echten-Deckert G, Zschoche A, Bar T, Schmidt RR, Raths A, Heinemann T, & Sandhoff K (1997) *J Biol Chem* **272,** 15825-15833.

75. Triola G, Fabrias G, Dragusin M, Niederhausen L, Broere R, Llebaria A, & van Echten-Deckert G (2004) *Mol Pharmacol* **66,** 1671-1678.

76. Ridgway ND & Merriam DL (1995) *Biochim Biophys Acta* **1256,** 57-70.

77. van Echten-Deckert G, Giannis A, Schwarz A, Futerman AH, & Sandhoff K (1998) *J Biol Chem* **273,** 1184-1191.

78. Memon RA, Holleran WM, Uchida Y, Moser AH, Grunfeld C, & Feingold KR (2001) *J Lipid Res* **42,** 452-459.

79. Scarlatti F, Sala G, Somenzi G, Signorelli P, Sacchi N, & Ghidoni R (2003) *Faseb J* **17,** 2339-2341.

80. Gomez del Pulgar T, Velasco G, Sanchez C, Haro A, & Guzman M (2002) *Biochem J* **363,** 183-188.

81. Lehtonen JY, Horiuchi M, Daviet L, Akishita M, & Dzau VJ (1999) *J Biol Chem* **274,** 16901-16906.

82. Wang H, Maurer BJ, Reynolds CP, & Cabot MC (2001) *Cancer Res* **61,** 5102-5105.

83. Billi de Catabbi SC, Setton-Advruj CP, Sterin-Speziale N, San Martin de Viale LC, & Cochon AC (2000) *Toxicology* **149,** 89-100.

84. Jeong T, Schissel SL, Tabas I, Pownall HJ, Tall AR, & Jiang X (1998) *J Clin Invest* **101,** 905-912.

85. Hanada K, Nishijima M, & Akamatsu Y (1990) *J Biol Chem* **265,** 22137-22142.

86. Adachi-Yamada T, Gotoh T, Sugimura I, Tateno M, Nishida Y, Onuki T, & Date H (1999) *Mol Cell Biol* **19,** 7276-7286.

87. Hojjati MR, Li Z, & Jiang XC (2005) *Biochim Biophys Acta* **1737,** 44-51.

88. Dedov VN, Dedova IV, Merrill AH, Jr., & Nicholson GA (2004) *Biochim Biophys Acta* **1688,** 168-175.

89. Daigo M, Arai Y, Oshida K, Kitamura Y, Hayashi M, Shimizu T, & Yamashiro Y (2008) *Pathobiology* **75,** 330-334.

90. Wang H, Charles AG, Frankel AJ, & Cabot MC (2003) *Urology* **61,** 1047-1052.

91. Reynolds CP, Maurer BJ, & Kolesnick RN (2004) *Cancer Lett* **206,** 169-180.

92. Wang H, Maurer BJ, Liu YY, Wang E, Allegood JC, Kelly S, Symolon H, Liu Y, Merrill AH, Jr., Gouaze-Andersson V*, et al.* (2008) *Mol Cancer Ther* **7,** 2967-2976.

93. Schiffmann S, Sandner J, Schmidt R, Birod K, Wobst I, Schmidt H, Angioni C, Geisslinger G, & Grosch S (2009) *Journal of lipid research* **50,** 32-40.

94. Jiang Q, Wong J, & Ames BN (2004) *Ann N Y Acad Sci* **1031,** 399-400.

95. Scarlatti F, Bauvy C, Ventruti A, Sala G, Cluzeaud F, Vandewalle A, Ghidoni R, & Codogno P (2004) *J Biol Chem* **279,** 18384-18391.

96. Hojjati MR, Li Z, Zhou H, Tang S, Huan C, Ooi E, Lu S, & Jiang XC (2005) *J Biol Chem* **280,** 10284-10289.

97. Sawamura N, Ko M, Yu W, Zou K, Hanada K, Suzuki T, Gong JS, Yanagisawa K, & Michikawa M (2004) *J Biol Chem* **279,** 11984-11991.

98. Batheja AD, Uhlinger DJ, Carton JM, Ho G, & D'Andrea MR (2003) *J Histochem Cytochem* **51,** 687-696.

99. Moore JD, Caufield WV, & Shaw WA (2007) *Methods in enzymology* **432,** 351-367.

100. Sullards MC & Merrill AH, Jr. (2001) *Sci STKE* **2001,** PL1.

101. Sullards MC, Allegood JC, Kelly S, Wang E, Haynes CA, Park H, Chen Y, & Merrill AH, Jr. (2007) *Methods Enzymol* **432,** 83-115.

102. Liu B & Hannun YA (2000) *Methods Enzymol* **311,** 164-167.

103. Mizutani Y, Kihara A, & Igarashi Y (2005) *Biochem J* **390,** 263-271.

104. Mizutani Y, Kihara A, & Igarashi Y (2006) *Biochem J* **398,** 531-538.

105. Pewzner-Jung Y, Ben-Dor S, & Futerman AH (2006) *J Biol Chem* **281,** 25001-25005.

106. Riebeling C, Allegood JC, Wang E, Merrill AH, Jr., & Futerman AH (2003) *J Biol Chem* **278,** 43452-43459.

107. Lahiri S & Futerman AH (2005) *J Biol Chem* **280,** 33735-33738.

108. Mandon EC, Ehses I, Rother J, van Echten G, & Sandhoff K (1992) *J Biol Chem* **267,** 11144-11148.

109. Alvarez SE, Milstien S, & Spiegel S (2007) *Trends in endocrinology and metabolism: TEM* **18,** 300-307.

110. Chalfant CE & Spiegel S (2005) *J Cell Sci* **118,** 4605-4612.

111. Coward J, Ambrosini G, Musi E, Truman JP, Haimovitz-Friedman A, Allegood JC, Wang E, Merrill AH, Jr., & Schwartz GK (2009) *Autophagy* **5**.

112. Sanchez AM, Malagarie-Cazenave S, Olea N, Vara D, Cuevas C, & Diaz-Laviada I (2008) *Eur J Pharmacol* **584,** 237-245.

113. Kumagai K, Yasuda S, Okemoto K, Nishijima M, Kobayashi S, & Hanada K (2005) *J Biol Chem* **280,** 6488-6495.

114. Hanada K, Kumagai K, Tomishige N, & Kawano M (2007) *Biochim Biophys Acta* **1771,** 644-653.

115. Futerman AH & Riezman H (2005) *Trends Cell Biol* **15,** 312-318.

116. Seufferlein T & Rozengurt E (1994) *J Biol Chem* **269,** 27610-27617.

117. Wang F, Nobes CD, Hall A, & Spiegel S (1997) *Biochem J* **324 (Pt 2),** 481-488.

118. Formigli L, Meacci E, Sassoli C, Chellini F, Giannini R, Quercioli F, Tiribilli B, Squecco R, Bruni P, Francini F*, et al.* (2005) *J Cell Sci* **118,** 1161-1171.

119. Carton JM, Uhlinger DJ, Batheja AD, Derian C, Ho G, Argenteri D, & D'Andrea MR (2003) *J Histochem Cytochem* **51,** 715-726.

120. Yerokun T & Stewart J (2006) *Int J Environ Res Public Health* **3,** 252-261.

121. Tamehiro N, Zhou S, Okuhira K, Benita Y, Brown CE, Zhuang DZ, Latz E, Hornemann T, von Eckardstein A, Xavier RJ*, et al.* (2008) *Biochemistry* **47,** 6138-6147.

122. Bonifacino JS & Dell'Angelica EC (2001) *Curr Protoc Cell Biol* **Chapter 7,** Unit 7 2.

123. Lacoste J, Ma A, & Parsons JT (1998) *Methods Enzymol* **298,** 89-102.

124. Dignam JD, Lebovitz RM, & Roeder RG (1983) *Nucleic Acids Res* **11,** 1475-1489.

125. Andrin C & Hendzel MJ (2004) *The Journal of biological chemistry* **279,** 25017-25023.

126. Lampugnani MG (1999) *Methods Mol Biol* **96,** 177-182.

127. Lee AS (2005) *Methods* **35,** 373-381.

128. Pellegrin S & Mellor H (2007) *J Cell Sci* **120,** 3491-3499.

129. Hanada K, Hara T, Fukasawa M, Yamaji A, Umeda M, & Nishijima M (1998) *J Biol Chem* **273,** 33787-33794.

130. Frisch SM & Screaton RA (2001) *Curr Opin Cell Biol* **13,** 555-562.

131. Han G, Gable K, Yan L, Natarajan M, Krishnamurthy J, Gupta SD, Borovitskaya A, Harmon JM, & Dunn TM (2004) *J Biol Chem* **279,** 53707-53716.

132. Yard BA, Carter LG, Johnson KA, Overton IM, Dorward M, Liu H, McMahon SA, Oke M, Puech D, Barton GJ*, et al.* (2007) *J Mol Biol* **370,** 870-886.

133. Puntervoll P, Linding R, Gemund C, Chabanis-Davidson S, Mattingsdal M, Cameron S, Martin DM, Ausiello G, Brannetti B, Costantini A*, et al.* (2003) *Nucleic acids research* **31,** 3625-3630.

134. Sierralta J & Mendoza C (2004) *Brain Res Brain Res Rev* **47,** 105-115.

135. Kim E & Sheng M (2004) *Nat Rev Neurosci* **5,** 771-781.

136. Okuhira K, Fitzgerald ML, Sarracino DA, Manning JJ, Bell SA, Goss JL, & Freeman MW (2005) *J Biol Chem* **280,** 39653-39664.

137. Buechler C, Boettcher A, Bared SM, Probst MC, & Schmitz G (2002) *Biochem Biophys Res Commun* **293,** 759-765.

138. Keep NH (2000) *Neurol Sci* **21,** S929-937.

139. Haenggi T & Fritschy JM (2006) *Cell Mol Life Sci* **63,** 1614-1631.

140. Boadu E, Bilbey NJ, & Francis GA (2008) *Curr Opin Lipidol* **19,** 270-276.

141. Murata N, Sato K, Kon J, Tomura H, Yanagita M, Kuwabara A, Ui M, & Okajima F (2000) *Biochem J* **352 Pt 3,** 809-815.

142. Argraves KM, Gazzolo PJ, Groh EM, Wilkerson BA, Matsuura BS, Twal WO, Hammad SM, & Argraves WS (2008) *J Biol Chem.*

143. Hogan A, Shepherd L, Chabot J, Quenneville S, Prescott SM, Topham MK, & Gee SH (2001) *The Journal of biological chemistry* **276,** 26526-26533.

144. Kadrmas JL & Beckerle MC (2004) *Nat Rev Mol Cell Biol* **5,** 920-931.

145. Hermanson O, Glass CK, & Rosenfeld MG (2002) *Trends Endocrinol Metab* **13,** 55-60.

146. Urs AN, Dammer E, Kelly S, Wang E, Merrill AH, Jr., & Sewer MB (2007) *Mol Cell Endocrinol* **265-266,** 174-178.

147. Mizutani Y, Tamiya-Koizumi K, Nakamura N, Kobayashi M, Hirabayashi Y, & Yoshida S (2001) *J Cell Sci* **114,** 3727-3736.

148. Modrek B & Lee C (2002) *Nat Genet* **30,** 13-19.

149. Caceres JF & Kornblihtt AR (2002) *Trends Genet* **18,** 186-193.

150. Wen F, Li F, Xia H, Lu X, Zhang X, & Li Y (2004) *Trends Genet* **20,** 232-236.

151. Burset M, Seledtsov IA, & Solovyev VV (2000) *Nucleic Acids Res* **28,** 4364-4375.

152. Charles AG, Han TY, Liu YY, Hansen N, Giuliano AE, & Cabot MC (2001) *Cancer Chemother Pharmacol* **47,** 444-450.

153. Adams ME, Butler MH, Dwyer TM, Peters MF, Murnane AA, & Froehner SC (1993) *Neuron* 11, 531-540.